The Integration of Annular Thermoelectric Generators in a Heat Exchanger for Waste Heat Recovery Applications

THE INTEGRATION OF ANNULAR THERMOELECTRIC GENERATORS IN A HEAT EXCHANGER FOR WASTE HEAT RECOVERY APPLICATIONS

By

MOHAMMED ZAHER, B.Sc.

A Thesis Submitted to the School of Graduate Studies

In Partial Fulfillment of the Requirements for the Degree

Master of Applied Science

McMaster University

Master of Applied Science (2017) McMaster University

Mechanical Engineering Hamilton, Ontario, Canada

TITLE: The Integration of Annular Thermoelectric Generators in a Heat Exchanger for Waste Heat Recovery Applications

AUTHOR: Mohammed Zaher, B.Sc.

SUPERVISOR: Dr. James Cotton

NUMBER OF PAGES: xvii, 128

Abstract

Growing concerns regarding climate change, the increase in demand for energy and the efficient utilization of energy have become of major interest in applications of heating and power generation. A large portion of the energy input to these applications is lost, due to their typical inefficiencies, in the form of waste thermal energy which, if captured and utilized, can offer an abundant source of energy for electricity generation and heating purposes. The use of thermoelectric generators (TEGs) of different designs in waste heat recovery applications has been pursued over the past few decades as the generation of electrical power using TEGs has become viable compared to other conventional systems at low temperatures. This study focuses on the implementation of an annular design for integrated TEG modules in a heat exchanger device for waste heat recovery and the investigation of the effect of different TEG design parameters on the device performance.

The integration of the annular TEG design in the heat exchanger was studied using a developed numerical model to investigate the interaction between the heat transfer and the thermoelectric effects and evaluate the performance under specific operating conditions. The heat transferred from the exhaust to the water flow through the TEGs was modelled using a thermal network for the heat flow, coupled with an electrical circuit for the power output. The model was validated using experimental results of the first generation of the TEG device with good agreement (3-6 %) between the predicted and measured performance results: power output, efficiency and the exhaust and water flow temperatures.

With the objectives of maximizing the power output and improving the power characteristics, a half annular TEG design was presented. It was able to generate the same power output with double the voltage and half the current, thus improved the power characteristics required for functional operation, compared to the full annular design. The effect of the annular TEG design dimensions on the device performance was studied for a multi-row heat exchanger using the numerical model. The results showed that a maximum power output can be obtained at optimum TEG diameter ratio and thickness.

In addition, the TEGs performance was studied under different electrical connection configurations in series and in parallel. The series connection between TEG rows showed better power output characteristics with lower current output, minimal power loss due to temperature mismatch and higher voltage output. The effect of heat exchanger design considerations such as the axial heat conduction was also investigated using the numerical model and the results were compared with an ANSYS model for verification. Good agreement was demonstrated and the results showed a decrease in the total power output of multiple TEG rows when axial conduction of heat was allowed between the TEGs hot-side surfaces in the heat exchanger.

A dimensions map was created for annular TEGs integrated in a heat exchanger combining the effects of varying the TEG diameter ratio and thickness on the power output. Further, a dimensionless design parameter (β) was introduced to locate the maximum power region on the map. Using the map as a design tool, the dimensions of the annular TEG modules in a heat exchanger were determined to maximize the power output under a typical current output constraint in order to improve the system power characteristics. Using the map, it was shown that the current output could be reduced by 46 % of its value at the maximum power available on the map and the resultant power output could be maintained at 98 % of its maximum value. This also resulted in a 48% reduction in the TEG material volume and an increased voltage output of the device. As a result, the power output was maximized, the current output was limited to reduce losses in the power management system components and material volume reduction was achieved which would increase the device power density and reduce its overall cost.

Acknowledgments

In the name of Allah, the Most Gracious and the Most Merciful, all praises to Allah for blessing me with strength and knowledge to complete this work.

I would like to express my gratitude and genuine appreciation to my supervisor, Dr. Jim Cotton, for his endless support and indispensable guidance throughout the course of this work. Thank you for your patience, trust and help with every step along the way and for giving me the chance to be part of the AMAZING research team, TMRL.

I would like to extend my thanks to Dr. Hossam Sadek for guiding me through and for lending a helping hand in times when I needed it the most. I would also like to express my sincere appreciation to Dr. Chan Ching for motivating me to do more while keeping me in high spirits and Dr. Vickram Lakhian for his invaluable contribution to the progress of this project.

To Yasser and Ali who have always got my back and are the reason that I am still pursuing my dream. To Zizo who had to put up with my lengthy discussions. To Sarah who joined me in my numerous early morning attempts to work. To Romina for helping with my presentations. To Raf, Jeff, Mustafa, Paul, Mike and Donal, the TEG team, who guided me and helped make this work possible. To all members of TMRL. I would like to thank you for your selfless support and cherished company.

I would also like to acknowledge the project sponsors Gerard Campeau at TEGTEC Corp., Pizza Pizza Ltd., OCE and NSERC. Thank you for providing the resources to accomplish this project.

To my beloved parents, my dear brother and my loving sisters, I would like to express my utmost gratitude, appreciation and unbounded respect. Thank you for believing in me and for your continuous support and motivation. This would not have happened if it were not for you.

Contents

List of Figures

List of Tables

Nomenclature

Variables

A	Thermoelement Leg Cross-sectional Area	[m^2]
D	Diameter	[m]
I	Current Output	[A]
J	Current Density	[A/m^2]
K	Thermal Conductance	[K/W]
L, l	Thermoelement Leg Length	[m]
L_{pipe}	Pipe Length	[m]
m_L	External Electrical Load Ratio	[ ]
N	Number	[ ]
P	Power Output	[W]
Q	Heat Transfer Rate (Flow)	[W]
$\tilde{r}$	Raduis	[m]
r, R	Electrical Resistance	[ohm]
R_{th}	Thermal Resistance	[W/K]
S	Spacing	[m]
t	Thickness	[m]
T	Temperature	[°C or K]
v	Velocity	[m/s]
V	Voltage Output	[V]
Z	Figure of Merit	[1/K]
α	Seebeck Coefficient	[V/K]
β	Annular TEG Dimensionless Parameter	[ ]
ϵ	Joule Heat Distribution Ratio	[ ]
η	Efficiency	[ ]
λ	Thermal Conductivity	[W/m.K]

μ	Viscosity	[Pa.s]
π	Peltier Coefficient	[V]
ρ	Electrical Resistivity	[ohm.m]
τ	Thomson Coefficient	[V/K]

Subscripts

A	Axial
av	Average
cd	Conductor
c, ct	Contact
C	Cold-side
g	Gas
G	Gap
H	Hot-side
HX	Heat Exchanger
i	Inner
m	Row Number
mat	Material
N	N-Type Semiconductor
n	Node Number
o	Outer
OC	Open Circuit
P, p	P-Type Semiconductor
r	Radius
S	Surface
SC	Short Circuit
th	Thermal
T, TEG	Thermoelectric Generator (TEG)
w	Water

Chapter 1

Introduction

Different applications utilize heat from energy resources for power generation and heating purposes which contributes to a major part of the world's energy consumption. Large portions of this energy is lost to the surroundings, as waste heat through exhaust from industrial or commercial processes or power generating heat engines. Typical thermal efficiencies of such applications range from 10-50% for ovens and industrial furnaces, 25-44% for power production cycles and heating applications as boilers with efficiencies in the range of 80-90% [1], [2].

Waste heat recovery systems strive to put this lost thermal energy to use but challenges exists depending on the characteristics of heat sources. These sources can have a wide range of temperatures and flow rates, often with unsteady conditions and dispersed among a number of small-scale sources [3]. Such conditions impose challenges on recovering waste heat energy especially for electricity generation by conventional Rankine type systems which require sources with stable and steady output. This offers a huge potential for using thermoelectric generators in waste heat recovery applications.

Thermoelectric generators (TEGs) have a number of advantages due to their ability for generating electricity over a wide range of temperature differences and their solid state nature provides a maintenance-free reliable operation over prolonged periods of time and they can operate under unstable conditions [3]. These properties enabled TEGs to be used for power generation in a broad range of applications from example wearable electronics, autonomous sensors, automotive and industrial waste heat recovery systems and space applications.

As heat engines, TEGs are subject to the laws of thermodynamics with efficiency limits represented in Carnot efficiency and the material properties denoted in the thermoelectric figure of merit (Z) [3]. The higher the thermoelectric material figure of merit and the temperature difference, the higher the efficiency and the electrical power output of the TEGs. The figure of merit (Z) is temperature dependent and it varies between different thermoelectric materials

depending on the temperatures range as shown in Fig.(1.1). Depending on the application temperature range, the thermoelectric material with the highest Z is selected. Common semiconductors as bismuth alloys combined with antimony, tellurium and selenium are used as thermoelectric materials for low-temperature applications up to 450 K compared to materials based on lead telluride and silicon germanium alloys for intermediate-temperature (up to 850 K) and high-temperature (up to 1300 K) applications respectively [3].

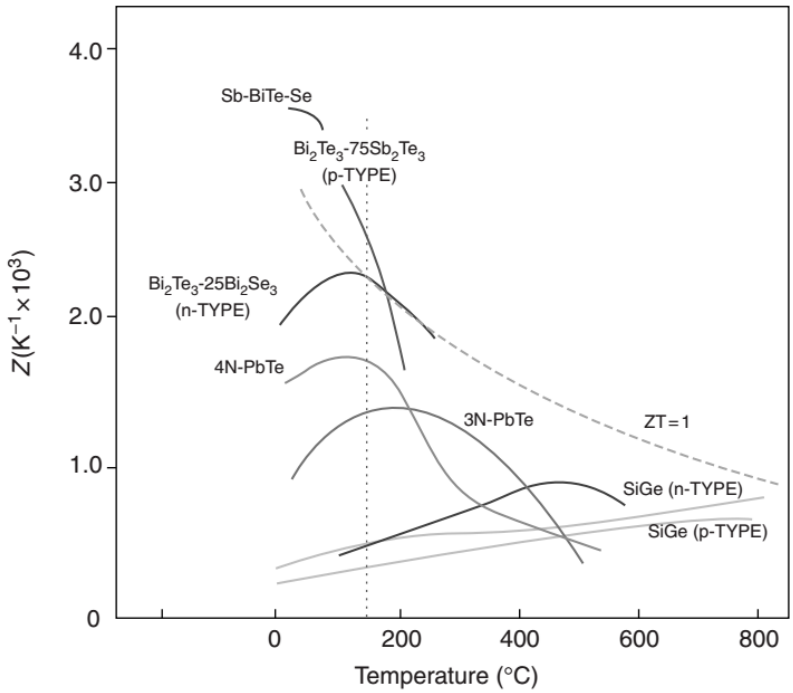

Fig.(1.1) – The figure of merit (Z) of different thermoelectric materials as function of temperature [3]

The temperature of waste heat energy depends on the type of the application. For low temperature applications (up to 200 °C), bismuth telluride alloys offer the highest figure of merit which make it suitable for designing TEG modules for this temperature range with a maximum average figure of merit of $2.5 \times 10^{-3}\, K^{-1}$ for a thermoelectric couple [1] limiting the generator theoretical efficiency at 5.8 % when operating at 175 K temperature difference. Although a TEG efficiency might seem relatively low, for a system designed for power generation using waste heat, the power output is a main priority compared to the efficiency since waste heat can be considered a free source of energy [4]–[7].

Considering waste heat from gas-fired appliances used in commercial applications as food industry, conventional natural gas fired ovens operating continuously can generate an output of 10 kW of waste heat with steady rate during operation, to maintain a temperature of 260 °C for baking purposes, the majority (90%) of heat is lost through the exhaust gas stream to the atmosphere. This indicates that huge amount of energy is lost from heating processes in commercial applications which can be utilized for power generation using TEGs.

A waste heat recovery system has been developed, to capture the energy lost from conventional natural gas fired ovens to generate electricity and provide thermal energy needed for hot water purposes, using a heat exchanger device with integrated TEGs [8] which is referred to as "Thermal-Electric Generator Pizza Oven Waste Energy Recovery (TEG POWER)" to save on natural gas and electricity and provide energy resiliency in power outage.

The first generation of TEG POWER heat exchanger uses commercial TEG modules with flat geometry to generate electricity and transfer waste heat to a cooling loop connected to a water tank. The device is able to generate 79 W of electricity with an efficiency of 2% for exhaust flow rate of 0.044 kg/s at temperature 265 °C and water with flow rate of 0.07 kg/s and temperature of 8 °C while recovering 3.9 kW of thermal energy to be stored in the hot water tank for later use. The TEGs are connected electrically to a DC circuit to charge a battery. Proper matching between the TEG electrical resistance and the external load resistance is required to attain a maximum power output from the TEGs due to its linear V-I characteristics. A maximum power point tracking (MPPT) system is used to ensure proper TEG load matching under different operating conditions.

The TEG modules used consists of 126 thermoelectric couples, made of bismuth telluride alloy with flat geometry for the thermoelectric legs, connected electrically in series and packed in between two ceramic substrates which transfer the heat from the heat exchanger to the thermoelectric legs [9]. Despite their compact design, the modules suffer from temperature drop across the substrates which affect the performance adversely, moreover the TEG material properties and manufacturing process tolerances cause a significant variation of the performance of individual modules from the manufacturer specifications [10].

As a result, the efficiency of the TEG modules is lower when compared to a theoretical TEG operating under the same temperature difference in TEG POWER heat exchanger which would allow a maximum theoretical efficiency of 4.4 % using a maximum figure of merit for bismuth

telluride alloys of $2.5 \times 10^{-3}\, K^{-1}$. This shows that the actual of efficiency of the system can further be improved which will increase the system power output under the same conditions. In addition, the thermal resistance of the flat TEG modules is not optimized for this heat exchanger design. Studies [4]–[7], [11] have shown that, for a given heat exchanger design, the power output can be increased by optimizing the TEG thermoelectric couples geometry. Finally, although the current commercial TEG module flat design has been extensively used in heat exchangers for waste heat recovery applications, it requires more consideration in the design to decrease the inherent heat exchanger thermal resistance, this often increases the heat exchanger complexity and cost.

An annular TEG module design was manufactured and tested by Min and Rowe [12], the design is more suitable for implementation in typical heat exchangers due to the annular geometry which allow the modules to be fitted around pipes and integrated in heat exchanger designs. In addition, the geometry provides a larger outer surface area which is advantageous for heat transfer from exhaust gases and the design if well suited for mass production process would lead to reduce the device total cost compared to labor-intensive manufacturing techniques used for flat TEG modules.

A next generation of TEG POWER heat exchangers is introduced in this study that uses an annular bismuth telluride alloys module design. The heat exchanger is a cross flow design with multiple rows of TEG modules. The comparison is based on fixed heat exchanger overall dimensions, design and operating conditions. The current assessment uses similar exhaust side heat transfer surface design compared to the first generation TEG POWER device. However the water side heat exchanger design is replaced with simple coolant flow pipes due to the annular shape of the TEGs but a low heat transfer thermal resistance is maintained.

Several studies have considered the annular TEG module design [12]–[18], however the effect of TEG dimensions on the overall performance of a heat exchanger and the power output characteristics has not been investigated. The dimensions of the annular TEGs can significantly affect the heat flow through the heat exchanger since it is considered the component of highest thermal resistance. This is mainly due to the relatively lower thermal conductivity of the TEG material compared to other components of the heat exchanger, and it also affects the total power output and efficiency of the TEG modules.

1.1. Objectives

The objective of this study is to develop a numerical model to investigate the performance of the next generation TEG POWER heat exchanger with integrated annular thermoelectric generators. The numerical model methodology is verified using the results of the 1st generation TEG POWER device for exhaust, water and TEG surface temperatures, power output and efficiency. Furthermore, the results for the annular TEGs will be compared against the results of a simulation model using ANSYS to provide insight into the temperature distribution and heat flow.

The model takes into account the interaction between the heat transfer and the thermoelectric effects through the TEG modules in the heat exchanger, the temperature variation within the exhaust gas and water streams, the electrical connection between the TEG modules and the effect of different heat exchanger and TEG design aspects on the performance. The effect of TEG outer diameter and thickness is studied on the heat flow through the heat exchanger, the voltage and current output of the TEGs.

1.2. Scope of work

The scope of this study is the investigation of the effect of the annular TEGs dimensions of the next generation TEG POWER heat exchanger on performance using a numerical model. The TEG dimensions affect the thermal resistance, which alters the heat flow and the temperature difference across the TEG, and the electrical resistance, which affect the voltage, current and thus power output of TEG modules, and the material volume.

The annular TEG outer diameter and thickness are characterized using a parametric analysis to obtain the maximum electrical power output for given heat exchanger design and operating conditions. A performance map using the key dimensions is developed as a design criterion for the TEG dimensions. An electrical current limit will be used as a constraint to improve the power output characteristics and minimize the volume of material used.

Chapter 2

Literature Review

2.1. Introduction

In this chapter, the principles of thermoelectricity and theory of thermoelectric generators (TEGs) will be outlined. Different methodologies for modelling of TEGs operation in heat exchangers will be discussed through a review of open literature. The effect of TEG geometrical parameters will be presented and optimization studies of these parameters will be discussed. Finally, different TEG geometries, including research studies focusing on annular shaped TEGs, will be presented.

2.2. Principles of thermoelectricity

Thermoelectricity is the basis for solid-state technology that enabled the use of simple and reliable devices in power generation applications where using conventional processes could be challenging and, in some cases, impractical. A simple definition would state that thermoelectric effects are a result of coupling of Ohm's law and Fourier's law [19], these effects occur due to the interaction between electrical current and heat flow allowing heat to be converted directly into electricity [3]. In thermoelectricity, the three effects of concern are Seebeck, Peltier and Thomson effect which will be discussed in brief below.

2.2.1. The Seebeck effect

For an open circuit of a thermocouple consisting of two dissimilar metals, known as thermo-elements or legs, (a & b) connected at two junctions (A & B), electrically in series and thermally in parallel, as shown in Fig (2.1). An electromotive force is generated creating a voltage output across the terminals (C & D) when the junctions maintained at different temperatures (T_H & T_C) where ($T_H > T_C$). This is known as the Seebeck effect [3].

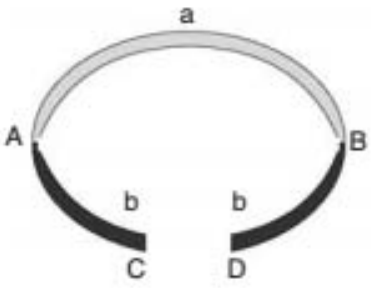

Fig.(2.1) – Basic thermocouple schematic [3]

The voltage output depends on the Seebeck coefficient (α) which is the difference between the Seebeck coefficients of both metals. To maximize Seebeck effect in a circuit of a generator with multiple couples (N), semiconductors are used which can be doped, creating a P-type with a positive Seebeck coefficient and N-type with a negative Seebeck coefficient, maximizing the circuit Seebeck coefficient. The open circuit voltage (V_{OC}) can be written as:

$$V_{OC} = N\ \alpha\ (T_H - T_C) \quad (2.1)$$

2.2.2. The Peltier effect

A thermal effect occurs in a thermocouple circuit shown in Fig.(2.1) at a junction maintained at constant temperature as heat is transferred, as a result of the current flow, to or from the junction when a voltage difference is applied, which is known as the Peltier effect or heat. The ratio of the current (I) to the heat (q) is defined as the Peltier coefficient (π) [19] and it is related to the Seebeck coefficient (α) as:

$$\pi = \alpha\ T \quad (2.2)$$

$$Q = \alpha\ I\ T \quad (2.3)$$

The Peltier heat is considered as the reversible component of heat [3] which can have the same direction as heat conduction in case of a generator or the opposite in case of a cooler, since it depends on the direction of the current flow, it is calculated using eqn.(2.3) and it can be summed to the conduction component [3].

2.2.3. The Thomson effect

Due to the dependence of the Seebeck coefficient on temperature and the presence of a temperature gradient along the thermoelectric material, generation of reversible heat takes place as a result of the current flow, which is known as the Thomson effect. Thomson heat is caused by the temperature gradient along the thermo-element leg which causes Peltier heat to be absorbed or released within the thermoelectric material in case of temperature dependent Seebeck coefficient. It can be written as:

$$\tau = T \frac{d\alpha}{dT} \quad (2.4)$$

All thermoelectric effects, shown in eqns. (2.1 – 2.4), depend on the material Seebeck coefficient (α) which is a temperature dependent material property. For the case of constant average Seebeck coefficient with temperature, the Thomson coefficient (τ) is equal to zero. Ioffe et al. [20] stated that Thomson effect can be modelled by taking the mean Seebeck coefficient across the thermo-element. Sunderland [21] showed that the power output of a thermoelectric generator can increase or decrease depending on the sign of the Thomson coefficient.

Different approaches, with varying complexity and computational costs, were taken in literature for modelling of temperature dependent thermoelectric properties and Thomson effect in thermo-elements subject to a hot-side temperature (T_H) and a cold-side temperature (T_C). These approaches include cases; 1) Simplified model with averaging of properties using the mean temperature ($T_m = T_H + T_C/2$) [20], 2) Same simplified model with integral averaging of properties [22], 3) Finite element model (including Thomson heat) [22], [23].

Lau et al. [22] and Fraisse et al. [23] compared case (1) of averaging using the mean temperature neglecting Thomson effect with case (3) of finite element modelling including the effect of Thomson heat. Both studies [22], [23] investigated the performance of thermo-elements as generators under temperature differences up to 200 K. The results of Fraisse et al. showed that case (1) overestimated the power output by 9% at 200 K compared to case (3) while Lau. P et al. showed a higher deviation of 11% at 200 K.

By using integral averaging of properties i.e. case (2), the results of Lau et al. [22] showed improved accuracy of the simplified model with deviation less than 5% compared to case (3) for temperature differences up to 200 K. It can also be concluded from the results that the deviation

decreases significantly as the temperature difference decreases since the power output estimation of case (2) coincides with case (3) at 150 K. Other improved simplified models that includes an average Thomson coefficient were also presented in [21], [23], [24].

Typically (as in the current study) for comparative and optimization studies as [4]–[7], Thomson effect is neglected as the Seebeck coefficient is assumed constant within the thermo-elements length. The thermoelectric properties are calculated using integral averaging between the hot and cold side temperatures of each row for improved accuracy.

2.3. Theory of thermoelectric generators

A thermoelectric generator (TEG) is a device that converts thermal energy into electricity by means of thermoelectric effects generated in semiconductors under a temperature gradient. By applying a temperature difference across a TEG, voltage is generated across the junctions as a result of Seebeck effect and heat is transferred irreversibly by conduction and Joule heating through the thermoelectric material and reversibly due to Peltier effect [1,2]. For power generation using TEGs, modern semiconductors are used in which the material properties and geometry can be tailored for the application temperature range to generate a considerable power output.

A typical TEG module configuration is shown in Fig.(2.2) operating between constant temperatures, it consists of (N) thermoelement couples, made of P and N-type semiconductor thermoelectric materials, connected in series using metallic electrical conductors. A heat source of high temperature (T_H) and a heat sink of low temperature (T_C) are used to provide a temperature difference between the TEG hot-side and cold-side junctions which creates a voltage output (V). By connecting the generator to an external load resistance (R_L), current (I) will flow through the TEG and a power output (P) is generated according to Ohm's law.

The TEG performance can be evaluated by modelling the heat and current flows through the TEG using the material thermoelectric properties. Several modelling methodologies have been presented in literature, steady state ideal models [20], [25], [26], the effect of the electrical contact resistances on performance [26] and temperature dependent thermoelectric properties [22].

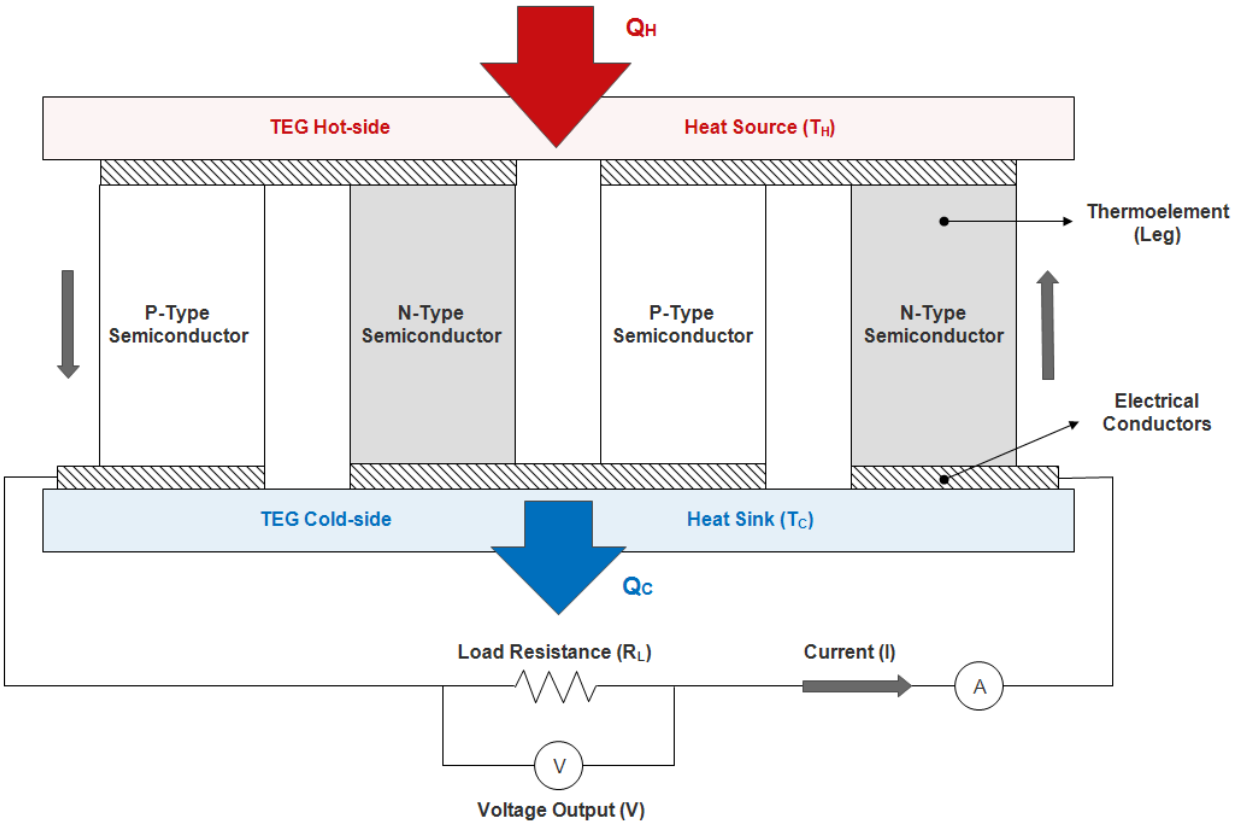

Fig.(2.2) – Thermoelectric generator (TEG) module operating between constant temperatures heat source and sink

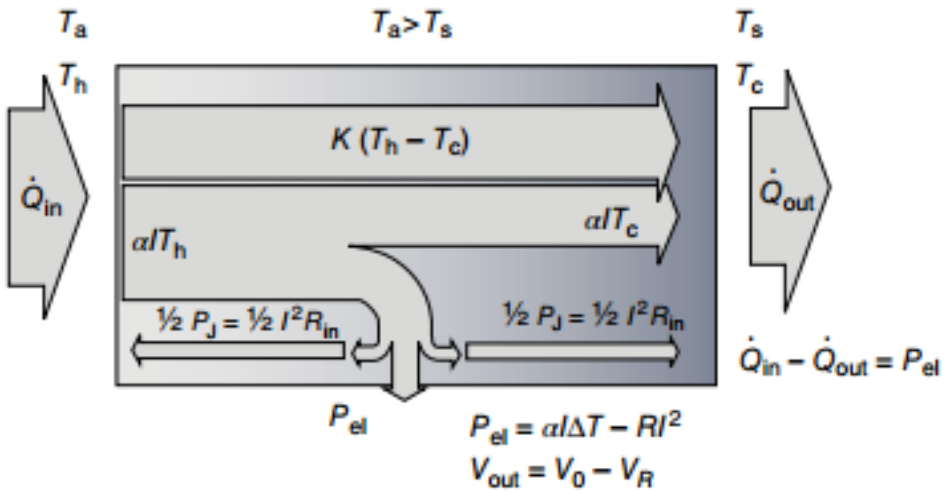

Fig.(2.3) – Modelling of heat flow through a TEG using Ioffe CPM [19]

An ideal model was presented by Ioffe [20] to model the coupling between heat conduction, Peltier heat and Joule heating through a TEG couple with constant cross sectional area operating between constant temperatures using constant thermoelectric properties which is often referred to as Ioffe's constant properties model (CPM) shown as a representation in Fig.(2.3) [19]. The heat flow at the TEG hot-side (Q_H) and cold-side (Q_C) can be written as:

$$Q_H = K_T(T_H - T_C) + \alpha\, I\, T_H - \frac{1}{2}I^2 r_T \quad (2.5)$$

$$Q_C = K_T(T_H - T_C) + \alpha\, I\, T_C + \frac{1}{2}I^2 r_T \quad (2.6)$$

The figure of merit of TEGs was introduced [20], [25] for a generator as:

$$Z = \frac{\alpha^2}{Kr} = \frac{(\alpha_P - \alpha_N)^2}{[(\lambda_P \rho_P)^2 + (\lambda_N \rho_N)^2]^{1/2}} \quad (2.7)$$

The efficiency of the generator can be calculated using the figure of merit in eqn.(2.7) as the ratio of the power output to the heat flow at the TEG hot-side, the efficiency for a generator can be written as [20]:

$$\eta = \frac{P}{Q_H} = \frac{T_H - T_C}{T_H} \times \frac{\frac{m_L}{m_L + 1}}{1 + \frac{1}{Z} \times \frac{m_L + 1}{T_H} - \frac{1}{2}(T_H - T_C)\frac{1}{m_L + 1} \times \frac{1}{T_H}} \quad (2.8)$$

The efficiency shown in eqn.(2.8) depends on the external load ratio ($m_L = R_L / r_{TEG}$) and the maximum efficiency occurs when the load ratio is equal to $\sqrt{1 + Z\bar{T}}$ and the leg length (L) to the cross section area ratio (A) of the device is equal to [25]:

$$\frac{L_N A_P}{L_P A_N} = \left(\frac{\lambda_N \rho_P}{\lambda_P \rho_N}\right)^{\frac{1}{2}} \quad (2.9)$$

The maximum efficiency of a generator can then be rewritten as:

$$\eta = \frac{P}{Q_H} = \frac{T_H - T_C}{T_H} \times \frac{\sqrt{1 + Z\bar{T}} - 1}{\sqrt{1 + Z\bar{T}} + \frac{T_C}{T_H}} \quad (2.10)$$

Considering constant hot-side and cold-side temperatures, the efficiency is independent of the TEG leg length as it only depends on the figure of merit (Z) as shown in eqn.(2.10). Varying the TEG leg length affects both the power output and the heat flow for a constant temperature difference, since it equally affects the TEG thermal and electrical resistance, causing the efficiency to remain constant.

Other resistances can also affect the TEG power output and efficiency. Cobble studied the effect of electrical contacts on the performance of a multi-couple TEG [26]. The study introduced the electrical contacts resistance between the conductors and the thermoelectric material to the constant properties model [20] and showed a resulting decrease in power output and efficiency. The resistance of the electrical contacts depends on the generator manufacturing process of joining the conductors to the TEG material.

In a heat exchanger, TEG surface temperatures can vary significantly between rows which can affect the performance of each row in case of temperature dependent thermoelectric properties which is considered in this study, properties as Seebeck coefficient, thermal conductivity and electrical resistivity of the P and N-type materials are calculated for every row using integral averaging between the TEG hot-side and cold-side temperatures.

2.4. Modelling methodologies of heat exchangers with integrated thermoelectric generators for performance optimization

Due to coupling between the heat transfer through a TEG and the thermoelectric effects due to current flow, the performance of TEGs in heat exchangers requires modelling of the heat transfer through the heat exchanger to study their effect on the TEG surface temperatures which results a set of non-linear equations. Different modelling methodologies have been presented in literature several of which are discussed in this section followed by studies on the geometrical aspects of the TEG design of performance.

Typically in a heat exchanger, heat is transferred between a fluid at high temperature and another fluid at a relatively lower temperature. The integration of TEGs in a heat exchanger, where the hot fluid acts as the heat source for the TEG and the cold fluid becomes the heat sink, requires the modelling of the heat transfer mechanisms between the fluids and the TEG junctions.

These mechanisms include convection from the fluid to the heat exchanger surface, conduction through the heat exchanger structure and contacts at the TEG surfaces. Thermal resistances associated with these mechanisms affects the TEG performance due to the temperature difference between the fluids and the TEG material at junctions. Another parameters as the fluids flow rates has a major influence on performance due to the temperature variation in the fluids temperatures in the heat exchanger.

2.4.1. Modelling techniques of heat exchangers

Different modelling techniques have been presented in literature for heat exchangers with integrated TEGs. The heat flow through the heat exchanger components at the TEG hot-side and cold-side surfaces is modelled as a function of the heat exchanger thermal conductance (K), the heat source temperature ($T_{S,H}$), the heat sink temperature ($T_{S,C}$) and the TEG hot-side ($T_{T,H}$) and cold-side ($T_{T,C}$) surface temperatures. By combining the heat exchanger modelling equations with Ioffe's CPM equations described in eqns.(2.5 & 2.6), the result is a set of non-linear equations that determines the surface temperatures, the heat flow and the power output of the TEG. The total heat flow model equations can be written as:

$$Q_H = K_H\left(T_{S,H} - T_{T,H}\right) \quad (2.11)$$

$$Q_H = K_T\left(T_{T,H} - T_{T,C}\right) + \alpha\, I\, T_{T,H} - \frac{1}{2} I^2 r_T \quad (2.12)$$

$$Q_C = K_T\left(T_{T,H} - T_{T,C}\right) + \alpha\, I\, T_{T,C} + \frac{1}{2} I^2 r_T \quad (2.13)$$

$$Q_C = K_C\left(T_{T,C} - T_{S,C}\right) \quad (2.14)$$

$$I = \frac{\alpha\left(T_{T,H} - T_{T,C}\right)}{r_T\,(m_L + 1)} \quad (2.15)$$

Assuming constant heat source and sink temperatures, several studies [4]–[7], [11], [27]–[30] have investigated the performance of TEGs in a heat exchanger by solving the model equations (2.11 - 2.15) to study the effect of TEG design parameters. Different solution techniques were used in these studies by applying simplifying assumptions.

A simplified model was used in [4]–[7], [11], [28], [29], referred to "first level model". It neglects the current flow (I) through the TEG and hence neglecting Peltier and Joule heat effects in the heat flow equations (2.11 - 2.15). This assumption resulted in a linear set of equations that can be used to obtain a closed form solution. The power output was found to be [7]:

$$P = \frac{\alpha^2}{2\rho} \times \frac{A\,N}{(n+1)\left(1 + \frac{2r l_c}{l}\right)^2} \times (T_H - T_C)^2 \quad (2.16)$$

More accurate exact models were presented in [28], [30] that take into account Peltier and Joule heat components in eqns. (2.11 - 2.15). The solution was obtained by Freunek et al. using taylor expansion by neglecting second and higher order terms and the power output was written as [30]:

$$P = (\Delta T m \alpha)^2 \left(\frac{K_g}{K_g + K_C + K_H}\right)^2 \frac{R_l}{(R_l + R_{TEG}^{eff})} \quad (2.17)$$

The solution of the developed simplified model shown in eqn.(2.17) was compared with that of the first level in eqn.(2.16) by Freunek et al. [30] in Fig.(2.4). The results show the effect of simplifying assumptions on the power output calculations, the first level model significantly overestimates the TEG power output by 40% compared to the simplified model. This highlights the importance of modelling of Peltier and Joule heating effect for accurate performance calculations.

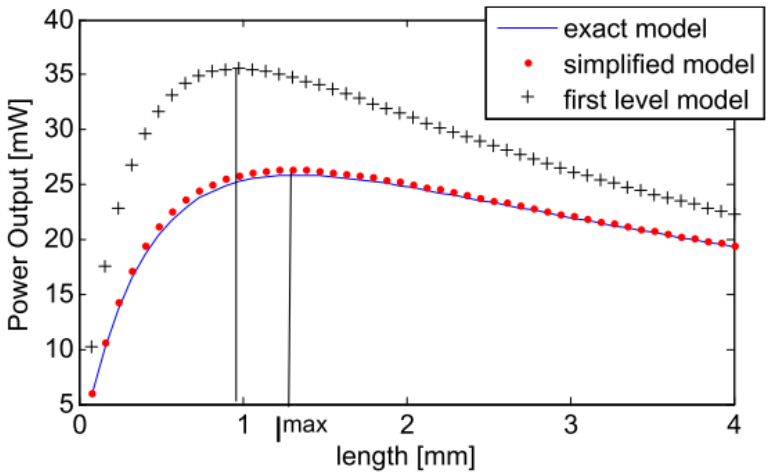

Fig.(2.4) – Power output estimation using different modelling techniques [30]

Since the TEG power output is a function of the load ratio (m_L) which is the ratio between the external electrical load to the TEG internal resistance, the power output is maximized when the external load resistance is matched with the internal resistance ($m_L = 1$). This is true only when a TEG is operating between constant hot-side and cold-side temperatures. However, in a heat exchanger, these temperatures are a function of the heat flow through the TEG as shown in eqns.(2.11-2.15).

Freunek et al. [30], [31] first investigated the effect of the heat exchanger thermal resistance on load matching. The study estimated the load ratio at maximum power for a TEG in a heat exchanger using the simplified model in [30], the maximum power output was found to occur when an external load resistance is equal to an effective TEG internal resistance which can be written as [31]:

$$R_{TEG}^{eff} = R_{TEG} + T_{s,C}\alpha^2(K_C + K_H) \times \frac{K_{TEG}}{K_{TEG} + K_C + K_H} \quad (2.18)$$

This result shows that the matched load occurs at an effective TEG internal resistance (R_{TEG}^{eff}) which is higher than the TEG calculated internal resistance (R_{TEG}) due to the effect of the heat exchanger thermal resistances. This effect was not considered by Strasser et al. [32] and Glatz et al. [28] in their exact models. Freunek et al. [31] compared the load matching results using the effective TEG resistance compared to matching using the TEG material resistance. The results

showed that although the calculated maximum power output increased only by 5%, the voltage output increased significantly by 20%.

2.4.2. Effect of TEG geometrical parameters on performance

For a TEG integrated in a thermal circuit of a heat exchanger operating at constant heat source and sink temperatures, the TEG hot-side and cold-side temperature are dominated by the TEG thermal resistance. Varying the dimensions of TEGs affects their thermal resistance which in turn will change the temperature difference across them and hence the power output. Additionally, this also affects the TEGs electrical resistance. Therefore, modelling of the coupled mechanisms of heat transfer and thermoelectric effects using the equations, as discussed in section (2.4.1.), is required. Several research studies of the TEG geometry and its effect on performance will be discussed in this section.

Henderson [27] developed a numerical model to investigate the performance of TEGs in a heat exchanger for an ocean thermal energy application under small temperature differences, the study was done on a single thermoelectric element of flat geometry with taking into consideration the heat exchanger and the TEG electrical thermal resistances and neglecting electrical contact resistances. The thermoelectric material properties were also assumed constant over the temperature range.

The effect of TEG cross sectional area to leg length (γ) on the power output was studied and the results show that the power output can be maximized by matching the TEG thermal resistance, which is a function of (γ), with the summation of the heat exchanger hot-side and cold-side thermal resistances. The same result was also shown by Stevens [11] in which the analysis was done using a first level model for a fixed heat exchanger thermal resistance and the TEG thermal resistance was varied. This study [11] was done for applications of small temperature difference (1-10 K) and the heat flow through the TEG was assumed to be equal for both the hot and cold sides by neglecting the effect of current flow to obtain a closed form solution. Although this assumption might be valid for TEG operating under small temperature differences, it could result in overestimation of the power output as shown by Freunek et al. [30] in Fig.(2.4).

Min and Rowe [4]–[7] studied the optimization of the flat TEG module geometry for waste heat recovery applications in which it was suggested that the thermoelement geometry should be

optimized to maximize the power output rather than efficiency due to the abundance of waste energy in such applications and it can significantly reduce the cost per watt. A first level model was used that takes into consideration the electrical contact resistance and the thermal contact resistance of the ceramic plates at the TEG junctions, neglecting the Peltier heat through the module and assuming constant thermoelectric properties.

The effect of the thermoelement leg length was investigated experimentally by using three different TEG modules operating between a heat source of 120 °C and a cold side at ambient temperature. The results showed that by decreasing the leg length by 55%, the power output increased by 48% while the efficiency decreased by less than 10% [5]. Such decrease in the thermoelement leg length corresponds to a reduced volume of the module which in turn can significantly reduce the cost of the module.

The inter-thermoelement separation, which is the gap distance between the legs in a flat TEG module, was studied by Rowe et al. [6]. The results showed that the power per unit area of a module can significantly increase by reducing the spacing between the TEG legs. To achieve higher power output requirements, the modularity of the optimized TEG design was also shown important as it facilitates the system design up-scaling [7].

Increasing the TEG modules power output was shown possible in studies [4]–[7], [11], [27] as shown in Fig.(2.5) by optimizing the module geometry. However, a simple modelling technique was used to simplify the analysis which provided a good understanding for the dependence of the power output on the TEG geometry but might result in an inaccurate estimation of % increase in power output as shown in Fig.(2.4). Additionally, the effect of temperature distribution in flow streams on the TEG modules surface temperature in a system was not investigated in [7] which can have a significant effect on the geometry optimization. Furthermore, decreasing the TEG thermal resistance by decreasing the TEG leg length also results in a decrease in the TEG electrical resistance which affects the power output characteristics as the TEG voltage output decreases and the current output increases as shown in Fig.(2.5).

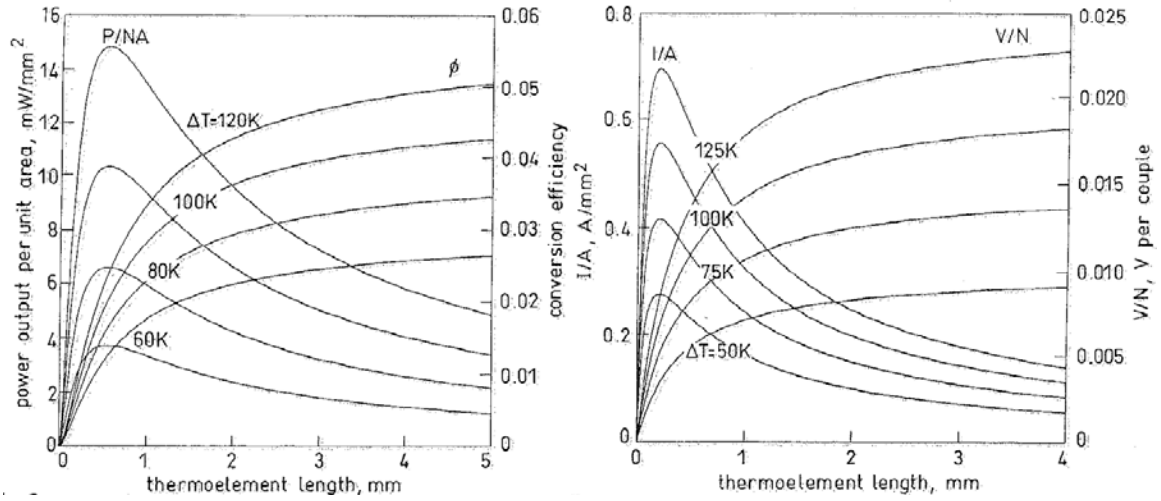

Fig.(2.5) – The effect of thermo-element leg length of power output per unit area, efficiency, current per unit area and couple voltage output of a TEG module [3], [6], [7]

By optimizing the thermoelement leg length for maximum power output, although it can reduce the volume of the TEG material used, it results in an increase in the current output and a decrease in voltage of the TEG module as shown in Fig.(2.5) [4]–[6]. In an actual system, the TEG requires a maximum power point tracking (MPPT) device connected to power a DC-microgrid that would operate at a higher voltage. Therefore, a high step up gain for a DC/DC converter is required, achieved at higher duty cycles, resulting in a significant drop in efficiency [33] due to switching and Joule heating losses.

Glatz et al. [28] studied the optimization of micro-TEGs performance integrated in flexible polymers for possible applications as wearable electronics using an exact model developed by Strasser et al. [32] that takes into account the Joule heating and Peltier effects. The study compared the general model with the first level model, the results showed an increased optimized leg length compared to the first level model due to Joule heating losses and Peltier heat effects.

A modified model was introduced by Freunek et al. [31] for the investigation of Peltier effects and Joule heating on the optimized TEG geometry and external load matching for constant material properties. A closed form solution for an optimum design ratio, which is equal to TEG leg length to the cross sectional area, was derived using the developed modified model. The ratio depends on parameters including the heat exchanger thermal resistances, material properties and the heat sink temperature. It can be written as [31]:

$$\frac{l}{A} = N\left(\lambda_n + \lambda_p\right)(K_H + K_C)\sqrt{1 + ZT_{s,C}} \qquad (2.19)$$

The ratio shown in eqn.(2.19) indicates that the optimum TEG geometry is not only a function of the heat exchanger thermal resistances but also the temperature of the heat sink as well as the TEG material properties. The results obtained by Freunek et al. [31] showed the temperature dependence of the TEG optimum geometry when Joule heating, Peltier effects, electrical contact resistance and accurate external load matching were included in the analysis with neglecting Thomson effect.

Brownell and Hodes [34] studied the optimization of the height and number of thermo-elements of a flat TEG in a thermal resistance network for waste heat recovery applications. The study considered constant heat source and sink temperatures, equal thermal resistances of the hot and cold sides, equal electrical contact resistance and constant thermoelectric properties implying no Thomson effect. The load ratio was set for maximum efficiency. The study showed that an optimal number (N) and height (H) of thermo-elements exist for a prescribed area in a thermo-elements array that maximizes the power output as shown in Fig.(2.6).

A numerical model was developed to solve for the maximum power output for combinations of N and H. The optimization of these parameters was studied for a module made of bismuth telluride of fixed total area of 1562 square mm with packing density of 40% operating between 100 °C and 20 °C. The results shown in Fig.(2.5) indicate the effect of varying the thermoelement height (H) and the thermoelement area (A), where (A) is inversely proportional to the number of thermo-elements (N).

The TEG power output is maximized when its thermal resistance equals the sum of that of the heat exchanger as found by Stevens [11] using a simplified first level model. Since the TEG thermal resistance is a function of the thermo-elements height (H) and area (A) and by varying both parameters, the TEG thermal resistance will change accordingly. A certain value of thermal resistance maximizes the power output at N = 250 and H = 1mm approximately as shown in Fig. (2.6).

However the study did not investigate the effect of the ratio of the thermo-element leg height (H) to the area (A) on the power output. As shown by Freunek et al. [31] in eqn.(2.19), using the TEG material properties and the heat exchanger thermal resistances, the ratio (H/A) can be determined that maximizes the TEG power output. In addition, the TEG dimensions was only optimized for a

constant external electrical load (R_L) equals to 5 ohms although the maximum power output occurs when R_L is matched with the TEG effective internal electrical resistance (R_{TEG}^{eff}) as described in Section (2.4.1). This might cause the TEG to underperform for different groups of N and H due to external electrical load mismatching since R_{TEG}^{eff} is a function of N and H. This is avoided by connecting the TEG to a maximum power point tracker (MPPT) that ensures external electrical load matching ($R_{TEG}^{eff} = R_L$).

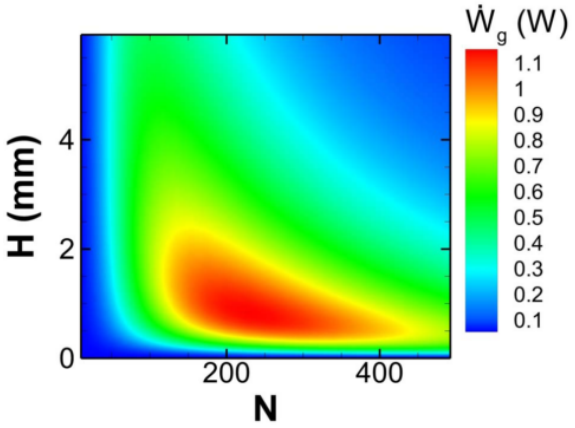

Fig.(2.6) – Power output contours created by varying two independent variables: the thermo-element leg height (H) and no. of thermo-elements (N) [34]

All research studies investigated earlier [4]–[7], [11], [27]–[31], [34] considered only constant heat source and sink temperatures assuming infinite heat reservoirs which might be applicable in some cases. However, the temperature variation within a heat exchanger in the flow direction, due to finite heat source and sink fluids flow rates, can have an effect of the TEG geometry optimization. The fluid flow rate can also have a significant impact especially when either the heat source or the heat sink is a fluid of low heat capacity as air or exhaust gas.

A numerical model was developed by Crane et al. [35] to simulate the performance of the heat exchanger and TEGs, using temperature dependent thermoelectric properties model, neglecting Thomson effect. The analysis considered the heat conducted axially through the walls in the flow direction. The heat exchanger is discretized into cells along the hot fluid flow direction with a cell length equivalent to a multiple of the distance between adjacent TEG rows and the non-linear equations are solved using Newton-Raphson method. The results showed that by decreasing the TEG leg length which in turn decreases the TEG thermal resistance, the power output of the heat exchanger increased due to the increase in the heat flow [35]. The model was validated using

experimental data for bismuth telluride TEG modules integrated in a counter-flow heat exchanger with hot water and cooling air channels [36].

Crane et al. [36] studied the optimization of cross flow heat exchangers with integrated TEGs for waste heat recovery applications with focus on optimizing the heat exchanger design using the model described in [35]. The study also included the TEG geometry to maximize the net power output and included losses due to pressure drop. The study focused on relatively small TEG leg length to avoid causing a significant drop in the heat transferred through the heat exchanger when integrating TEGs in the design.

Crane et al. [37] investigated the performance of a flat plate heat exchanger assembly for waste heat recovery with integrating 60 high power density bismuth telluride TEGs, connected electrically in series-parallel arrangement. The heat source was organic oil and heat sink a water/ethylene glycol mixture with flow rates of 30.3 and 8.85 liters per minute respectively with maximum temperature difference of 205 °C. High power density was achieved using a novel TEG and Y-shaped conductors design with small TEG elements leg length, large cross sectional area and low electrical contact resistance as discussed by Crane and Bell in [38]. By using this design, the TEG thermal and electrical resistances were decreased which increased the heat and current flow through the TEGs and hence increasing their power density. A maximum power output of 130 W for one row/layer was achieved at the maximum temperature difference with voltage output of approximately 6.5 V and current of 20 A [37]. However, the device efficiency results were not included.

Kumar et al. [39] developed a numerical model for thermoelectric generators in a heat exchanger for automotive waste heat recovery. The heat exchanger was a parallel plate-fin design for the exhaust side with skutterudite TEG modules. The flow domain was discretized along the exhaust flow direction. The temperature dependent thermoelectric properties were averaged over the junctions temperatures neglecting Thomson effect, and the model equations are then solved iteratively. The model results showed an output of 553.4 W can be generated when the exhaust gas flow rate is equal to 0.035 kg/s and temperature of 550 °C. The study did not include the conduction in the heat exchanger walls, as the heat transfer was modelled as one dimensional thermal network, which would have a significant impact on the temperature distribution in the direction of gas flow. The TEG effective electrical internal resistance, described in eqn.(2.18), was not considered in the

external load matching which could lead to inaccurate results as discussed by Freunek et al. [31]. Moreover, the electrical contact resistance was neglected.

The influence of the TEGs geometry was investigated by Kumar et al. [40] using the developed numerical model [39] on the performance of the heat exchanger. By keeping the material volume at 0.0036 m^3, for the same inlet flow conditions, and by varying the TEG dimensions, the results of the parametric analysis showed that TEGs, with larger cross sectional area and shorter leg length, can generate higher power output [40] which is a similar result to [38].

Hendricks et al. [1] studied TEG and heat exchanger integration design optimization with the goal to identify the optimum hot and cold side temperatures to maximize power output or efficiency for specific heat source and sink temperatures. The study also showed similar results to Freunek et al. [31] for external load matching for maximum power and maximum efficiency of TEG modules integrated in a heat exchanger as shown in eqn. (2.18). The matched load resistance at maximum power is a function the TEG temperature difference variation with the external load as result of the current flow, as well as the TEG material electrical resistance.

As a result of large temperature differentials in thermoelectric waste heat recovery devices, Hendricks et al. [1] introduced a "dual-sectioned TE design", shown in Fig.(2.7). The thermoelectric heat exchanger is split into sections where an optimized TEG dimensions are selected based on the temperatures of the section to maximize the output of each individual section. The study suggested that, as the temperature drops axially downstream of the high temperature section, the TEG elements should be thinner due to lower temperature gradients.

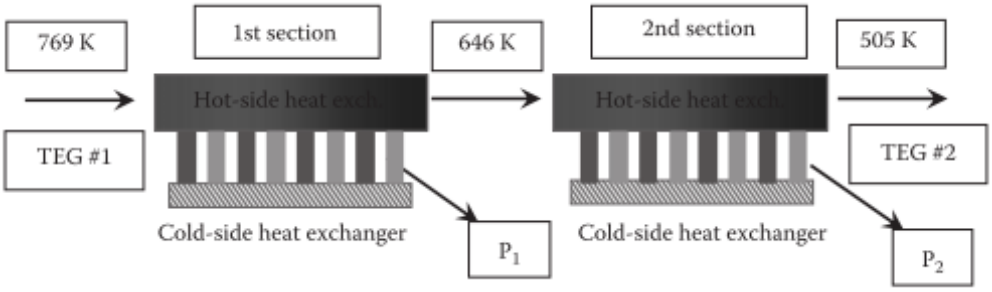

Fig.(2.7) – Schematic for dual-sectioned TE design [1]

For hot-side heat exchanger design of fixed thermal conductance, the TEGs dimensions of each section was optimized to maximize the total power output, starting with the upstream section as it

affects the gas inlet temperature of the following section downstream [1]. However, the study did not include the effect of the electrical connection, series or parallel, between TEGs in each section as well as other possible interactions as heat conduction through the heat exchanger structure.

Meng et al. [41] investigated the optimization of TEGs for automobile exhaust waste heat recovery considering the temperature variation along the flow direction in the exhaust and coolant channels, the TEG unit comprised of P and N legs of 0.5 x 0.5 mm (L x W) area and 1.2 mm leg length with spacing of 0.2 mm between legs. The material properties was assumed constant with temperature, the TEG module performance was calculated using a numerical model for different values of current and compared for different number of units per module.

By increasing the number of units in the exhaust direction, the total power output increased up to an optimum of 16 units then decreased, the power output of individual units in the module was found to decrease by increasing the number of units per module. This is due to lateral or axial heat conduction in the exhaust channel wall which caused the hot side temperature of the upstream units to drop as more units are added downstream as a result of the drop in the exhaust temperature along the direction of flow [41]. However the performance was not investigated in case of isolating the TEG units to impede the axial heat component.

The optimization of number of TEG units was done for a fixed length of the exhaust channel and fixed spacing between legs, the total power output was found to increase as the number of units increased, i.e. as TEG thickness L decreased, which means higher power output can be achieved for lower volume of material [41]. However, the increase in the power output would be limited by the electrical contact resistance, which will increase as the number of units increases, an important parameter not considered.

2.4.3. Summary of TEG modelling methodologies in a heat exchanger

Table (2.1) provides a summary of different modelling techniques that have been used in several studies of flat TEGs integrated in heat exchangers. It describes all model components for the TEGs and the heat exchanger, the simplifying assumptions and the solution technique as well as experimental results. In addition, the key results are summarized, showing the effect of different TEG design parameters included in the study on performance.

Table 2.1 – Summary of modelling methodologies of TEG integrated in exchanger and the effect of the TEG design on performance.

Author	TEG Model		Heat Exchanger Model			Solution Technique	Study Parameters	Experi-mental Results	Remarks
	Modelling Technique	Simplifying Assumptions	H.Ex. Model	Heat Source	Heat Sink				
Henderson 1979 [27]	Ioffe CPM [19]	▪ No Thomson effect. ▪ No elec. contact.	Flow convection	Water at 25 °C	Water at 5 °C	Numerical solution	TEG Leg Length	No	Maximum power is achieved when ΔT_{TEG} is approx. equal to $0.5\ \Delta T_{Total}$
Stevens 2001 [11]	First Level Model [28]	▪ No Peltier & Thomson effect. ▪ No Joule heating. ▪ No elec. contact.	Constant Thermal Resistance	Constant Temp.	Constant Temp.	Analytical	TEG Thermal Resistance	No	Similar results to Henderson [27]
Min 1992 [4]	First Level Model [28] ▪ Elec. contact.	▪ No Peltier & Thomson effect. ▪ No Joule heating.	Constant Thermal Contact Resistance	Constant Temp. 120 °C	Constant Temp. 20 °C	Analytical	TEG Leg Length	$P \sim L_{TEG}$	Power output increased by 48% when the leg length decreased by 55%
Rowe 1998 [6]	First Level Model [28] ▪ Elec. contact.	▪ No Peltier & Thomson effect. ▪ No Joule heating.	Constant Thermal Contact Resistance	Constant Temp.	Constant Temp.	Analytical	TEG Leg Length and Spacing	$P \sim L_{TEG}$ $P \sim A_{TEG}$	Power output increased by decreasing the TEG leg length and the spacing between elements
Glatz 2006 [28]	First Level Model [28] / Ioffe CPM [19]	▪ No Thomson effect. ▪ No elec. contact.	Constant Thermal Resistance	Constant Temp.	Constant Temp.	Analytical as [32]	TEG Leg Length	$P \sim \Delta T$ to validate model	Deviation in optimum leg length and max. power calculations due to Peltier and Joule heating
Freunek 2009 [31]	Ioffe CPM [19] ▪ Constant Thomson Coeff. ▪ Elec. contact.	▪ Thomson effect was neglected to simplify solution	Constant Thermal Resistance	Constant Temp.	Constant Temp.	Analytical, neglecting high order terms [30]	TEG Leg Length	$P \sim \Delta T$ to validate model	Max. power occurs when external load resistance matches the TEG effective elec. resistance
Brownell 2014 [34]	Ioffe CPM [19] ▪ Elec. contact.	▪ No Thomson effect. ▪ Constant R_L.	Constant Thermal Resistance	Constant Temp. 100 °C	Constant Temp. 20 °C	Numerical Solution	TEG Leg Length & No. of Elements	No	Power was maximized at certain TEG leg length and number of elements
Crane 2001 [35]	Ioffe CPM [19] ▪ Elec. contact.	▪ No Thomson effect. ▪ Constant R_L.	Flow over plate fins / Turbulent Pipe flow	Engine coolant 110 °C	Air 37 °C	Newton Raphson method	TEG Leg Length & Coolant flow rate	No	Power output increased by decreasing the leg length due to increased heat flow.

	▪ Temp. dependent TE properties.								
Kumar 2013 [39], [40]	Ioffe CPM [19] ▪ Temp. dependent TE properties.	▪ No Thomson effect. ▪ No elec. contact. ▪ $R_L = r_{TEG}$	Flow over plate fins / Coolant flow	Exhaust 550 °C	Engine coolant	Iterative method	Exhaust flow rate	No	At a constant material volume, power output increased by increasing the leg C.S. area and decrease its length
Meng 2016 [41]	3D Model [42]	▪ No Thomson effect (constant TE properties) ▪ No elec. contact.	Parallel / Counter flow	Exhaust 500 °C	Coolant 27 °C	Iterative method	No. of Elements under constant vol. / spacing constraints	No	For fixed total length and by increasing the no. of elements, power output increased under constant spacing constraint

2.5. Research studies of cylindrical TEG geometries

Flat TEG geometry offers compact rectangular module designs with equal surface areas for the hot and cold sides. Thus, it often requires tailored heat transfer surface designs with large surface areas and to ensure uniform temperature distribution on the module surface. This is particularly important in applications of exhaust gases with relatively low flow rates. Studies [37], [38] considered an alternative TEG couple design with Y-shaped copper conductors to be fitted to cylindrical pipes. However this design requires bulky machined conductors, with low electrical and thermal resistances to provide the uniform heat distribution with low temperature drop, which might lead to increased device cost and complex heat exchanger design. For common heat sources with cylindrical geometries as pipes in heat exchangers, TEG modules with cylindrical geometries can be easier to implement when compared to flat geometry. Different cylindrical TEG designs were adopted in literature; annular ring-structured design with π-shaped conductors [12]–[18] and another annular design with angular TEG elements [43], [44]. These designs will be discussed in details in this section.

Min and Rowe [12] first introduced a full ring-structured design for annular TEG modules consisting of coaxially arranged P and N-type rings which are electrically connected in series using copper rings. The TEG rings dimensions are 14 mm, 6.4 mm and 2 mm for the outer diameter, inner diameter and thickness (t) respectively. The ring arrangement forms a tube with hot water flow in the inner annulus as heat source. The assembly was immersed in a cold water tank which acted as the heat sink at the TEG outer surface. The temperature difference was measured using thermocouples located at the TEG surfaces.

The power output was measured at different temperature differences up to 70 K and compared against a simplified model for constant surface temperatures assuming constant thermoelectric properties with temperature, radial flow of heat and current and negligible electrical contact resistance. A significant deviation between the model and experimental results was reported due to experimental error in temperature and power measurements and short circuit through water, anisotropic thermoelectric properties and the poor quality of contacts [12].

In the analysis shown in [12], the electrical contact resistance, which increases as the contact area between the conductor and TEG material decreases, was neglected in the simplified model which

might have a major impact on the predicted power output results. This is particularly apparent due to the relatively small area of contact for the current flow between the ring thermo-elements and the copper conductors as shown in Fig.(2.8). In addition, it was reported that there was poor electrical contact between the TEG elements and the conductor rings. The assumption of radial flow of current and heat in this design might be inaccurate due to the conductor placement, shown in Fig.(2.8). It would have a two dimensional effect on the current flow as well as the heat bypass through the conductors to the sides of the rings.

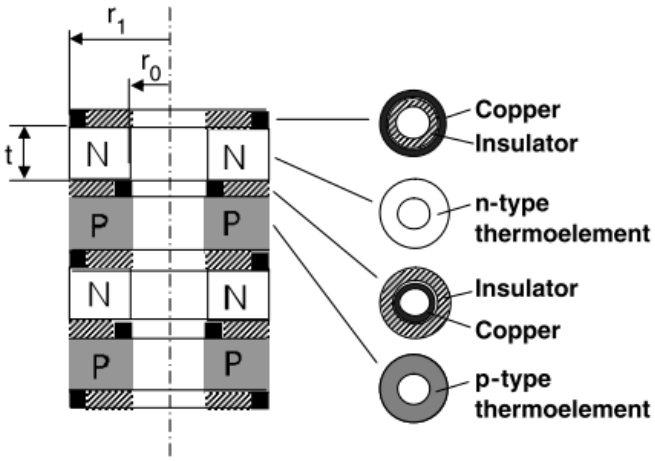

Fig.(2.8) – Section view of the annular TEG modules used by Min and Rowe showing the copper conductors placement in between the rings [12]

Bauknecht et al. [13] studied the effect of non-uniform heat flux on the circumference of annular TEGs due to asymmetric exhaust gas flow patterns for automotive waste heat recovery applications. The study used a similar annular or washer design to the full ring module design introduced in [12] with different electrical conductor design. In Bauknecht's design, the conductors are metal tubes directly attached to the TEG inner and outer surfaces. The TEG rings are incased between outer and inner pipes with heat supplied by exhaust gas flow over the outer pipe circumference and absorbed using coolant flow through the inner pipe. The performance was simulated, at constant surface temperature profiles along the circumference, using a 3D model using commercial software that incorporates temperature dependent thermoelectric properties. The results showed that the inhomogeneity in temperature along the TEG outer circumference up to 300 K can cause the efficiency to drop to 4.75% compared to 5.1% for the homogeneous case.

This is due to the volume averaged deviation in angle of the electric current flow density vector from the radial direction in case of homogeneous temperature distribution [13].

Schmitz [14] studied manufacturing of annular TEG modules made of lead telluride using spark plasma sintering (SPS), with a full ring design similar to [12] but using cylindrical conductors as shown in Fig.(2.9). The electrical conductors are directly attached to the TEG inner and outer surfaces. The rings dimensions are 14.3 mm, 9.3 mm and 1 mm for the outer diameter, inner diameter and thickness (t) respectively, the conductors are designed to counteract the mechanical stresses due to thermal expansion by providing tensile and compressive stresses on the TEG outer and inner surfaces. The outer surface was chosen for heat transfer from exhaust gas due to the larger surface area compared to the inner surface which is used as heat sink using the liquid coolant. A module consisting of four annular TEG couples was produced but the performance was not investigated and high electrical resistance was reported due to poor electrical contacts resulted from the assembly process.

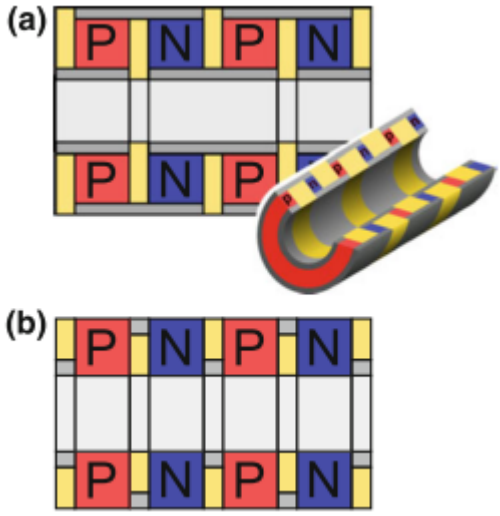

Fig.(2.9) – Schmitz A. compared two annular TEG module designs: a) Cylindrical conductors – b) Ring conductors [12] used by Min G. and Rowe D. [14]

Takahashi et al. [15] introduced a tubular design for a TEG with tilted layers of bismuth telluride and nickel for heat exchangers in waste heat recovery applications, the device uses a traverse thermoelectric design manufactured by solder-pasting of the thermoelectric material and metal creating a tubular module using SPS with 14 mm and 10 mm outer and inner diameters. Hot water

of temperature 95 °C flows through the tube and cold water at 10 °C flows on the outside surface in a shell and tube heat exchanger design with flow rate of 20 liter per minute for both streams. A maximum power output of 2.7 W was generated at low voltage of approximately 0.12 V and high current of 22 A due to the low internal resistance of the module (0.0045 ohms).

The design offered a very high thermal conductance, which is suitable for heat exchangers in waste heat recovery, and high volume to power density compared to conventional annular TEG designs. The device efficiency was 0.2 % due to the low value of ZT (0.144) as the design uses nickel metal for N-type elements. The device is capable of achieving similar power density as conventional devices but at a lower efficiency requiring heat flow an order of magnitude higher [15].

Sakai et al. [16] manufactured an annular TEG π-shaped module, as shown in Fig.(2.9 – a), using a design similar to Schmitz [14] made of 51 couples of N-type and P-type bismuth telluride using SPS with outer diameter of 14.7 mm, inner diameter of 9.3 mm and 1 mm thickness. The device had an internal resistance value of 0.114 ohms which 54% higher than calculated with estimated high electrical contact resistance of 1.1×10^{-7}ohm.m^2. The performance was tested under same flow temperatures as Takahashi et al. [15] and flow rates of 5 liter per minute. The test resulted in a maximum power of 4.8 W at voltage approximately 0.75 V and 6.4 A achieving a power density of 0.9 kW per unit transfer surface area at 85 K temperature difference. The results also showed that the electrical contact resistance caused the power output to decrease by 36% from the calculated value.

Other researchers [17], [18] reported some challenges facing the annular ring design. The challenges include cracking of the TEG material during operation at temperatures 400 K at the outer surface and 800 K at the inner surface due to thermal stresses which caused severe tensile stresses inside the material [17] and cracking of the TEG rings during manufacturing and operation due to the material brittleness [18].

Kyono et al. [43] studied another cylindrical design for TEG modules, similar to Shen's [44] shown in Fig.(2.10), for steam power plant condensers. The design consists of angular P and N couples arranged around the coolant pipe circumference and vapor condensation on the outer surface providing the temperature difference for power generation. The TEG performance was modelled using simplified analysis neglecting Peltier and Joule heating through the TEG in heat flow calculations and neglecting any thermal or electrical contact resistance. The total power output and

the condenser size were investigated under the effect of module length (l) under constraint of 7 °C increase in the coolant temperature and full condensation of steam.

The results showed that by increasing the module length (l), the total power reaches a theoretical maximum of 200 kW, however the size of condenser, i.e. the condenser pipe length (L), has to increase in order to achieve full steam condensation [43]. The effect of Peltier heat, which decreases the TEG thermal resistance, was not considered in this study which would have led to a smaller condenser size due to increases heat flow.

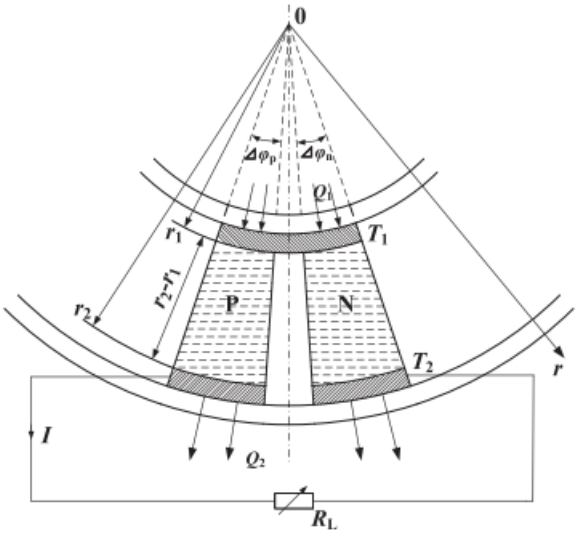

Fig.(2.10) – Annular TEGs design with angular legs operating between constant temperatures heat source and sink [44]

Shen et al. [44] presented a theoretical study of the performance of an annular TEG design with couples consisting of angular P and N legs arranged along the circumference of cylindrical heat source and sink at constant temperatures. The study introduced a one-dimensional steady state model for TEGs in cylindrical coordinates, for constant thermoelectric properties with temperature, including Joule heating and Peltier effect into the analysis. It was shown that the equations for heat transfer on the annular TEG hot and cold sides, power output and efficiency are the same as flat TEGs.

The performance of annular TEGs was compared with flat TEGs using a non-dimensional analysis in which an annular TEG power output is compared to a reference flat TEG with thermal

conductance (K_o) and internal resistance (R_o), the external load resistance was chosen to be a multiplier of the reference internal resistance, which is equal to (R_L/R_o). The analysis was done for a range of diameter ratios from 0 to 4, noting that at diameter ratio equal to 1, infinite inner and outer diameters are assumed and the annular TEG performs as a reference flat TEG fitted in between the source and the sink. By varying the annular TEG diameter ratio, the dimensionless power output was found to be maximum at diameter ratio equals to 1 which indicates the performance of the flat TEG. Also the efficiency was found to be largely dependent on the diameter ratio for different (R_L/R_o) [44]. These findings are inconsistent with Ioffe et al. [20], Min and Rowe [12] and other studies discussed in [19] as the efficiency is shown to be independent of the TEGs shape for constant thermoelectric properties. Upon review, this discrepancy is due to Shen impractical treatment of the external load matching ratio as shown in the following analysis.

The maximum efficiency is a function of the load ratio and the material figure of merit (ZT) [20], [25], for constant load ratio and figure of merit, the efficiency should not depend on the TEG dimensions which contradicts with the results of Ioffe [20] for the relation of efficiency shown in eqn.(2.8). By replacing (R_L/R_o) with ($\frac{R_L}{R}\times\frac{R}{R_o}$) and keeping the load ratio (R_L/R) instead of (R_L/R_o) in the Shen's efficiency relation [44] as follows:

$$\eta = \frac{2(ZT)(\theta-1)\left(\frac{R_L}{R}\times\frac{R}{R_o}\right)\left(\frac{R}{R_o}\right)}{(\theta+1)\left[\left(\frac{R_L}{R}\times\frac{R}{R_o}\right)+\left(\frac{R}{R_o}\right)\right]^2+2\theta(ZT)\left(\frac{R}{R_o}\right)\left[\left(\frac{R_L}{R}\times\frac{R}{R_o}\right)+\left(\frac{R}{R_o}\right)\right]-(ZT)(\theta-1)\left(\frac{R}{R_o}\right)^2} \quad (2.20)$$

By simplifying eqn.(2.20):

$$\eta = \frac{2(ZT)(\theta-1)\left(\frac{R_L}{R}\right)}{(\theta+1)\left[\left(\frac{R_L}{R}\right)+1\right]^2+2\theta(ZT)\left[\left(\frac{R_L}{R}\right)+1\right]-(ZT)(\theta-1)} \quad (2.21)$$

The efficiency was found to be independent of the TEG dimensions as shown in eqn.(2.21). The improper constant load ratio (R_L/R_o) used by Shen [44] led to the conclusion that flat TEGs outperform annular TEGs and the latter need more attention regarding the external load ratio [44]. This conclusion is inaccurate as the external load (R_L) should be kept constant with respect to the annular TEG internal resistance (R) not the reference resistance (R_o) as the ratio (R/R_o) is a function of the diameter ratio. The variation of (R/R_o) with the diameter ratio in the analysis [44] caused the annular TEG internal resistance (R) to change compared to the external load (R_L).

By comparing the ring design of annular TEGs [12]–[18] shown in Fig.(2.9) with the angular design [43], [44] shown in Fig.(2.10), the ring modules are preferred in the current study as they offer several advantages over the angular design. While both module designs have a cylindrical shape that enables them to be fitted around pipes, higher packing density, defined as the area of TEG elements footprint to the total heat transfer surface area available [45], can be achieved using the ring design. This is due to the gaps between elements in the angular design used for spacing along the circumference, typically filled with insulating material, which are eliminated in the ring design. Higher packing density can increase the device heat flow and hence its power density which is more suitable for a heat exchanger. The ring-shaped elements also provide a simpler design with fewer number of parts per module, when compared to the angular design, which leads to more cost effective manufacturing and assembling processes.

Table (2.2) shows a summary for several studies of ring-shaped annular TEGs in literature. It describes the TEG design including the thermoelectric material used, the heat source and sink characteristics and the TEG dimensions as the outer and inner diameters and thickness as well as the conductor design. The output of the TEGs is also listed including the maximum power and its characteristics of voltage and current.

Table 2.2 – Summary of studies on annular TEGs including design description and output characteristics.

Authors	Study Objective	Type of TE material	Heat Source	Heat Sink	TEG Module Design				Max. Power (P_{max})	Output Characteristics		Remarks
					Outer / Inner Diameter	P-Type / N-Type Thickness	No.of Cou-ples	Conductor Type		Voltage at P_{max}	Current at P_{max}	
Min 2007 [12]	Module Assembly / Performance Testing	Bi_2Te_3	Hot Water on inner surface	Cold Water on outer surface	14 mm / 6.4 mm	2 mm / 2 mm	2	Copper rings 1mm thick [π-shaped design]	33 mW at 70 K	×	×	Reduced power due to poor elec. contact and error in measurements
Schmitz 2013 [14]	Module Assembly	PbTe	Exhaust on outer surface	Coolant on inner surface	14.3 mm / 9.3 mm	1 mm / 1 mm	4	Nickel Cylinders [π-shaped design]	N/A	N/A	N/A	High internal elec. resistance due to poor elec. contact
Takahashi 2013 [15]	Module Assembly / Performance Testing	Bi_2Te_3 / Nickel	Hot Water on inner surface	Cold Water on outer surface	14 mm / 10 mm	1.3 mm / 1.3 mm	×	N/A [Transverse design]	2.7 W at 85 K	0.12 V	22 A	Low voltage / high current output characteristics
Sakai 2015 [16]	Module Assembly / Performance Testing	Bi_2Te_3	Hot Water on inner surface	Cold Water on outer surface	14.7 mm / 9.3 mm	1 mm / 1 mm	51	Cylinders [π-shaped design]	4.8 W at 85 K	0.75 V	6.4 A	The power output decreased by 36% due elec. contact resistance
Mansouri 2016[17]	Module Assembly / Performance Testing	Skutter-udites	Exhaust on inner surface	Coolant on outer surface	×	×	×	Cylinders [π-shaped design]	×	×	×	Failure due to cracking as a result of thermal stresses

[×] Not reported by the authors.

2.6. Summary

In this study for the next generation TEG POWER devices with integrated annular TEGs, the performance of the multi-row heat exchanger is investigated. Annular ring-structured TEG modules with π-shaped conductors, similar to Schmitz design [14], are modelled using Ioffe constant properties model (CPM) with taking into account the electrical resistance of the contacts and the conductors. The thermal resistance of the heat exchanger components are considered and the resulting set of equations are solved numerically in a developed multi-row heat exchanger model. Although previous studies [12]–[18] have considered an annular TEG designs, the performance of annular TEGs in a multi-row heat exchanger system and the impact of the annular TEG dimensions on the power output have not been investigated. In addition, annular TEGs showed unfavorable power output characteristics, i.e. lower voltage / higher current output, in previous studies, however the improvement of the annular TEG power characteristics through the design dimensions has not been studied. As a result, the power output is calculated in parametric analysis to find the suitable TEG dimensions to maximize power under a certain current limit to increase the heat exchanger power density while maintaining an improved power output characteristics.

Chapter 3

TEG Heat Exchanger Modelling

3.1. Introduction

In this chapter, modelling of a heat exchanger with integrated annular TEGs will be discussed. Different modelling techniques will be presented to study the performance of annular TEGs and the effect of simplifying assumptions of the heat exchanger and the TEG models on calculations. Simple modelling approaches will be discussed to investigate the effect of thermal resistances of a heat exchanger design on maximum power point calculations. A developed numerical model for single row and multi-row configurations will be presented to study the performance of annular TEGs in the heat exchanger design of the next generation of TEG POWER systems. In addition, the verification of the numerical model methodology using an ANSYS model will be discussed.

3.2. Modelling of TEGs in heat exchangers

In a heat exchanger with integrated TEGs, the performance depends on several parameters including heat exchanger design and operation parameters, TEGs design parameters, material properties and electrical load characteristics. The thermoelectric equations are studied to model the coupling between the heat transfer and the thermoelectric effects in TEGs integrated in a heat exchanger that uses exhaust gas flow as a source of heat and water flow as a heat sink

3.2.1. Model description

In the thermal network shown in Fig.(3.1), a TEG, operating between a hot-side temperature ($T_{T,H}$) and a cold-side temperature ($T_{T,C}$), has a thermal resistance ($R_{th,TEG}$), an electrical resistance (r_{TEG}) and Seebeck coefficient (α). The TEG is integrated in a heat exchanger of thermal resistance ($R_{th,H}$) for exhaust gas hot-side with inlet temperature ($T_{g,in}$), outlet temperature ($T_{g,out}$) and gas

mass flow rate ($\dot{m}_{gas}$), and thermal resistance ($R_{th,C}$) for water cold-side with inlet temperature ($T_{w,in}$), outlet temperature ($T_{w,out}$) and water mass flow rate ($\dot{m}_{water}$).

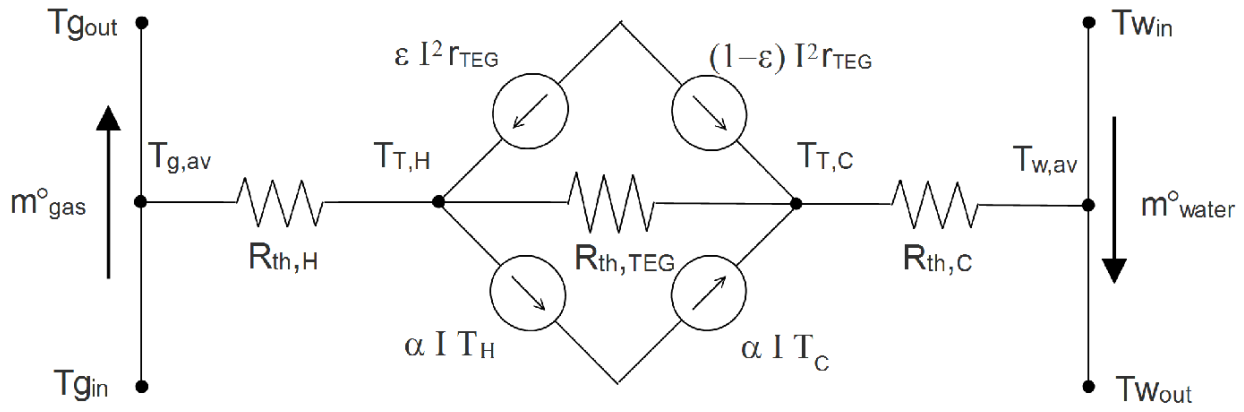

Fig.(3.1) – Thermal network for a TEG in a heat exchanger.

For fixed inlet temperatures of gas and water, the temperature difference across the TEG is a function of the heat exchanger thermal resistances and flow rates, the TEG thermal and electrical resistances and the current flow which depends on the external electrical load characteristics. The heat transferred through the TEG consists of heat conduction component represented in the material thermal conductivity, Peltier heat component represented in the material Seebeck coefficient and the current flow, and Joule heating component represented in the material electrical resistivity and the current flow which affects the heat flow between the hot-side and cold-side by the ratio (ϵ) depending on the geometry and dimensions.

The heat flow input (Q_H) to the TEG hot-side and the heat flow output (Q_C) from the TEG cold-side can be expressed using Ioffe constant properties model [19], [20] as described in Section (2.3):

$$Q_H = K_{TEG}\left(T_{T,H} - T_{T,C}\right) + \alpha\, I\, T_{T,H} - \epsilon\, I^2 r_{TEG} \quad (3.1)$$

$$Q_C = K_{TEG}\left(T_{T,H} - T_{T,C}\right) + \alpha\, I\, T_{T,C} + (1-\epsilon)\, I^2 r_{TEG} \quad (3.2)$$

$$\alpha = |\alpha_P| + |\alpha_N| \quad (3.3)$$

Where K is the thermal conductance and it is equal to ($1/R_{th}$), (ϵ) is the ratio of Joule heat distribution between the hot-side and cold-side of the TEG, α_P and α_N are P-type and N-type TEGs

Seebeck coefficients [31]. The current flow through the TEG, is a function of the temperature difference and the electrical load ratio (m_L) which is the ratio of the load resistance (R_L) and the TEG electrical resistance (r_{TEG}), can be expressed as:

$$I = \frac{\alpha\,(T_{T,H} - T_{T,C})}{r_{TEG}\,(m_L + 1)} \qquad (3.4)$$

By taking the arithmetic average between the inlet and outlet temperatures of water and gas, the heat flow input (Q_H) to the TEG hot-side and the heat flow output (Q_C) from the TEG cold-side can also be expressed in terms of the heat exchanger thermal resistances and flow rates as:

$$Q_H = \dot{m}_g\, C_{P,g}\left(T_{g,in} - T_{g,out}\right) = K_H\left(\frac{T_{g,in} + T_{g,out}}{2} - T_{T,H}\right) \qquad (3.5)$$

$$Q_C = \dot{m}_w\, C_w\left(T_{w,out} - T_{w,in}\right) = K_C\left(T_{T,C} - \frac{T_{w,in} + T_{w,out}}{2}\right) \qquad (3.6)$$

Then, the power output can be expressed in terms of the TEG temperature difference and the load ratio (m) as:

$$P = \frac{\alpha^2\left(T_{T,H} - T_{T,C}\right)^2}{r_{TEG}} \times \frac{m_L}{(m_L + 1)^2} \qquad (3.7)$$

For constant hot-side and cold-side temperatures of the TEG, the maximum power occurs at matched load ($m_L = 1$) where the load resistance (R_L) is equal to the TEG electrical resistance (r_{TEG}). Considering the case of TEG integrated in a heat exchanger, the TEG temperatures are a function of the current flow which means by changing the load (R_L) on the TEG, the temperatures across the TEG change accordingly leading to a maximum power at ($m_L > 1$) [1], [31]. This is due to the effect of the thermal resistances of the heat exchanger and is discussed in detail later in this chapter. The TEG performance can be investigated by solving for all temperatures in the thermal network shown in Fig.(3.1) for fixed inlet temperatures of gas and water using a set of non-linear equations shown in eqns.(3.1 – 3.7).

3.2.2. Modelling equations for annular geometry of TEGs

For fixed heat exchanger design and operating conditions, the power output of integrated annular TEGs is influenced by their dimensions. They can affect the TEGs thermal and electrical

resistances which in turn change the TEG hot-side and cold-side temperatures as well as the gas and water temperature profiles through the heat exchanger.

Considering the annular geometry of the TEGs, the modelling equations for the thermal resistance for heat conduction and electrical resistance of current flow for Peltier and Joule heat are studied for cylindrical coordinates. The relationship between the TEG geometry dimensions and the material properties are investigated and their effect on the power output and efficiency is discussed.

Fig.(3.2) shows an annular TEG couple integrated in a heat exchanger, the couple consists of P and N ring-shaped TEG thermo-elements, with cylindrical conductors similar to the design adopted by Schmitz et al. [14] shown in Fig.(2.9a). The thermo-elements are connected in series as shown in a cross section in Fig.(2.2). The spacing gap between elements are filled with an insulating material. To model an annular TEG couple, one dimensional radial flow of heat and current is assumed through the TEG with uniform outer and inner surface temperatures. Convection or radiation heat transfer through the spacing gaps was neglected due to the presence of an insulating material and are not included in the analysis.

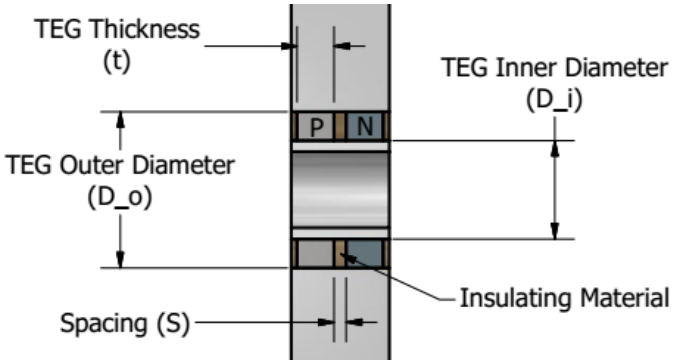

Fig.(3.2) – Annular TEG couple integrated in a heat exchanger element.

3.2.2.1. Heat conduction through annular TEGs

The conduction through annular TEGs can be evaluated using the steady state heat conduction equation for the irreversible heat flow [3] that takes into account the heat conduction and Joule heat generation components within the TEG, it can be written as:

$$\nabla(\lambda \nabla T) = -T\frac{d\alpha}{dT} J \nabla T - \rho J^2 \quad (3.8)$$

For steady one dimensional heat flow in cylindrical coordinates, and constant average thermal conductivity and Seebeck coefficient with temperature, the equation can be written as:

$$\frac{\lambda}{\tilde{r}}\frac{\partial}{\partial \tilde{r}}\left(\tilde{r}\frac{\partial T}{\partial \tilde{r}}\right) = -\rho J^2 = -q''' \quad (3.9)$$

Where (J) is the current density, (ρ) is the material electrical resistivity and (q''') is the heat generated within the TEG per unit volume. Eqn.(3.9) was solved by Shen et al. [44] for an annular TEG with the following boundary conditions; outer surface at temperature ($T_{T,o}$) and diameter (D_o), and inner surface at temperature ($T_{T,i}$) and diameter (D_i) to obtain the temperature distribution in the radial direction. The heat transfer rate can calculated at the TEG outer and inner surfaces using:

$$Q_r = -\lambda A_r \left(\frac{\partial T}{\partial \tilde{r}}\right)_r \quad (3.10)$$

The Joule heat distribution ratio (ϵ) is used to calculate the effect of Joule heating on the heat flow at the TEG hot and cold sides, the heat flow decreases by a value of ($\epsilon\, I^2 r_T$) at the TEG hot-side and increases by ($(1-\epsilon)\, I^2 r_T$) at the TEG cold-side as shown in eqns.(3.1 & 3.2) [20], [31]. By solving eqn.(3.10) to estimate the conduction and Joule heat components, Shen et al. [44] found that the Joule heating distribution ratio for annular TEGs is similar to ($\epsilon = 1/2$) for flat geometry of TEGs.

The thermal resistance of an annular TEG, consisting of P-type and N-type rings, can be expressed in terms of their material thermal conductivity (λ) as:

$$R_{th,TEG} = \frac{1}{2\pi t\lambda} \times \ln\left(\frac{D_o}{D_i}\right) \quad (3.11)$$

So the TEG thermal conductance (K_T) can be calculated for parallel flow of heat between the TEG rings as:

$$K_T = \frac{1}{R_{th,TEG}} = K_P + K_N = \frac{2\pi}{\ln\left(\frac{D_o}{D_i}\right)} \times \left(\lambda_p t_p + \lambda_n t_n\right) \quad (3.12)$$

The electrical resistance of the annular TEG (r_T) expressed in terms of P-type and N-type rings materials' electrical resistivity (ρ) connected electrically in series:

$$r_T = r_P + r_N = \frac{\ln(\frac{D_o}{D_i})}{2\pi} \times \left(\frac{\rho_p}{t_p} + \frac{\rho_n}{t_n}\right) \quad (3.13)$$

Where (D_o) is the outer diameter, (D_i) is the inner diameter and (t) is the TEG ring thickness as shown in Fig.(3.2).

3.2.2.2. The annular TEGs thickness ratio for maximum power and maximum efficiency configurations

The dimensions of a TEG can be optimized according to the material thermal conductivity and electrical resistivity to maximize performance. For an equal P and N leg lengths of a flat TEG, the legs cross sectional area ratios for maximum efficiency (ME) and maximum power (MP) were found to be [11], [20], [46]:

$$\left(\frac{A_p}{A_n}\right)_{ME} = \sqrt{\frac{\rho_p}{\rho_n} \times \frac{\lambda_n}{\lambda_p}} \quad (3.14)$$

$$\left(\frac{A_p}{A_n}\right)_{MP} = \sqrt{\frac{\rho_p}{\rho_n}} \quad (3.15)$$

Similarly for an annular TEG with equal P and N ring diameter ratios, the P and N rings thickness ratio can be derived for maximum efficiency and maximum power configurations. The annular TEG efficiency, for constant hot and cold side temperatures, can be expressed using eqns.(3.1 & 3.7) as:

$$\eta = \frac{P}{Q_H} = \frac{T_{TH} - T_{TC}}{T_{TH}} \times \frac{\frac{m_L}{m_L + 1}}{1 + \frac{K_T r_T}{\alpha^2} \times \frac{m_L + 1}{T_{TH}} - \frac{\epsilon(T_{TH} - T_{TC})}{T_{TH}(m_L + 1)}} \quad (3.16)$$

For maximum efficiency (ME) configuration, the term $(K_T r_T)$ should be minimized to find the thickness ratio (t_p/t_n) that maximizes efficiency for the same diameter ratio:

$$K_T r_T = \left(\lambda_p t_p + \lambda_n t_n\right) \times \left(\frac{\rho_p}{t_p} + \frac{\rho_n}{t_n}\right) = \lambda_p \rho_p + \lambda_n \rho_n + \lambda_p \rho_n \left(\frac{t_p}{t_n}\right) + \lambda_n \rho_p \left(\frac{t_n}{t_p}\right) \quad (3.17)$$

By differentiating eqn.(3.17), the annular TEG thickness ratio for maximum efficiency can be expressed as:

$$\left(\frac{t_p}{t_n}\right)_{ME} = \sqrt{\frac{\rho_p}{\rho_n} \times \frac{\lambda_n}{\lambda_p}} \qquad (3.18)$$

For maximum power (MP) configuration, the power can be maximized for a fixed TEG couple length ($L_C = t_n + t_p$) using eqns.(3.7 & 3.13), for constant hot and cold side temperatures and matched load ($m_L = 1$), as follows:

$$P = \frac{\alpha^2 \left(T_{T,H} - T_{T,C}\right)^2}{4\, r_{TEG}} = \frac{\alpha^2 \pi \left(T_{T,H} - T_{T,C}\right)^2}{2 \ln\left(\frac{D_o}{D_i}\right) \left(\frac{\rho_p}{t_p} + \frac{\rho_n}{L_C - t_p}\right)} \qquad (3.19)$$

To maximize the power output, the term $\left(\frac{\rho_p}{t_p} + \frac{\rho_n}{L_C - t_p}\right)$ should be minimized by differentiating with respect to (t_p). The annular TEG thickness ratio for maximum power can be expressed as:

$$\left(\frac{t_p}{t_n}\right)_{MP} = \sqrt{\frac{\rho_p}{\rho_n}} \qquad (3.20)$$

The annular TEGs thickness ratio for ME and MP configurations are similar to the legs cross sectional area ratios for flat TEGs. The thickness in an annular TEG affects the thermal and electrical resistances equally as shown in eqns.(3.11 & 3.13) since heat and current flow radially through an area controlled by the thickness for the same diameter ratio

The annular TEGs thickness ratios are calculated using eqns.(3.18 & 3.20) for maximum efficiency and maximum power, the effect of the thickness ratio on performance will be studied in Chapter (5) for annular TEGs in a heat exchanger. In addition, the effect of varying the TEGs thickness will be investigated by varying the N-type TEG thickness while the thickness ratio is kept constant and the P-type TEG changes accordingly.

3.2.3. Solution techniques

In order to obtain the surface temperatures of TEG couples arranged in a heat exchanger as described in Fig.(3.2) and evaluate their performance, the model equations will be solved using

simplified modelling techniques to obtain an analytical solution. The solution technique of a developed numerical model will also be discussed to investigate the effect of different parameters on the performance of a heat exchanger consisting of a single or multiple TEG rows.

3.2.3.1. Simplified models

Simplified analytical models are used to study the effect of changing the geometric parameters of annular TEGs on performance and investigate the effect of the heat exchanger thermal resistances on the external electrical load matching conditions at maximum power. Two approaches were implemented to simplify the analytical model solution by linearizing the model equations set using assumptions that will be discussed in this section.

First, the model was simplified using assumptions similar to the first level model [28]–[31] discussed in Section (2.4.1). This approach takes into account the heat conduction only through TEGs using the thermal resistances of a heat source, a heat sink and a TEG in a heat exchanger i.e. neglect the current flow and hence the Peltier and Joule heat effects. The average temperatures of gas and water are assumed to be constant. The heat flow, described in eqns.(3.1 & 3.2), can be rewritten as:

$$K_H\left(\overline{T_g} - T_{TH}\right) = K_T(T_{TH} - T_{TC}) \quad (3.21)$$

$$K_T(T_{TH} - T_{TC}) = K_C(T_{TC} - \overline{T}_w) \quad (3.22)$$

The temperature difference between the hot and cold sides of a TEG ($\Delta T_{TEG} = T_{TH} - T_{TC}$) can be found by solving eqn. (3.21) and (3.22).

$$\Delta T_{TEG} = T_{TH} - T_{TC} = \frac{\overline{T}_g - \overline{T}_w}{1 + K_T\, R_{th,HX}} \quad (3.23)$$

$$R_{th,HX} = R_{th,H} + R_{th,C} = \frac{1}{K_H} + \frac{1}{K_C} \quad (3.24)$$

The term ($R_{th,HX}$) is the total of thermal resistances of the heat source and sink in a heat exchanger. The power output of TEGs in heat exchanger can be calculated as follows:

$$P = \frac{\alpha^2\left(\overline{T}_g - \overline{T}_w\right)^2}{r_T} \times \frac{m_L}{(m_L + 1)^2} \times \left(\frac{1}{1 + K_T\, R_{th,HX}}\right)^2 \quad (3.25)$$

The annular TEG thermal conductance (K_T) and electrical resistance (r_T) are a function of the diameter ratio and thickness as shown in eqns.(3.12 & 3.13). By neglecting any electrical resistances of conductors and at contacts in TEG couples, the maximum power output can be achieved when TEG thermal resistance is equal to total of thermal resistances of the heat source and sink in a heat exchanger [11], [27]. This can be found by differentiating the power output in eqn.(3.25) with respect to the diameter ratio to find the condition for maximum power as:

$$K_T = \frac{1}{R_{th,TEG}} = \frac{1}{R_{th,HX}} \quad \rightarrow \therefore \quad R_{th,TEG} = R_{th,HX} = R_{th,H} + R_{th,C} \qquad (3.26)$$

Another approach was taken to consider heat conduction and Peltier effects through the TEGs and neglect the heat generation due to Joule heat effects. This was done to investigate the influence of the heat exchanger thermal resistances and Peltier heat on the external electrical load matching at maximum power. Peltier heat through the TEG is assumed to be the average ($\alpha\, I\, \bar{\bar{T}}$) between the hot and cold junctions where $\bar{\bar{T}}$ is the average temperature of the heat source and sink of TEG. The heat flow, described in eqns.(3.1 & 3.2), can be rewritten as:

$$K_H\left(\bar{T}_g - T_{TH}\right) = K_T(T_{TH} - T_{TC}) + \alpha\, I\, \bar{T} \qquad (3.27)$$

$$K_C(T_{TC} - \bar{T}_w) = K_T(T_{TH} - T_{TC}) + \alpha\, I\, \bar{\bar{T}} \qquad (3.28)$$

By solving for the temperature difference between the hot and cold sides of the TEG, the power output of TEGs in the heat exchanger was found as follows:

$$P = \frac{\alpha^2\left(\bar{T}_g - \bar{T}_w\right)^2}{r_T} \times \frac{m_L}{(m_L+1)^2} \times \left(\frac{1}{1 + K_T\, R_{th,HX} + \frac{\bar{T}\, R_{th,HX}}{(m_L+1)} \times \frac{\alpha^2}{r}} \right)^2 \qquad (3.29)$$

Differentiating the power output in eqn.(3.29) with respect to the load ratio (m_L), the maximum power was found to occur at a matched load ratio ($m_{L,Pmax}$) which is equal to:

$$m_{L,Pmax} = 1 + \frac{\alpha^2 \bar{T} R_{th,HX}}{r_T(K_T\, R_{th,HX} + 1)} \qquad (3.30)$$

The relation, described in eqn.(3.30) for ($m_{L,Pmax}$), shows the effect of the heat exchanger thermal resistance ($R_{th,HX}$) and the Peltier effects on the calculation of the matched load ratio at maximum

power. The maximum power output occurs at value of (m_L) equal to ($m_{L,Pmax}$) which is always higher than 1 for an actual case of a TEG in a heat exchanger due to Peltier heat, similar result was also found by [1], [31] as discussed in Section (2.4.1). In case of negligible heat exchanger thermal resistance ($R_{th,HX} = 0$), the matched load ratio will be equal to 1 as the TEG will be operating between constant temperatures. Using ($m_L = 1$) for a case of heat exchanger, which an assumptions often used in some models [28], [29], [39], can affect the calculations for the current and voltage at maximum power.

Using both approaches to simplify the model equations, it was shown that the TEG power output in a heat exchanger is dependent on the dimensions which affects both the thermal and electrical resistance of the TEG, as in eqn.(3.26). In addition, the maximum power output of a TEG in heat exchanger occurs at load ratio that is higher than 1 as in eqn.(3.30).

The simplified models offered a good understanding of the parameters affecting the performance, however accurate modelling of the Peltier and Joule heat through the TEG is required in order to find the dimensions of the TEG and the load ratio that maximizes the power output in a heat exchanger. The simplifying assumptions used can lead to inaccurate estimation of the TEG power output and optimum dimensions as shown in Fig.(2.4) by Freunek et al. [30].

3.2.3.2. Numerical Model:

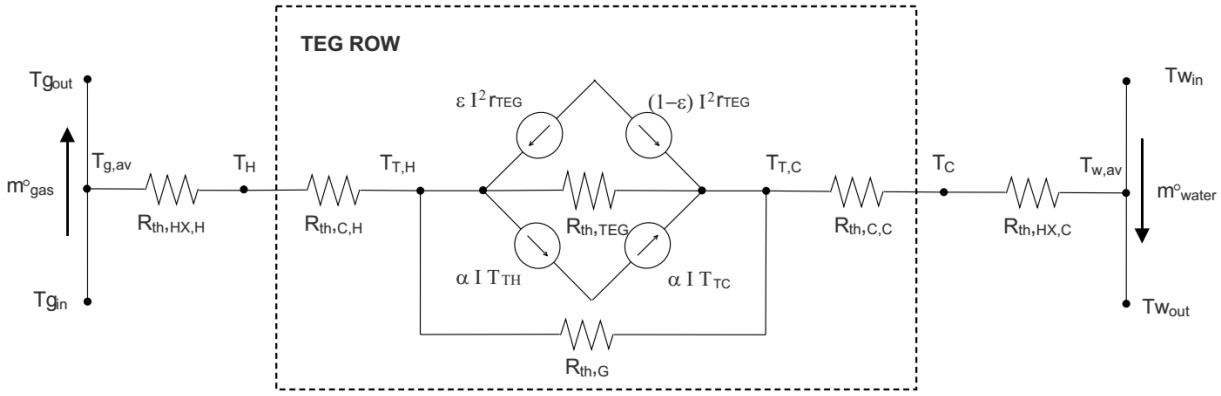

Fig.(3.3) – Thermal network for a TEG row including thermal contact resistances in a heat exchanger.

A numerical model was developed to evaluate the performance of TEGs in a single row, consisting of multiple TEG couples connected in series, integrated in a heat exchanger using a thermal network shown in Fig.(3.3). The model takes into consideration the effects of Peltier and Joule

heat, the thermal contact resistances ($R_{th,C}$) at the TEGs hot and cold sides, the gap thermal resistance ($R_{th,G}$) between TEGs due to the spacing (S) in Fig.(3.2), and the electrical contacts and conductors resistances of the TEGs.

For a single TEG row heat exchanger and for known inlet conditions of gas and water, the performance can be obtained by solving for the temperatures, for different values of current (I_m) numerically, using the equations as shown:

$$\dot{m}_g C^o_{P,g}\left(T_{g,n} - T_{g,n+1}\right) = K_{H,m}\left(\frac{T^o_{g,n} + T_{g,n+1}}{2} - T_{H,m}\right) \quad (3.31)$$

$$K_{H,m}\left(\frac{T^o_{g,n} + T_{g,n+1}}{2} - T_{H,m}\right) = K_{Ct,H,m}\left(T_{H,m} - T_{TH,m}\right) \quad (3.32)$$

$$K_{Ct,H,m}\left(T_{H,m} - T_{TH,m}\right) = K^o_{T,m}\left(T_{T,H,m} - T_{TC,m}\right) + \alpha^o_{T,m} I_m T_{T,H,m} - \epsilon\, I^2_m r^o_{mat,T,m} - I^2(r_{ct,H,T} + r_{cd,H,T}) + K_{G,m}\left(T_{T,H,m} - T_{T,C,m}\right) \quad (3.33)$$

$$K_{Ct,C,m}\left(T_{T,C,m} - T_{C,m}\right) = K^o_{T,m}\left(T_{T,H,m} - T_{TC,m}\right) + \alpha^o_{T,m} I_m T_{T,C,m} + (1-\epsilon) I^2_m r^o_{mat,T,m} + I^2(r_{ct,C,T} + r_{cd,C,T}) + K_{G,m}\left(T_{T,H,m} - T_{T,C,m}\right) \quad (3.34)$$

$$K_{C,m}\left(T_{C,m} - \frac{T^o_{w,n} + T_{w,n+1}}{2}\right) = K_{Ct,C,m}\left(T_{T,C,m} - T_{C,m}\right) \quad (3.35)$$

$$\dot{m}_w C^o_w\left(T_{w,n+1} - T_{w,n}\right) = K_{C,m}\left(T_{C,m} - \frac{T^o_{w,n} + T_{w,n+1}}{2}\right) \quad (3.36)$$

The TEG electrical resistance in eqns. (3.33, 3.34) is the summation of the TEG material, the electrical conductor resistance and the electrical contact resistance between the conductors and TEG material. It can be expressed as:

$$r^o_{T,m} = r^o_{mat,T,m} + r_{ct,T} + r_{cd,T} = \frac{\ln(\frac{D_o}{D_i})}{2\pi} \times \left(\frac{\rho^o_p}{t_p} + \frac{\rho^o_n}{t_n}\right) + 2 \times \left(\frac{R_{e,ct}}{A_{ct,H}} + \frac{R_{e,ct}}{A_{ct,C}}\right) + \rho_{cd} L_{cd}\left(\frac{1}{A_{cd,H}} + \frac{1}{A_{cd,C}}\right) \quad (3.37)$$

For a certain known value of (I_m), where (m) represents the TEG row number, the temperatures in the thermal network can be solved numerically using LU factorization method in MATLAB for known inlet conditions of gas and water to obtain initial solution to calculate the temperature

dependent properties of gas, water and TEG material that are used to calculate the terms denoted by a superscript (o).

By updating the temperature dependent properties, the temperatures are solved for iteratively until convergence is reached and the TEGs thermal performance is obtained. Since the solution is obtained for a certain known value of current (I_m), the model equations (3.31-3.36) become a set of linear algebraic equations that can be solved directly. Then the TEGs electrical performance is evaluated numerically for different values of current (I_m) using the following equations:

$$V = \alpha^o_{T,m}\left(T_{TH,m} - T_{TC,m}\right) - I_m r^o_{T,m} \qquad (3.38)$$

$$P = \alpha^o_{T,m} I_m\left(T_{TH,m} - T_{TC,m}\right) - I^2_m r^o_{T,m} \qquad (3.39)$$

Using the developed numerical model, single TEG row performance will be investigated for different TEG diameter ratios and thicknesses to determine the TEG dimensions that maximizes performance with taking into consideration all thermoelectric effects which will be discussed later in details in Chapter (5).

3.3. Verification of the numerical model results:

The numerical model results was compared against an ANSYS model for an annular TEG under the same conditions to verify the model solution for the interaction between the heat transfer and the thermoelectric effects which will further be used in a multi row heat exchanger model. An annular TEG couple is simulated using ANSYS for the comparison under the same boundary conditions. The TEG couple is operating between a heat source and a heat sink of constant temperature, as shown in Fig.(3.4), with all other surfaces insulated, negligible gap thermal resistance, negligible thermal and electrical contact resistances, and fixed TEG dimensions. Details of the ANSYS model used are presented in Appendix (C).

The heat exchanger was modelled using a fixed thermal resistances on the TEG hot and cold sides, the thermal resistances are simulated in ANSYS using cylindrical blocks of known dimensions and thermal conductivity, as shown in Fig.(3.4), similar to the numerical model inputs. The flow of gas and water is not simulated in both models and they are replaced with a fixed temperature source and sink for simplicity. Further verification of the gas and water flow modelling will be presented in Chapter (5).

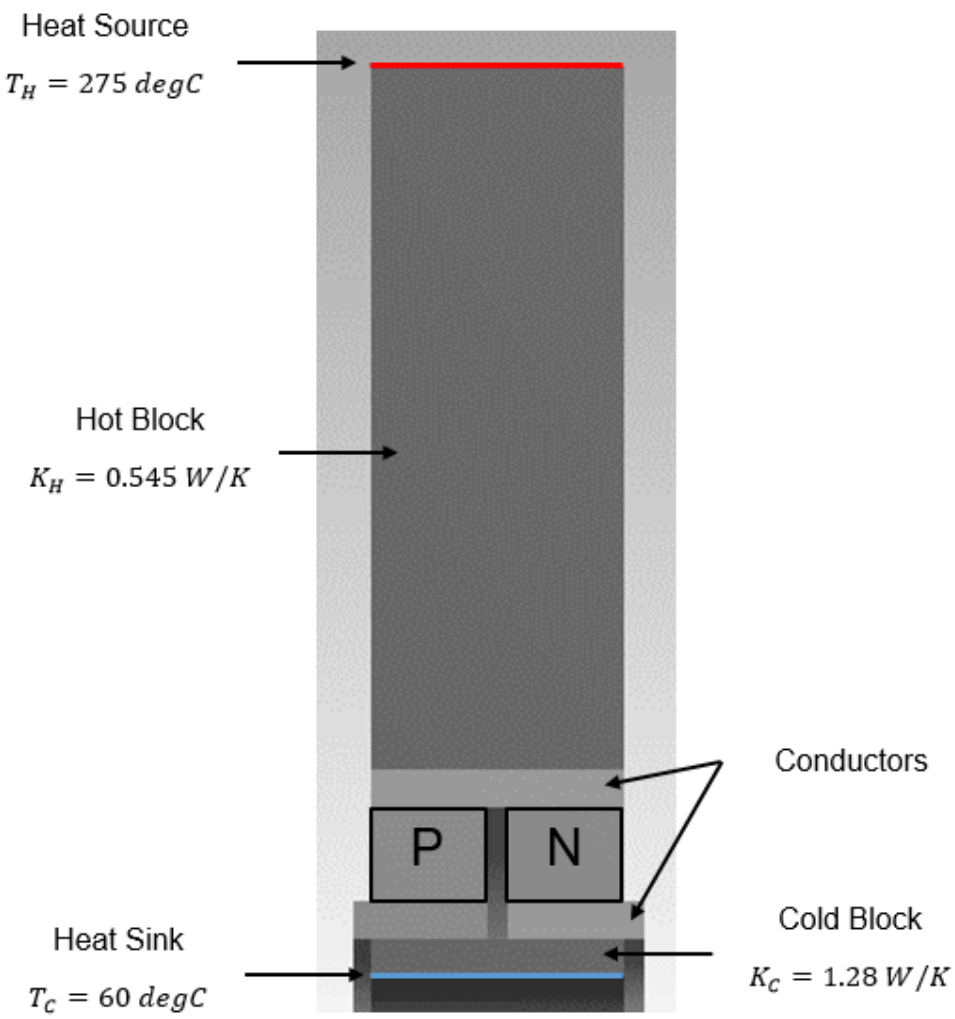

Fig.(3.4) – ANSYS model for an annular TEG couple with equivalent heat exchanger resistance and constant heat source and sink temperatures.

The performance of the TEG couple, shown in Fig.(3.4), was simulated using ANSYS under different electrical loads connected in series to the TEG couple. The couple consists of P and N materials with constant thermoelectric properties with temperature, all TEG outer surfaces are insulated including the spacing gap. The output voltage was calculated between the TEG terminals, the output current was calculated at the load and the heat flow was calculated using the heat flux and the surface area at the heat source. Finally, the power output and the efficiency was calculated and compared against the numerical model at different load resistances. The mesh independence was tested on five steps by decreasing the element size by half in each step, the results were found

to change within less than 0.6%. The element size was selected as a compromise between accuracy and computational cost.

The model geometry and boundary conditions represent a verification case study. The temperature boundary conditions and the thermal conductance of the heat exchanger components are selected based on the typical operation of TEG POWER system shown in Appendix (A). The TEG geometrical parameters were selected similar to the design used by Morsy [18], however the conductor design has been changed and the TEG thickness was set to be uniform and equal for the P and N rings. The TEG material properties was assumed constant with temperature and average values were calculated for bismuth telluride TE material [47]. The design and operating conditions are listed below:

- Operation conditions:
  Heat source temperature: $T_H = 275\ degC$.
  Heat sink temperature: $T_C = 60\ degC$.
- Design conditions:

TEGs

Design:

- Outer Diameter: $D_o = 12.7\ mm$
- Inner Diameter: $D_i = 7.9\ mm$
- Thickness: $t_p = t_n = 3\ mm$
- Spacing: $S = 0.5\ mm$

Material Properties:

- Seebeck coefficient: $|\alpha_P| = 2.37 \times 10^{-4}\ V/K$, $|\alpha_N| = 1.98 \times 10^{-4}\ V/K$
- Thermal conductivity: $\lambda_P = 1.34\ W/m.K$, $\lambda_N = 1.41\ W/m.K$
- Electrical resistivity: $\rho_P = 1.79 \times 10^{-5}\ ohm.m$, $\rho_N = 1.2 \times 10^{-5}\ ohm.m$

Heat Exchanger

Design:

- Hot-side thermal conductance: $K_H = 0.545\ W/K$
- Cold-side thermal conductance: $K_C = 1.28\ W/K$

By comparing the results of both models for power output and efficiency in Fig.(3.5), the numerical model shows a good agreement with the ANSYS model at different values of load resistance. This is because the ANSYS model was created to simulate a simple one dimensional case for the flow of heat and current through the annular TEG which can accurately be calculated using the analytical relations of the numerical model for the TEG thermal and electrical resistance. The results, shown in Fig.(3.6), for the TEG hot and cold side temperatures, show the effect of Peltier heat on the temperature difference across the TEG, the numerical model results coincides with the ANSYS results.

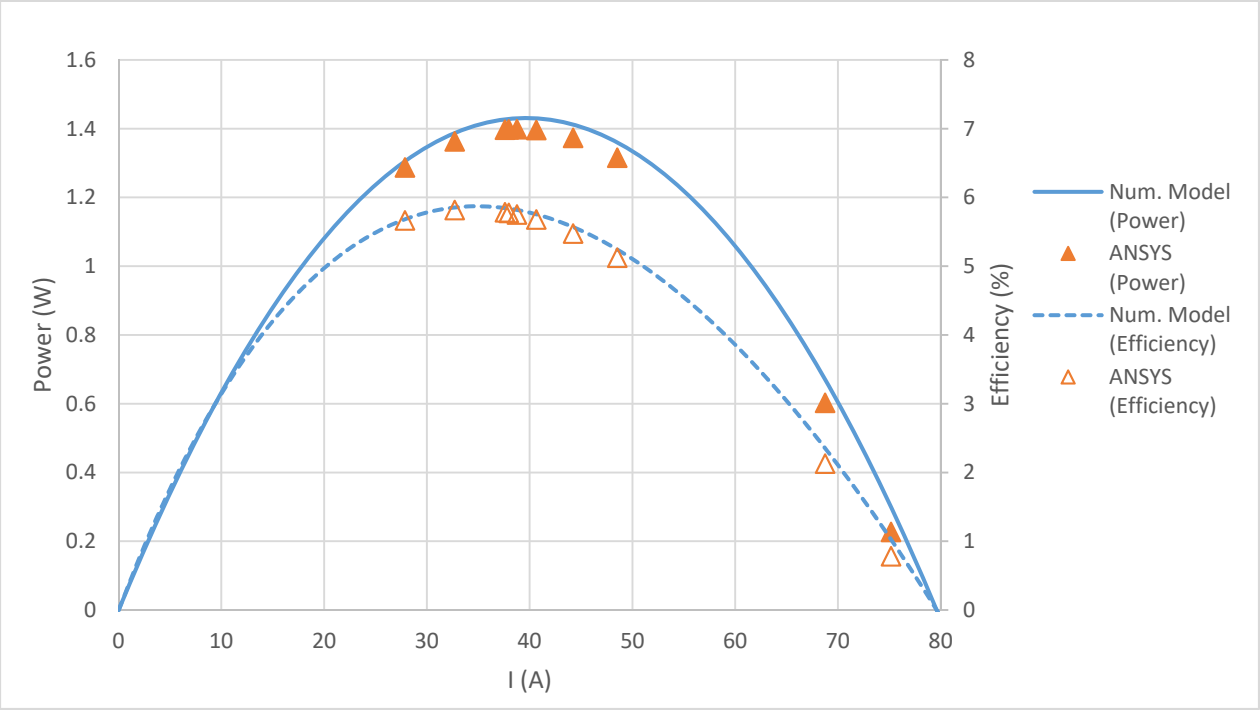

Fig.(3.5) – Comparison between results of ANSYS model and numerical model for the power output and efficiency of an annular TEG couple by varying the external load.

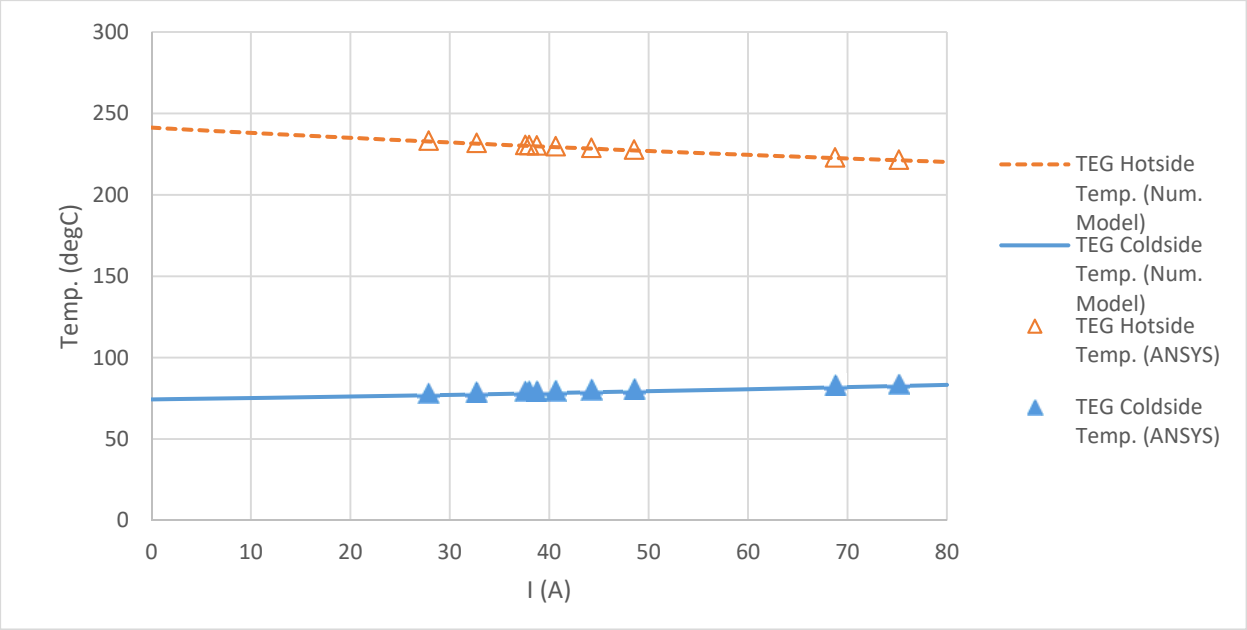

Fig.(3.6) – Comparison between results of ANSYS model and numerical model for the TEG hot-side and cold-side temperatures of an annular TEG couple by varying the external load.

There is a small deviation between the power output results of both models in Fig.(3.5). This deviation is due to the electrical resistance of the conductor in the ANSYS model which contributed to the slight drop in power output and it was neglected in the numerical model.

3.4. Maximum power point calculations

The Peltier heat affects the temperature difference across a TEG integrated in a heat exchanger as the current through the TEG increases, as shown in Fig.(3.6). It also affects the load ratio ($m_L = R_L/r_T$) at which the maximum power point (MPP) occurs as shown in eqn.(3.30). Accurate calculation of the load ratio at maximum power is required as it can affect the model estimation of the output voltage and current at MPP. The MPP is calculated in the numerical model by iteratively solving for the value of the short circuit current (I_{sc}) at which the value of the output voltage (V) is equal to zero. The short circuit current (I_{sc}) is initially estimated as:

$$I_{sc}^{o} = \frac{V_{oc,m}^{o}}{r_{T,m}^{o}} \quad (3.40)$$

Where ($V_{oc,m}^{o}$) is the open circuit voltage initial estimate of row (m), the initial temperatures solution is then obtained at (I_{sc}^{o}) and used to calculate a new value for $V_{oc,m}^{o}$ and I_{sc}^{o}. At every iteration, the output voltage (V) is checked and the error is calculated compared to zero. The iterations stops when the error in voltage reaches $< 1 \times 10^{-4}$. The current at MPP will be equal to half the value of (I_{sc}).

By plotting the power, current and voltage outputs of the annular TEGs case used in Section (3.3) for verification, MPP occurs at a value higher than one as shown in Fig.(3.7a). The results show that for this case, the short circuit current (I_{sc}) is found to be 80 A which means that the current at MPP is equal to 40 A and a load ratio ($m_L \cong 1.2$). The load ratio ($m_L = 1$) does not correspond to MPP which leads to inaccurate calculations for current and voltage at MPP as shown in Fig.(3.7b) and Fig.(3.7c) with approximately 7.5% and 8.3% error in the output current and voltage calculations.

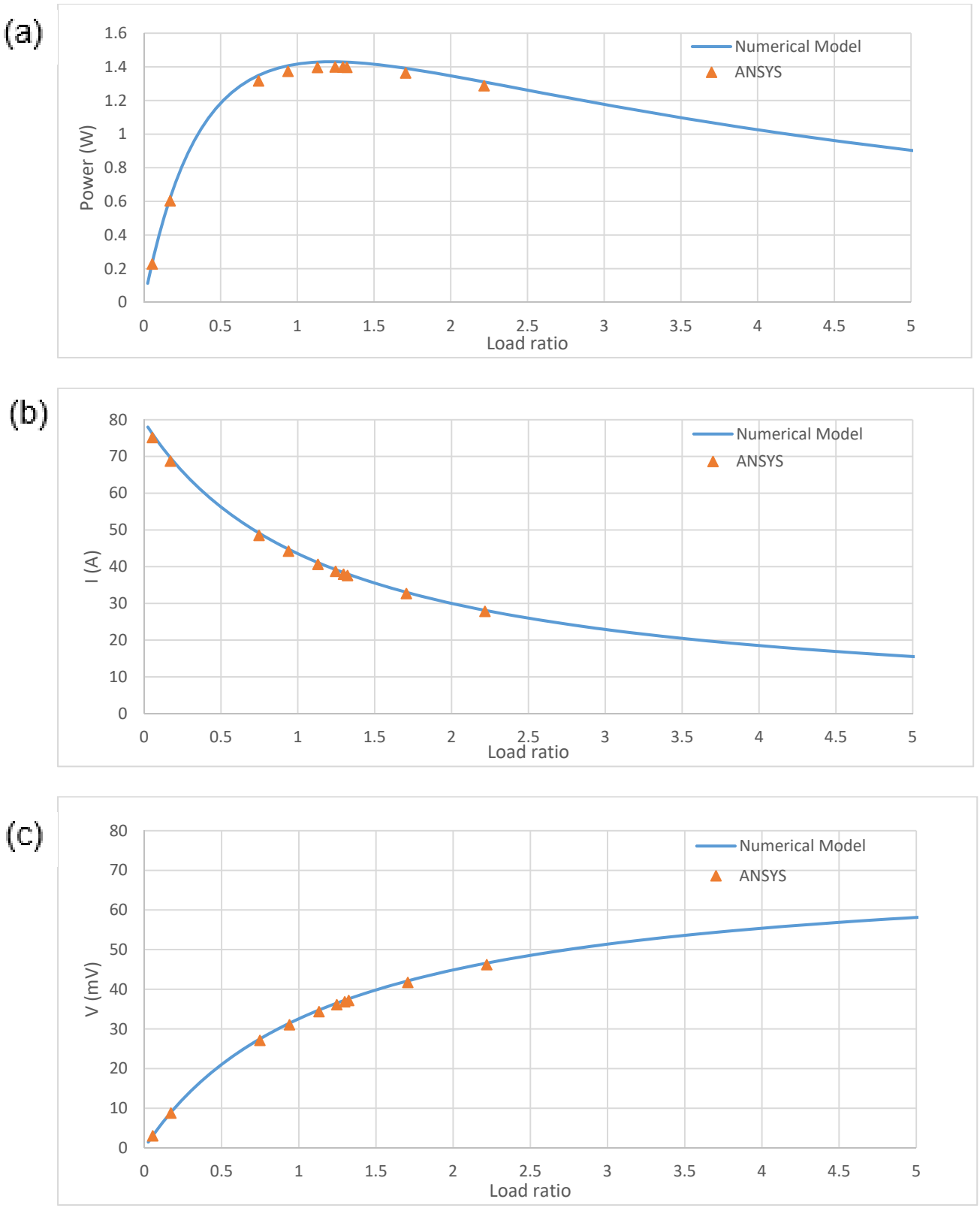

Fig.(3.7) – Comparison between results of ANSYS model and numerical model for an annular TEG couple by varying the load ratio (m) for: a) Power output – b) Current output – c) Voltage output

3.5. Multi-row TEG-HX numerical model

Using the developed numerical model for a single row heat exchanger as a building block, a multi-row heat exchanger model with integrated TEGs (TEG-HX) was developed to simulate the steady state performance of a heat exchanger consisting of multiple rows. The rows are connected together through the heat exchanger structure and the electrical connection between the TEGs can be either as series or parallel for comparison. The TEG-HX model will be used to study the effect of connection between the rows on the performance and determine the optimum TEG dimensions to maximize performance for a certain heat exchanger design.

The performance of the heat exchanger is evaluated based on the electrical power output of the TEGs and the amount of heat recovered. A thermal network, shown in Fig.(3.8), is solved to get the correct temperatures at all nodes in the heat exchanger for a certain known value of current (I_m) at every row, then an electrical network is further solved to get the correct current and voltage at every row based on the electrical configuration between rows. By applying energy balance on the TEG's hot and cold junctions as shown in Fig.(3.9), the equations are arranged to be solved for row (m) in the heat exchanger for a certain value of current (I_m).

$$\dot{m}_g C^o_{P,g}\left(T_{g,n} - T_{g,n+1}\right) = K_{H,m}\left(\frac{T^o_{g,n} + T_{g,n+1}}{2} - T_{H,m}\right) \quad (3.41)$$

$$K_{H,m}\left(\frac{T^o_{g,n}+T_{g,n+1}}{2} - T_{H,m}\right) = K_{A,H,n+1}\left(T_{H,m} - T^o_{H,m+1}\right) - K_{A,H,n}\left(T^o_{H,m-1} - T_{H,m}\right) + K_{Ct,H,m}\left(T_{H,m} - T_{TH,m}\right) \quad (3.42)$$

$$K_{Ct,H,m}\left(T_{H,m} - T_{TH,m}\right) = K^o_{T,m}\left(T_{T,H,m} - T_{TC,m}\right) + \alpha^o_{T,m} I_m T_{T,H,m} - \epsilon\, I^2_m r^o_{mat,T,m} - I^2\left(r_{ct,H,T} + r_{cd,H,T}\right) + K_{G,m}\left(T_{T,H,m} - T_{T,C,m}\right) \quad (3.43)$$

$$K_{Ct,C,m}\left(T_{T,C,m} - T_{C,m}\right) = K^o_{T,m}\left(T_{T,H,m} - T_{T,C,m}\right) + \alpha^o_{T,m} I_m T_{T,C,m} + (1-\epsilon) I^2_m r^o_{mat,T,m} + I^2\left(r_{ct,C,T} + r_{cd,C,T}\right) + K_{G,m}\left(T_{T,H,m} - T_{T,C,m}\right) \quad (3.44)$$

$$K_{C,m}\left(T_{C,m} - \frac{T^o_{w,n}+T_{w,n+1}}{2}\right) = K_{A,C,n+1}\left(T_{C,m} - T^o_{C,m+1}\right) - K_{A,C,n}\left(T^o_{C,m-1} - T_{C,m}\right) + K_{Ct,C,m}\left(T_{T,C,m} - T_{C,m}\right) \quad (3.45)$$

$$\dot{m}_w C^o_w\left(T_{w,n+1} - T_{w,n}\right) = K_{C,m}\left(T_{C,m} - \frac{T^o_{w,n} + T_{w,n+1}}{2}\right) \quad (3.46)$$

Equations (3.41 – 3.46) are a linear system of equations that can be solved directly using LU factorization method in MATLAB to get the temperatures at outlets of gas and water and at TEG junctions for a single row shown in Fig.(3.9). An initial solution is obtained by solving individual rows for known inlet conditions of the whole heat exchanger.

By adding an axial conduction component ($R_{th,A}$), shown in Fig.(3.9), to the numerical model for the hot and cold sides of the heat exchanger, it has enabled the study of the conduction within the heat exchanger structure which is often neglected in models [39], [40]. The effect of this component will be discussed in Chapter (5).

For all rows shown in Fig.(3.8), the equations are then solved iteratively for the heat exchanger. All terms with superscript (o) are obtained using solutions of previous iterations for temperature dependent properties and components that require adjacent rows' temperatures. Operation parameters such as water mass flow rate and number of inlets are set based on the design of the water cooling loop. The error in the energy balance of the heat exchanger and the error in temperature are used as convergence criteria for the thermal output solution, the convergence of the solution is considered when the error reaches $< 1 \times 10^{-5}$.

The electrical output solution is dependent on the electrical configuration of the heat exchanger rows i.e. series or parallel. After the thermal output solution is obtained, the electrical output is estimated using the voltage and current outputs of each TEG row. Different solution conditions are required for each type of electrical configuration, a series connection between the TEG rows requires equal current in all rows while a parallel connection requires equal voltage. Due to the model equations solution technique, the parallel configuration requires an additional outer iterations loop to obtain the output current of each row and ensure equal voltage outputs from all rows. On the other hand, the thermal and electrical output solution can be obtained for a series connection by directly setting the same value of current in all rows.

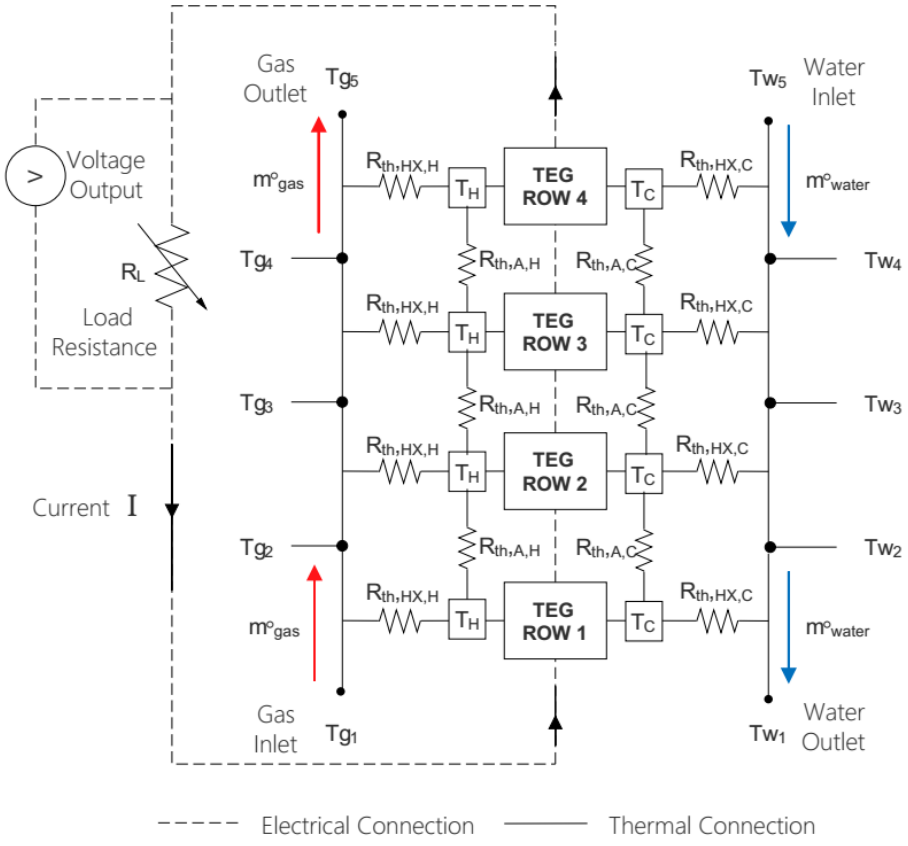

Fig.(3.8) – Thermal network for a multi-row heat exchanger with integrated TEGs including the electrical connection circuit between TEG rows.

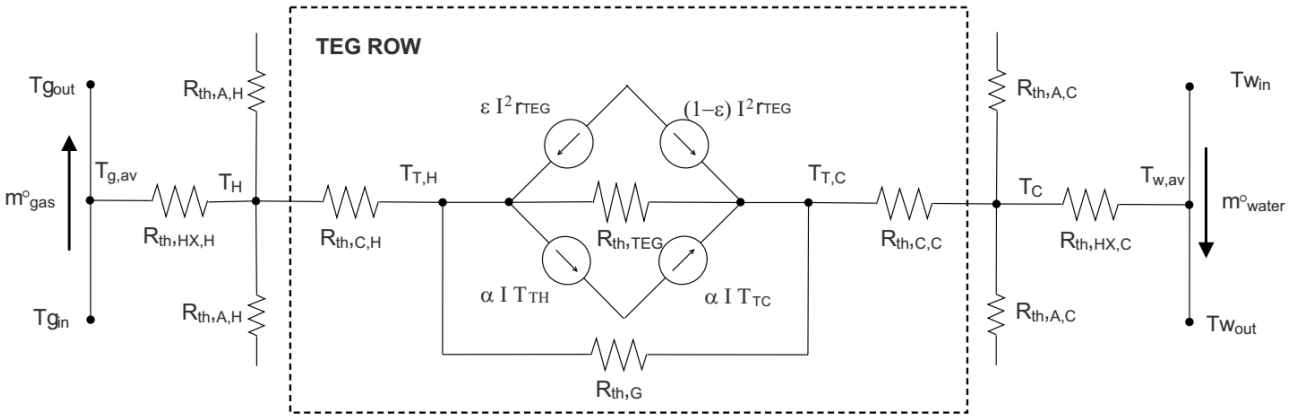

Fig.(3.9) – Thermal network for a TEG row including thermal contact resistances and axial conduction components in a heat exchanger.

3.6. List of modelling assumptions

The modelling of a heat exchanger with integrated TEGs using the multi-row TEG-HX model requires simplifying assumptions for the gas and water flows, the heat exchanger components and TEGs. The gas flow is assumed to be have a uniform velocity within the heat exchanger, a uniform temperature in X-Y plane and the temperature only varies in the Z-direction as the gas flows in Fig.(4.3) & Fig.(4.18). The average temperatures of gas and water are used between inlet and outlet of each row. Heat is transferred from gas to water through the heat exchanger components by convection and conduction. Radiation is neglected between the fins and the insulated ducting around the heat exchanger and between consecutive rows, this will be discussed in details in Section (5.6.1). The losses to the atmosphere from the heat exchanger are neglected by assuming that the exhaust gas duct, shown in Fig.(4.18), is perfectly insulated. The TEG hot-side and cold-side surfaces are assumed to have an average temperature due to the high thermal conductivity of aluminum in fins compared to the TEG material.

3.7. Summary

In order to study the performance of annular TEGs in the next generation TEG POWER heat exchanger, accurate modelling of the interaction between the heat transfer and thermoelectric effects is required. In this chapter, the modelling aspects of TEGs integrated in a heat exchanger were investigated, a thermal network was used to the coupling between the TEG model and the heat exchanger design thermal resistances. Different solution approaches for simplified models were discussed for the modelling equation of annular TEGs in a heat exchanger to study the effect of the heat exchanger and TEGs thermal resistances on the power output. A numerical model was developed to provide a more accurate solution for the TEGs and heat exchanger performance calculations, the results of the numerical model for a single row heat exchanger with TEGs were verified using ANSYS. A thermal network for a heat exchanger consisting of multiple TEG rows was presented and multi-row TEG-HX numerical model was developed to evaluate the thermal and electrical performance of the heat exchanger under fixed inlet conditions for different TEG dimensions and electrical configurations.

Chapter 4

Model Validation and Design Aspects

4.1. Introduction

A numerical model was developed to study the performance of annular TEGs in the heat exchanger design of the next generation of TEG POWER systems. The model was validated against the experimental results of 1st generation TEG POWER heat exchanger using flat TEGs. In this chapter, the model validation results will be presented and the annular TEG heat exchanger design aspects will be discussed.

4.2. Validation of multi-row TEG-HX numerical model using TEG POWER system

In order to validate the multi-row TEG-HX model results, results from TEG POWER system experimental testing facility described in [8] shown in Fig.(4.1), were used and compared against the numerical model results.

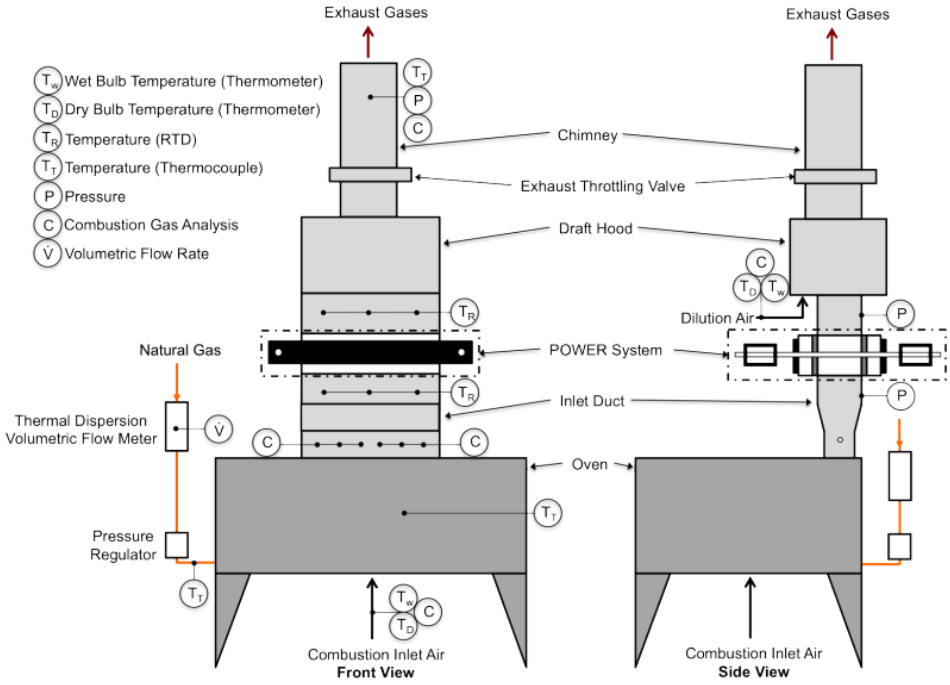

Fig.(4.1) – Experimental testing facility for TEG POWER systems [8]

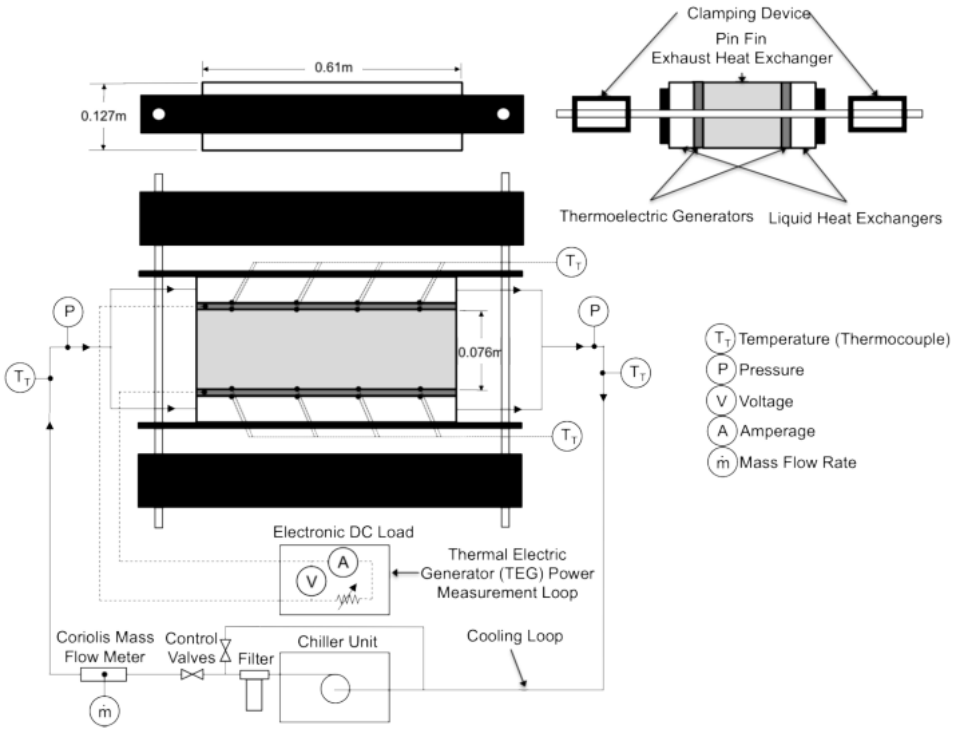

Fig.(4.2) – TEG POWER heat exchanger testing apparatus [8]

The testing facility consists of a natural gas oven as the exhaust gas source, TEG POWER heat exchanger for waste energy recovery system, a draft hood for exhaust control and a chimney. The TEG POWER heat exchanger is connected to a water cooling loop and an electronic DC load as shown in Fig.(4.2). The performance is experimentally evaluated through measurements of exhaust gas and water inlet and outlet temperatures and flow rates, TEGs hot-side and cold-side surface temperatures and power output. The experimental results are described in details in Appendix (A).

The heat exchanger uses 8 aluminum plate fin modules for the exhaust side heat exchanger, 48 flat TEG modules for power output, impinging jet heat exchanger for the water side and a clamping mechanism that provides 18 kN force on the TEGs to reduce contact resistance. The heat exchanger design is shown in Fig.(4.3). The heat exchanger performance data was tested for different exhaust gas mass flow rates using the experimental facility developed in [8]. The flat TEG modules performance is characterized to obtain the effective thermoelectric properties required which discussed in detail in the next section. The modelling of TEG power heat exchanger components

will be discussed. The modelling results will be compared against the experimental results for different exhaust gas flow rates.

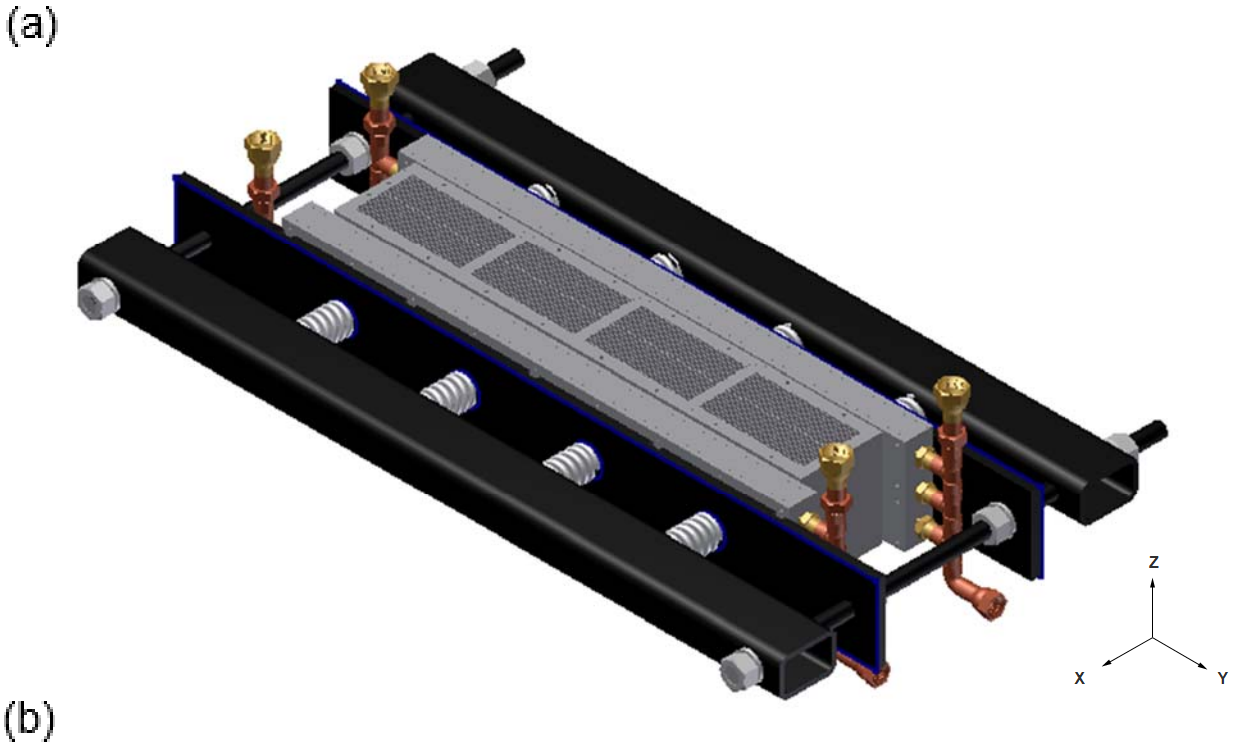

Fig.(4.3) – The 1st generation TEG POWER heat exchanger design: a) Isometric view showing the clamping mechanism and the cold-side heat exchanger arrangement – b) Hot-side heat exchanger design showing the TEGs arrangement on both sides – c) TEGs arrangement on the fin modules base. [Appendix (A)]

4.2.1. Characterization of flat TEG modules performance

The TEG POWER heat exchanger shown in fig.(4.3) is fitted with 48 flat TEG modules (TEG1-12610-5.1) with an area of 40 mm x 40 mm for the module, each consisting of 126 couples as shown in Fig.(4.4), arranged into two horizontal rows with 24 TEG modules each as shown in Fig.(4.3b) & Fig.(4.3c). The TEG module was characterized using the TEMTester which is developed by [10], to obtain properties as the module Seebeck coefficient, electrical resistance and thermal conductance.

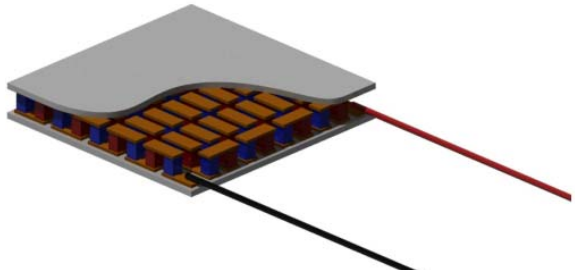

Fig.(4.4) – 3D schematic of Flat TEG module (TEG1-12610-5.1) [10]

Since the TEG properties are temperature dependent, the TEG was characterized between the average TEG hot-side and cold-side temperatures of the experimental results as shown in Fig.(4.5). From the experimental results, the average TEG temperatures are 168.5 °C for the hot-side and 40 °C for the cold-side which are used for the TEG characterization.

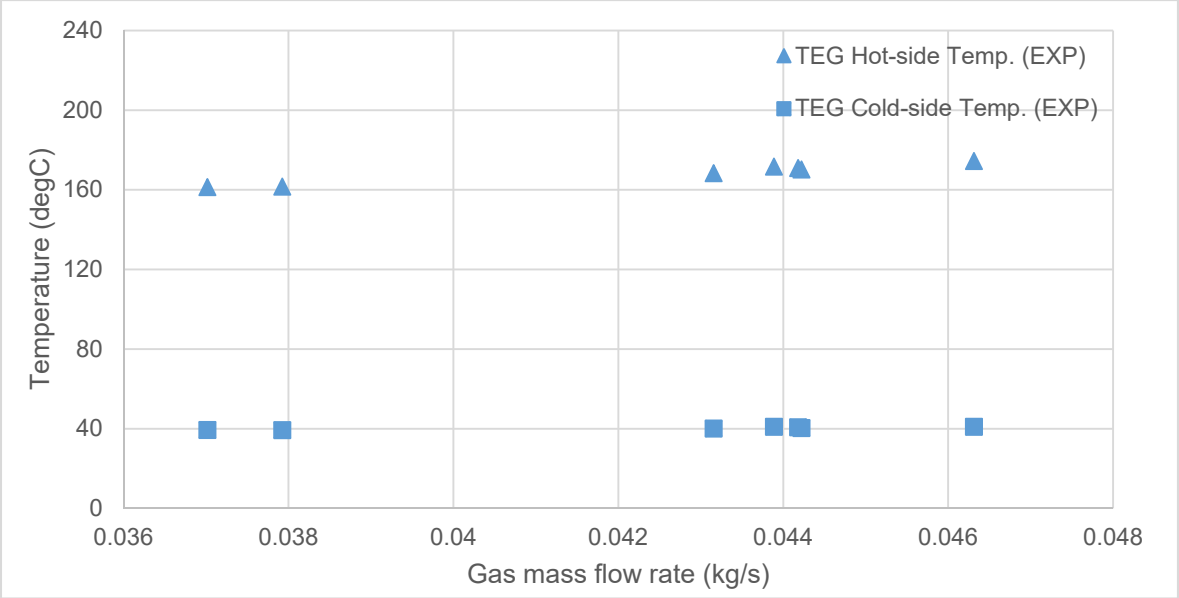

Fig.(4.5) – Experimental results of TEG hot-side and cold-side surfaces temperatures of 1st generation TEG POWER for different gas mass flow rates

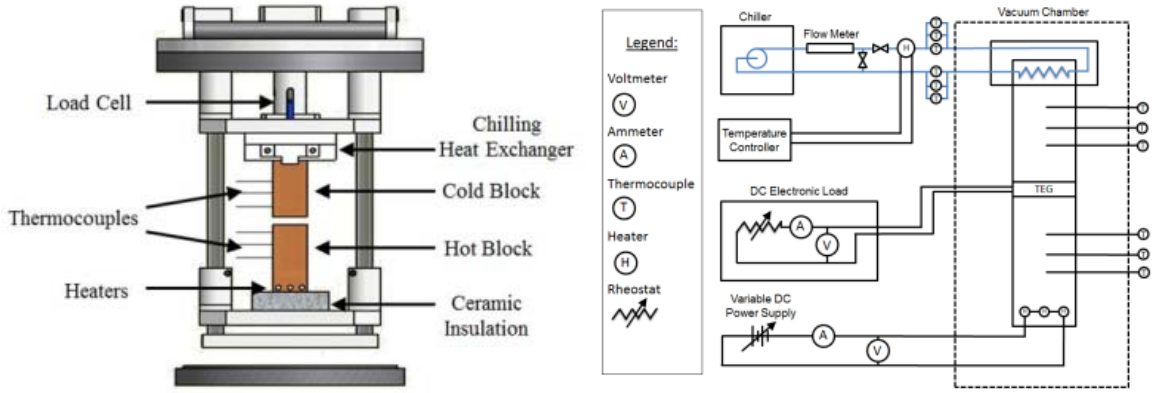

Fig.(4.6) – TEG characterization using TEMTester [10]

TEMTester is the testing apparatus for TEGs characterization, which is described in details by [10], it consists of a hot block and a cold block to provide controlled hot-side and cold-side temperatures for the TEG with 3 thermocouple fitted to each of them to measure the temperature gradient for heat flux and surface temperatures calculations, as shown in Fig.(4.6). The hot block is fitted with a heater, controlled with a variable DC power supply to control the TEG hot-side surface temperature, and the cold block is connected to a chiller unit to control the temperature of the TEG cold-side surface. A clamping mechanism provides pressure to reduce contact resistance which was investigated by [10] and considered negligible at 500 kPa applied pressure on the TEG which was used for the characterization test presented. This value of pressure is also equivalent to the pressure applied on the TEGs in the heat exchanger setup.

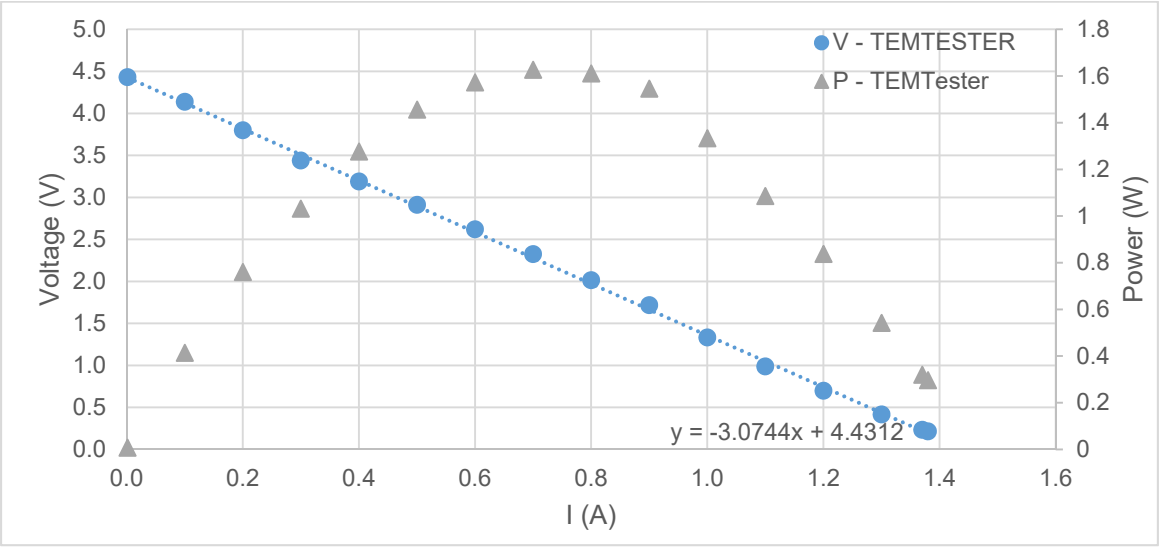

Fig.(4.7) – TEG characterization results for voltage and power outputs of (TEG1-12610-5.1) under hot-side and cold-side temperatures of 168.5 °C and 40 °C.

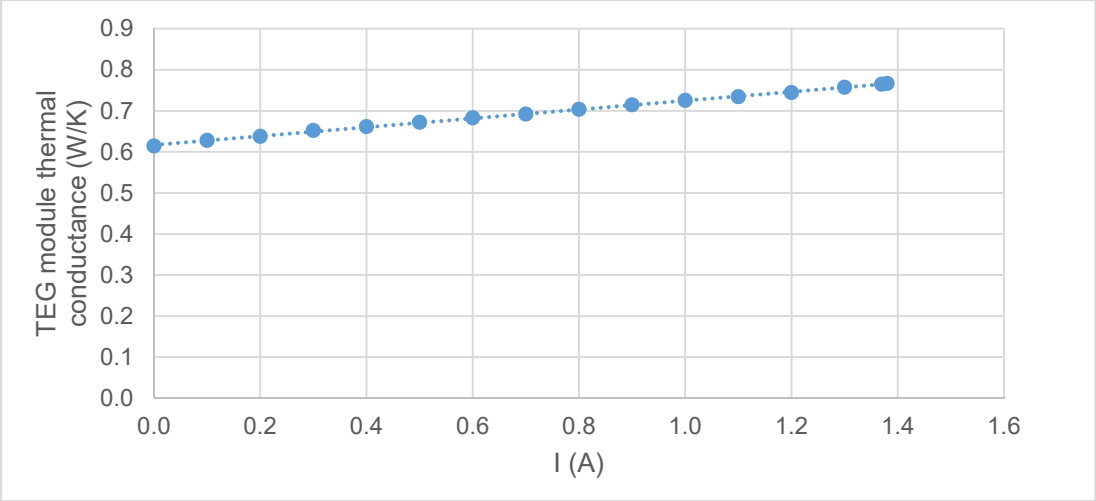

Fig.(4.8) – TEG characterization results for TEG1-12610-5.1 thermal conductance by varying the external load under hot-side and cold-side temperatures of 168.5 °C and 40 °C.

The characterization results are shown in Fig.(4.7) and Fig.(4.8) at hot-side temperature of 168.5 °C and cold-side temperature of 40 °C, the TEG performance including module Seebeck coefficient (α_{module}), electrical resistance (r_{module}) and thermal conductance (K_{module}) are obtained from these results as follows:

$$\alpha_{module} = \frac{V_{oc}}{T_H - T_C} = 4.43\ V$$

$$r_{module} = \frac{V_{oc}}{I_{sc}} = 3.07\ ohm$$

Where (V_{oc}) is open circuit voltage and (I_{sc}) is short circuit current. The module thermal conductance used for modelling is the value of open circuit since it changes by increasing current as shown in Fig.(4.8) due to Peltier heat. At open circuit, the module thermal conductance was found to be 0.614 W/K.

4.2.2. Modelling of the heat exchanger components

The heat exchanger consists of three main components: the exhaust side fins, the TEG modules and the water side heat exchanger. The TEG modules are modelled using the effective module properties obtained from experiments that are mentioned in the previous section. The modelling of gas and water flow through the heat exchanger will be discussed.

To model the heat transfer through the TEGs, the fins are divided equally into 2 rows which is equivalent to the TEGs number of rows and the TEGs are assumed to be centered with respect to the fins row as shown in Fig.(4.9). The gaps in between the TEGs are filled with insulating material and the heat transferred through it is neglected in the model.

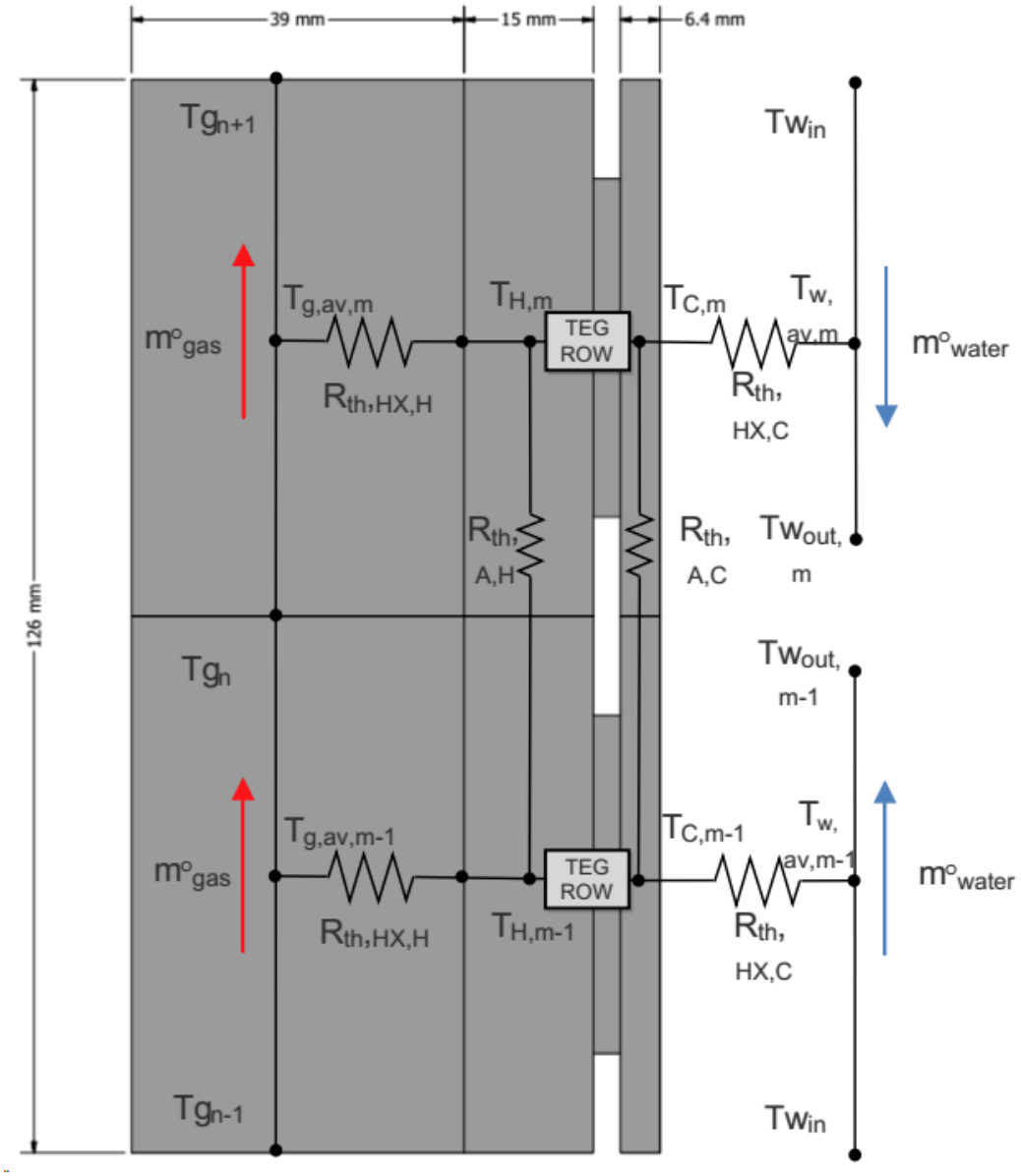

Fig.(4.9) – 1st generation TEG POWER heat exchanger with the modelling thermal network.

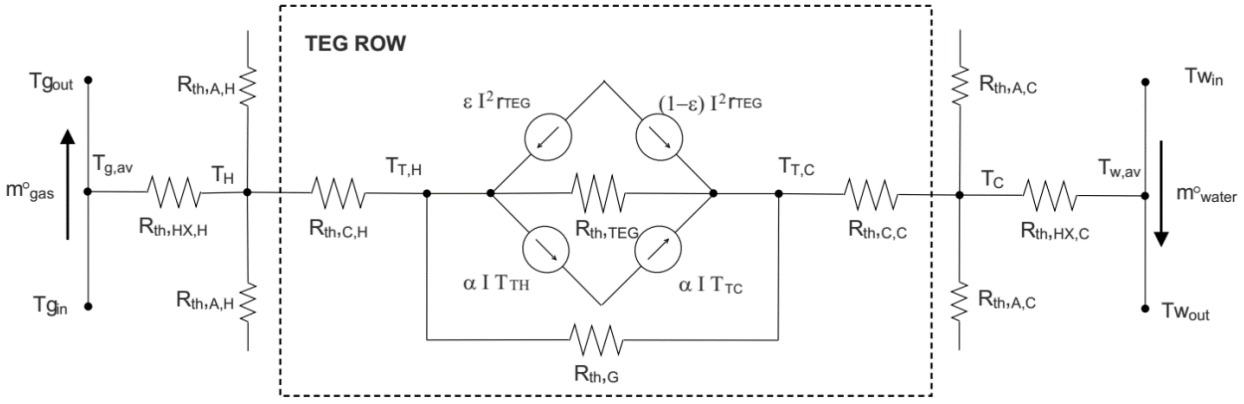

Fig.(4.10) – Thermal network for a TEG row including axial conduction components in a heat exchanger with neglecting thermal contact resistance

By setting up the thermal network for the heat exchanger consisting of two TEG rows, the multi-row TEG-HX numerical model will be used to investigate the performance of the heat exchanger by modelling the thermal resistance of the exhaust hot-side ($R_{th,HX,H}$), the water cold-side ($R_{th,HX,C}$) and the resistance of the axial conduction component in the fins base ($R_{th,A,H}$) and the cold-side plate ($R_{th,A,C}$) as shown in Fig.(4.9).

For TEG row model shown in Fig.(4.10), the heat transfer through the TEGs will be evaluated as described earlier in Section (3.5) by taking into consideration the flat geometry of the TEGs and negligible thermal contact resistances on TEGs hot-side and cold-side.

4.2.2.1. Exhaust side heat exchanger modelling

On the exhaust side, the heat exchanger consists of 8 plate fin modules made of aluminum ($\lambda = 200\ W/m.K$). The heat is transferred from the gas as it flows through the fins to the TEGs which transfer the heat to the water side heat exchanger. The TEGs performance depends on the thermal resistance of the fins ($R_{th,HX,H}$) which is calculated as follows:

$$R_{th,HX,H} = \frac{1}{\eta_o A_H h_{gas}} \quad (4.1)$$

$$\eta_o = 1 - \left(\frac{NA_f}{A_H}\right) \times \left(1 - \eta_f\right) \quad (4.2)$$

$$\eta_f = \frac{\tanh(mL_{cr})}{mL_{cr}} \quad (4.3)$$

To evaluate the fins efficiency (η_f) and the thermal resistance, the flow regime for the gas side was found to be laminar by calculating Reynolds number for a maximum mass flow rate of gas of 0.06 kg/s using properties of air as follows:

$$Re = \frac{\rho v \widetilde{D}_h}{\mu} \quad (4.4)$$

$$D_h = \frac{4A_c}{P} \quad (4.5)$$

The heat transfer coefficient was calculated using Nusselt number correlation for laminar gas flow between two parallel plates with the correction for the flow channels aspect ratio [48] for uniform surface temperature:

$$Nu_T = 7.541 \times (1 - 2.610\alpha^* + 4.970\alpha^{*2} - 5.119\alpha^{*3} + 2.702\alpha^{*4} - 0.548\alpha^{*5}) \quad (4.6)$$

$$Nu_T = \frac{h_{gas} L_c}{\lambda_{gas}} \quad (4.7)$$

Where (α^*) is the aspect ratio of the flow channel between the fins, the fluid properties are evaluated for air at an average temperature between the gas inlet and outlet temperatures. The entrance region effect was found to be negligible on the mean Nusselt number over the fins length as it would increase the value of (Nu_T) by less than 2% assuming a laminar flow between two parallel plates. The assumption of uniform surface temperature was used since the aluminum base of the fins spreads the heat over the length of the fin module.

By calculating the heat transfer coefficient of the gas flow and the fins efficiency, the total thermal conductance of the exhaust side heat exchanger is calculated to be used in the numerical model as:

$$K_H = \frac{1}{R_{th,HX,H}} \quad (4.8)$$

The thermal resistance of the fins base is neglected in the direction of heat flow perpendicular to the TEGs surface. It is only considered in the axial direction (parallel to the TEGs surface) of the gas stream due to higher temperature gradient of gas temperature profile, it can be calculated as:

$$R_{th,A,H} = \frac{L}{A_{CS,base}\lambda} \quad (4.9)$$

Where L in eqn.(4.9) is the distance between the centers of the TEG rows, and $A_{CS,base}$ is the base cross sectional area in the axial direction.

4.2.2.2. Water side heat exchanger modelling

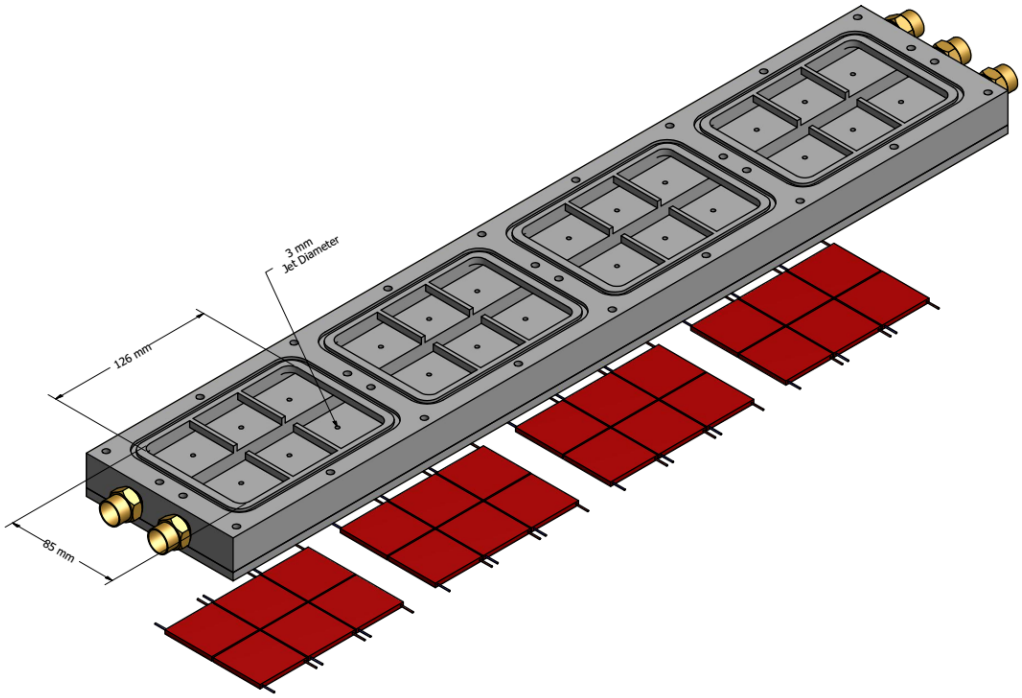

Fig.(4.11) – Cold-side heat exchanger jet impingement design of 1st generation TEG POWER with TEGs arrangement [Appendix (A)]

The heat exchanger on the water side dissipates the heat from the TEGs cold-side to the water by jet impingement. It consists of 48 jets positioned at the center of each TEG to provide a uniform temperature distributions. Fig.(4.11) shows the heat exchanger design for 24 TEGs on one side of the heat exchanger fins.

The same design was tested and presented by [49] for a heat exchanger consisting of 14 jets, shown in Fig.(4.12). The heat exchanger performance was investigated under a range of water flow rates in an experimental testing facility presented in [49] and a correlation was developed to calculate Nusselt number for the water impinging jet, shown in Fig.(4.13). This correlation was used to calculate the convective heat transfer coefficient as follows:

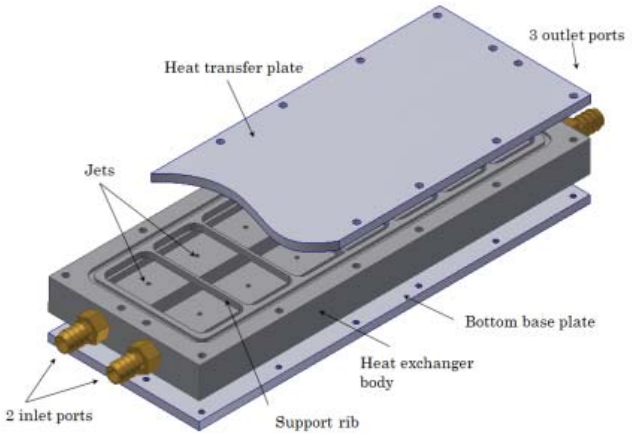

Fig.(4.12) – Jet impingement heat exchanger design tested by Hana [49]

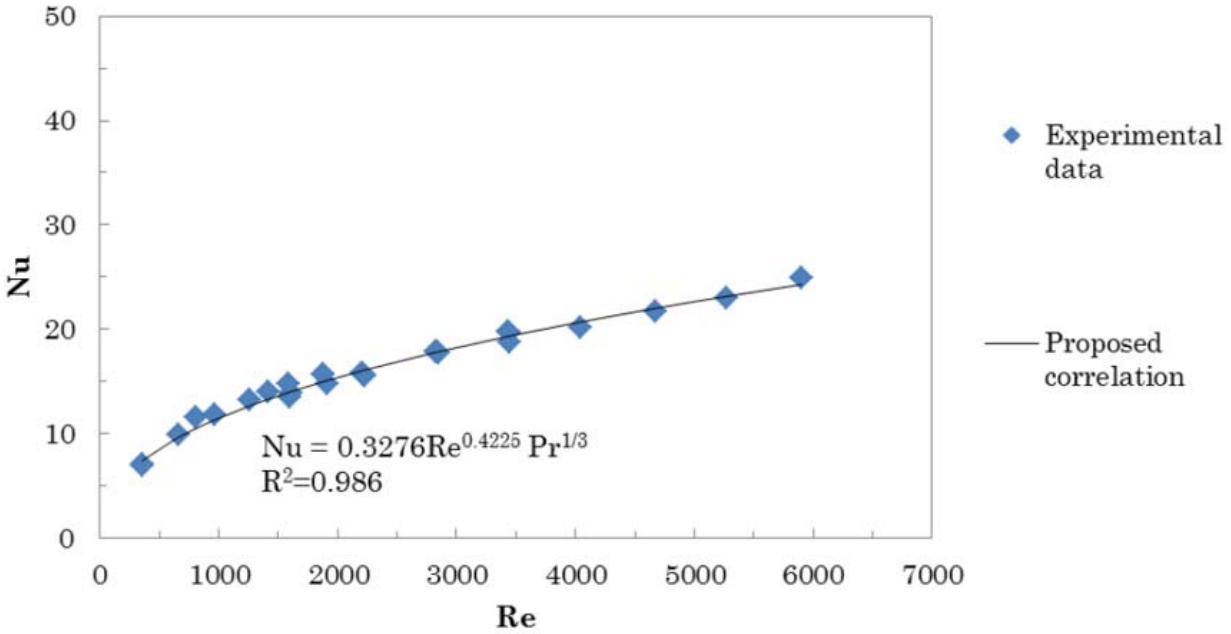

Fig.(4.13) – Nusselt number variation with Reynolds number for impinging jets – modified from [49]

$$Re = \frac{\rho v_j D_j}{\mu} \quad (4.10)$$

$$Nu = \frac{h_w D_j}{\lambda_w} = 0.3276\, Re^{0.4225} Pr^{1/3} \quad (4.11)$$

Where (V_j) is the jet velocity and (D_j) is the jet diameter (3 mm), all water properties are evaluated at the average temperature between the inlet and outlet. Using the thermal network shown in

Fig.(4.9), the cold-side heat exchanger is modelled using the heat transfer coefficient obtained by calculating the convection thermal resistance of the cold-side ($R_{th,HX,C}$) for each row as follows:

$$R_{th,HX,C} = \frac{1}{hA_C} \quad (4.12)$$

The water outlet temperature from the two rows of the heat exchanger shown in Fig.(4.9) is taken as the average of the water outlet temperature from each row since it is assumed that the water flow rate is equally distributed among all jets in the heat exchanger. The thermal conductance of the cold-side of each row can be written as:

$$K_C = \frac{1}{R_{th,HX,C}} \quad (4.13)$$

The thermal resistance of the aluminum plate between the TEGs and the cold-side heat exchanger is neglected in the direction of heat flow perpendicular to the TEGs surface. It is only considered in the axial direction (parallel to the TEGs surface) of the gas stream, it can be calculated as:

$$R_{th,A,C} = \frac{L}{A_{CS,plate}\lambda} \quad (4.14)$$

Where L in eqn.(4.14) is the distance between the centers of the TEG rows, and $A_{CS,base}$ is the base cross sectional area in the axial direction.

4.2.3. The model validation results using TEG POWER experimental results

The TEG POWER heat exchanger performance, shown in Fig.(4.3), is tested for different gas mass flow rates by varying the opening % of the exhaust draft hood between the heat exchanger and the chimney [8], the gas and water inlet temperatures, as well as the water flow rate, are kept constant during testing. By modelling the TEG POWER heat exchanger, the model results are compared against the experimental results for validation which are discussed in details in Appendix (A). Fig.(4.14) shows all the inlet conditions for the heat exchanger for each exhaust gas flow rate case which are used by the model.

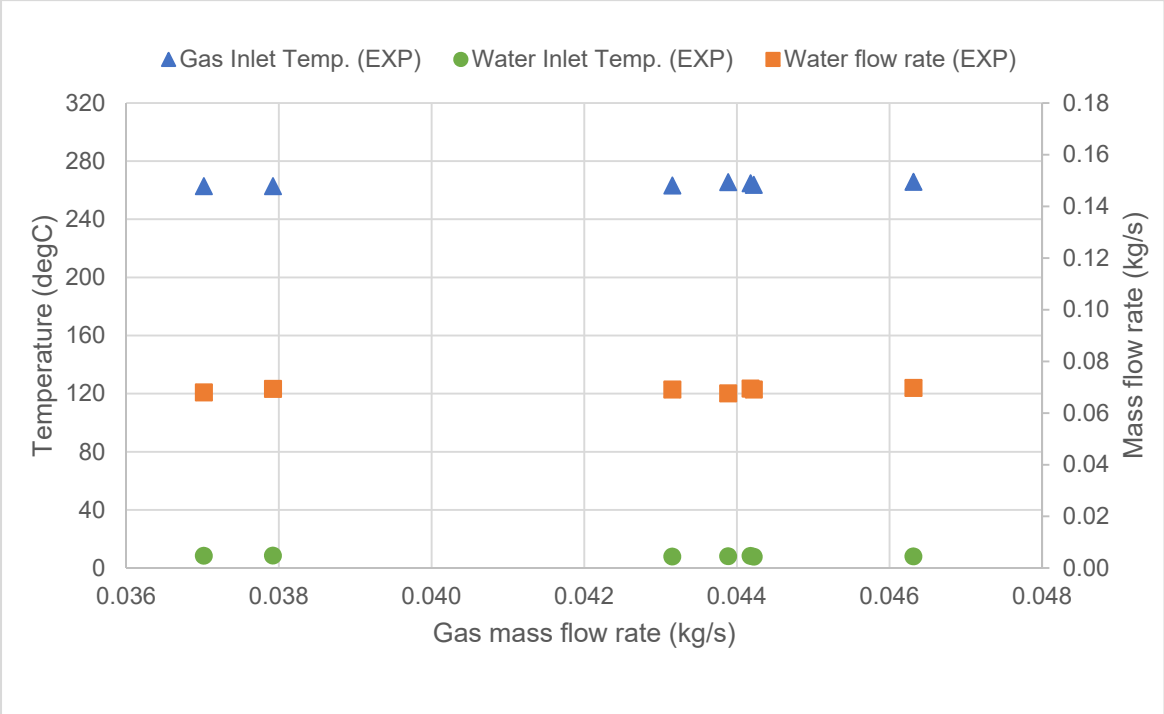

Fig.(4.14) – Heat exchanger gas and water inlet temperatures, and water flow rate.

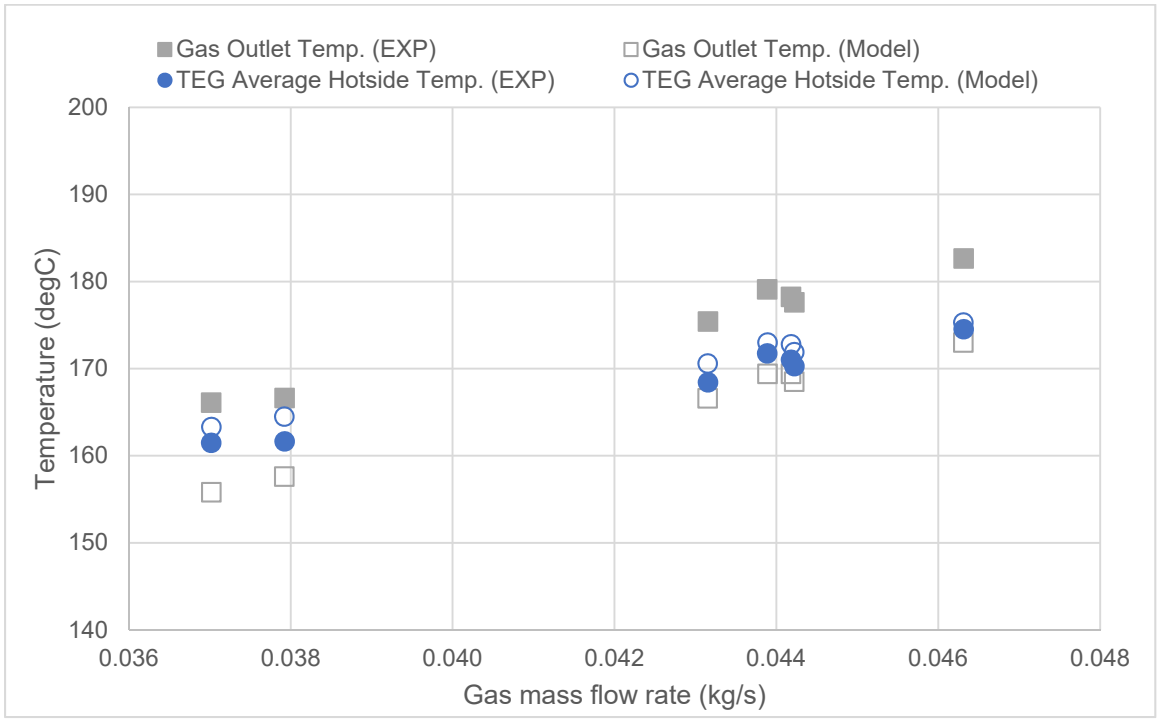

Fig.(4.15) – Comparison between experimental and model results for gas outlet temperature and TEG hot-side surface temperature under different gas flow rates.

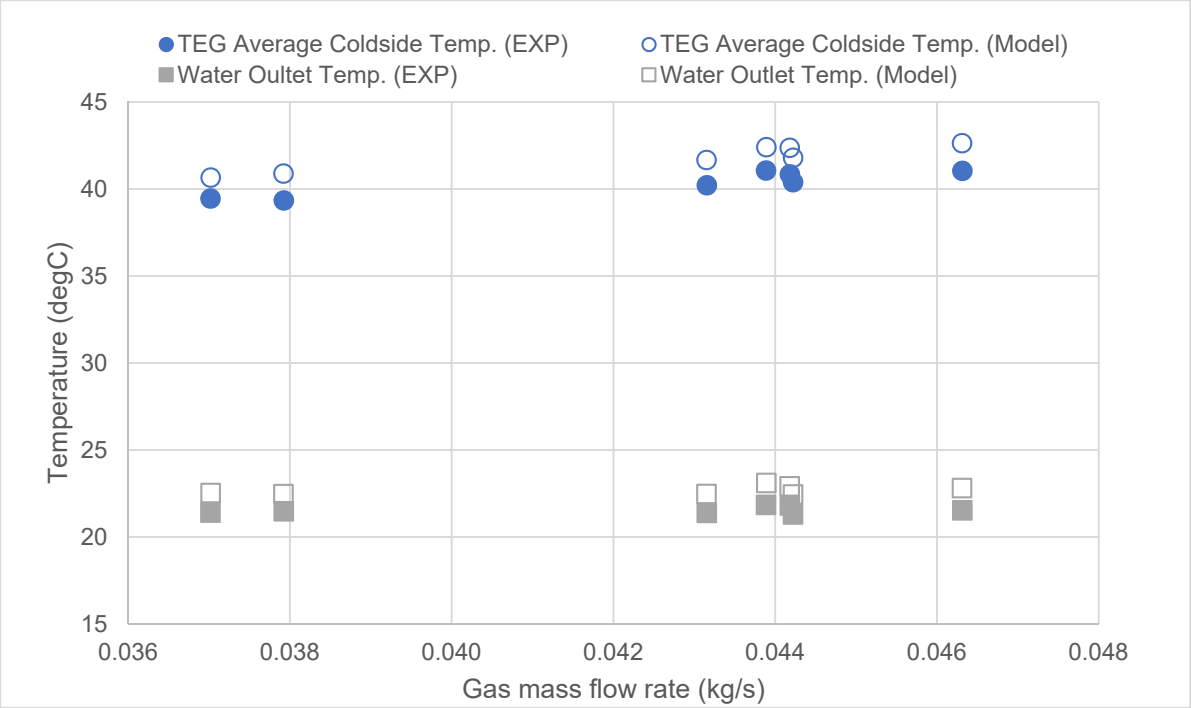

Fig.(4.16) – Comparison between experimental and model results for water outlet temperature and TEG cold-side surface temperature under different gas flow rates.

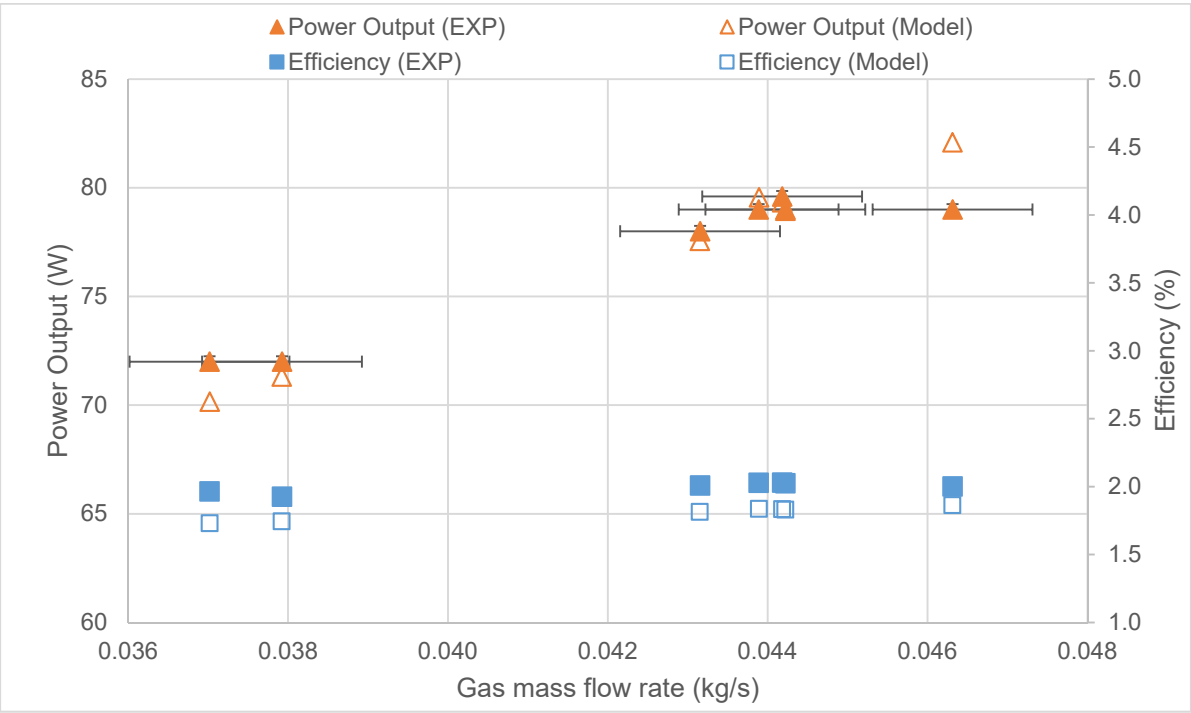

Fig.(4.17) – Comparison between experimental and model results for power output and efficiency under different gas flow rates.

The results show the increase in the power output, due to the increase in the available energy in the gas, as the gas mass flow rate increases as shown in Fig.(4.17). The power output of the TEGs in the model is calculated using the TEG hot-side and cold-side average temperatures shown in Fig.(4.15) & Fig.(4.16). Comparing the power output results of the model with the experiments, the results show good agreement with maximum error of 3.9 %.

The results of the model, for the gas and water outlet temperatures and the TEG hot-side and cold-side temperatures, show also a good agreement with the experimental results. The gas and water outlet temperatures results show a maximum error of 6% in the model results. The outlet temperature is measured at the channel mid-length of the fins outlet, however the calculated temperature is the gas average temperature. The error can be due to the averaging of temperature at the outlet and between calculation nodes along the gas and water streams, the low number of elements used for discretization of the gas and water domains which is limited by the number of TEG rows in the numerical model.

4.3. Design aspects of next generation TEG POWER heat exchanger with annular TEGs

For the next generation TEG POWER system, the heat exchanger consists of an exhaust side heat exchanger and a pipe for the water side heat exchanger fitted with annular TEG modules, connected to a water tank for thermal storage. The heat is recovered from the exhaust gases to be used for hot water purposes and electricity is generated to power a DC grid. The design's description and operating conditions will be discussed and the modelling aspects will be investigated.

4.3.1. Design description and operating conditions

The next generation TEG POWER heat exchanger is designed to be mounted on top of a natural gas oven described in [8]. An insulated ducting system is used for the oven exhaust to pass the gas through the heat exchanger to the chimney. The heat exchanger design used and operating conditions are described in Fig.(4.18).

The design consists of four TEG rows, each consists of 8 columns for the TEG modules, with a water pipe fitted through as shown. All TEG modules in the heat exchanger are considered to be

connected in series between all rows which are then connected to a DC circuit with a maximum power point tracking (MPPT) system.

The next generation TEG POWER heat exchanger uses a compact aluminum plate fin design for the exhaust side similar to that of the 1st generation TEG POWER, the TEG modules fit in a groove machined in the fins base plate as shown in Fig.(4.19). Pressure is applied on TEGs by clamping the base plates to control the thermal contact resistance in addition to thermal padding between the TEG modules, the water pipes and the fins base using thermal contact material of $\lambda = 17\ W/m.K$ [50].

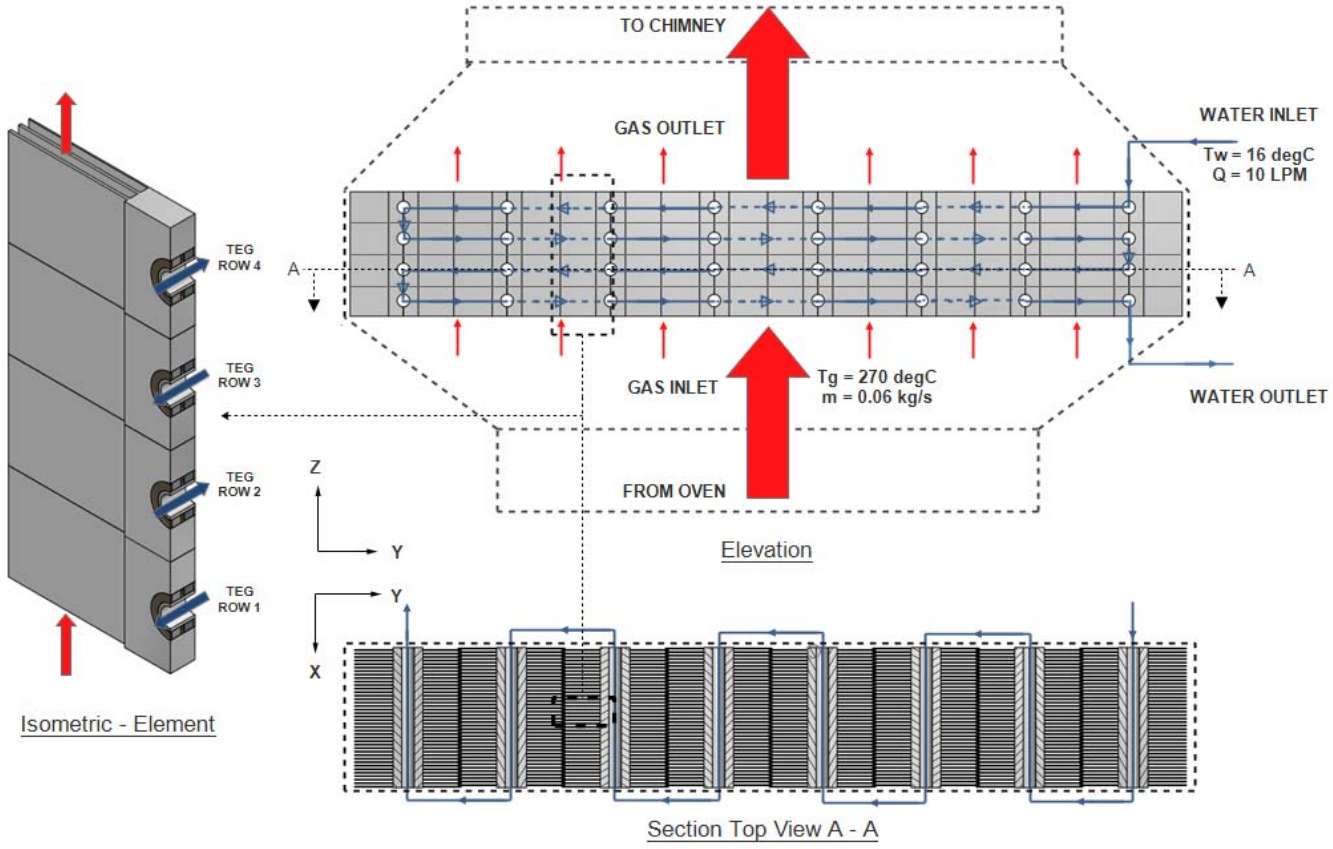

Fig.(4.18) – The next generation TEG POWER heat exchanger design with a list of operating conditions and directions of inlets of gas and water including a top view showing the water loop.

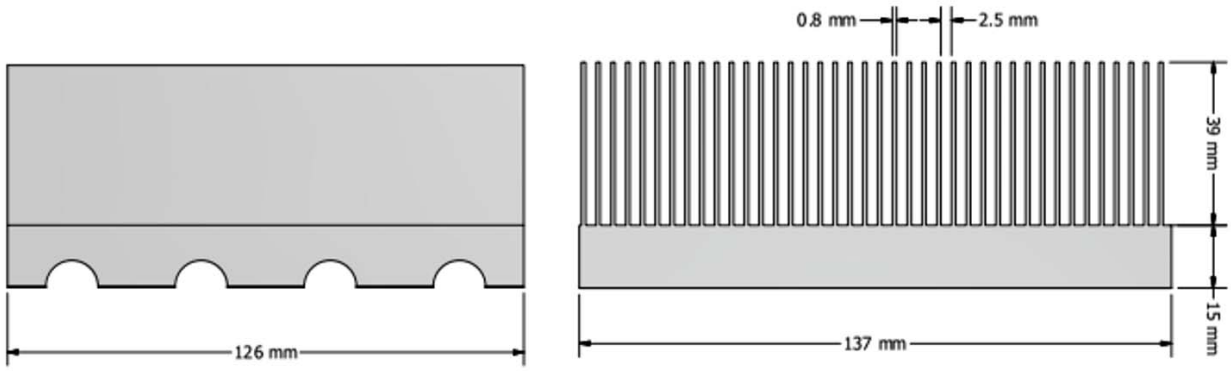

Fig.(4.19) – Fin modules design with half circular grooves for annular TEGs

The next generation heat exchanger was designed to have double the flow area of the 1st generation as the number of fin modules increased from 8 to 16 in the new design with the same air blockage ratio by fins of 24% as shown in Fig.(4.3) and Fig.(4.18). A detailed study of the pressure drop in the exhaust flow across the fins was presented by Girard in [8] for the 1st generation TEG POWER heat exchanger. In order to maintain the same flow pressure drop in the scaled up design of the next generation TEG POWER heat exchanger, the same fin design was used and the design operating conditions was chosen to ensure the same exhaust flow velocity at the inlet.

4.3.2. Modelling using multi-row TEG-HX numerical model

In order to model the next generation TEG POWER heat exchanger as shown in Fig.(4.20), components as exhaust side plate fins, annular TEG modules, water pipe and thermal contact materials will be modelled and implemented in TEG-HX numerical model. The modelling of the heat exchanger components will be discussed.

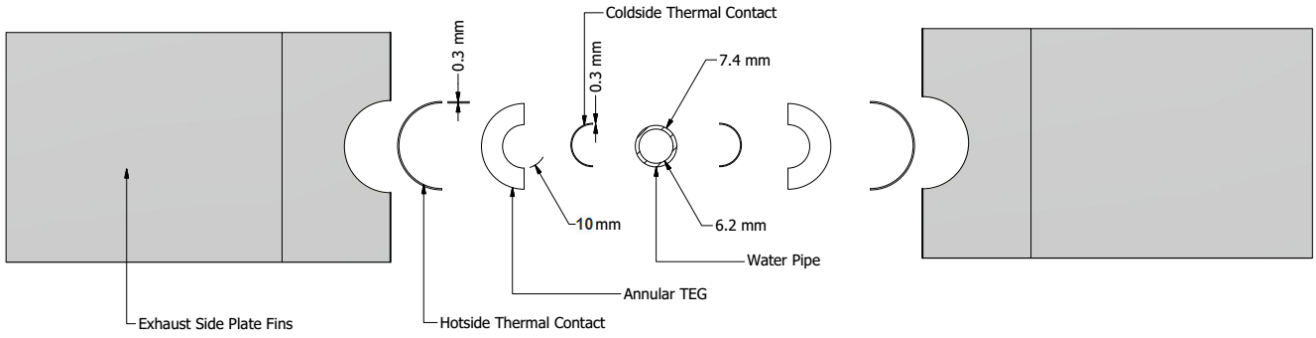

Fig.(4.20) – Heat exchanger with integrated one row of annular TEGs.

4.3.2.1. Annular TEG modules

The TEG material properties used for the modules is a crucial component for modelling since it affects performance calculations. The properties used are for spark plasma sintered bismuth telluride for P and N type rings which are characterized in [51], [52]. Since thermoelectric properties are temperature dependent and in order to model the performance in a heat exchanger with large temperature gradients between TEG rows, the properties are integrally averaged between the TEGs hot-side and cold-side temperatures for each row as follows:

$$\bar{x} = \frac{\int_{T_H}^{T_C} x(T)\, dT}{\Delta T} \qquad (4.15)$$

Eqn.(4.15) is used to calculate the average property of the TEG material where $\bar{x}$ represents the average Seebeck coefficient, electric resistivity or thermal conductivity of P-type and N-type materials. The temperature dependent function is obtained by using curve-fitted equations of the material characterization results [51], [52] in Appendix (B) which was specified for 120-180 μm particle sizes for P-type and N-type materials.

Using average thermoelectric material properties, the thermal conductance of annular TEG modules ($K^o_{T,m}$) can be calculated using eqn.(3.12) for TEG rows, the electrical resistance ($r^o_{T,m}$) can be calculated using eqn.(3.39) for an assumed electrical contact resistivity $R_{e,Ct} = 2 \times 10^{-9}\ ohm.m^2$ for soldering between the TEG material which in range with the values reported in literature [45], [53]. The copper conductors are assumed to be 1 mm thick.

4.3.2.2. Modelling of the heat exchanger components thermal resistances

The heat exchanger components consists of exhaust side plate fins, annular TEG modules, cooling water pipe and thermal contact materials at the interface between the heat exchanger and the TEG modules. The annular TEG modules, the thermal resistance of the contact materials and the pipe are modelled using the equations discussed in Section (3.5). The modelling of the exhaust side plate fins and the cooling water flow will be discussed.

The thermal network on the exhaust side for the numerical model is set up as shown in Fig.(4.21). The heat transfer through plate fins employs the same equations (4.1-4.9) as discussed in section (4.2.2.1) as the next generation heat exchanger shares the same design of fins for the 1st generation

TEG POWER. The axial thermal resistance of the fins base between rows is calculated using eqn.(4.9) neglecting the decrease in cross section due to the annular TEGs presence since the thermal conductivity of aluminum is two orders of magnitude higher than that of bismuth telluride. The validity of this assumption will be considered in Chapter (5). The temperature ($T_{H,m}$) is taken as the average temperature of the row fin base.

For the cooling water flow through the heat exchanger as shown in Fig.(4.18), the convection thermal resistance between the water flow and the pipe walls is modelled by calculating the convective heat transfer coefficient. Reynolds number is calculated for a water flow of 10 LPM which is found to be turbulent flow. Using the Dittus-Boetler [54] correlation for turbulent flow in circular pipes assuming developed flow, Nusselt number can written as:

$$Nu = 0.023\, Re_D^{0.8}\, Pr^{0.4} \qquad (4.16)$$

By calculating the convection thermal resistance ($R_{th,HX,C}$) and the thermal conductance (K_C) using eqns.(4.12) for the cold-side heat exchanger, the heat exchanger components thermal resistances are obtained for the operating conditions described in section (4.3.1.). The modelling approach of the annular TEG model is essentially identical to that presented in the flat TEG model and the performance is expected to be similar as they share the same hot-side heat exchanger design.

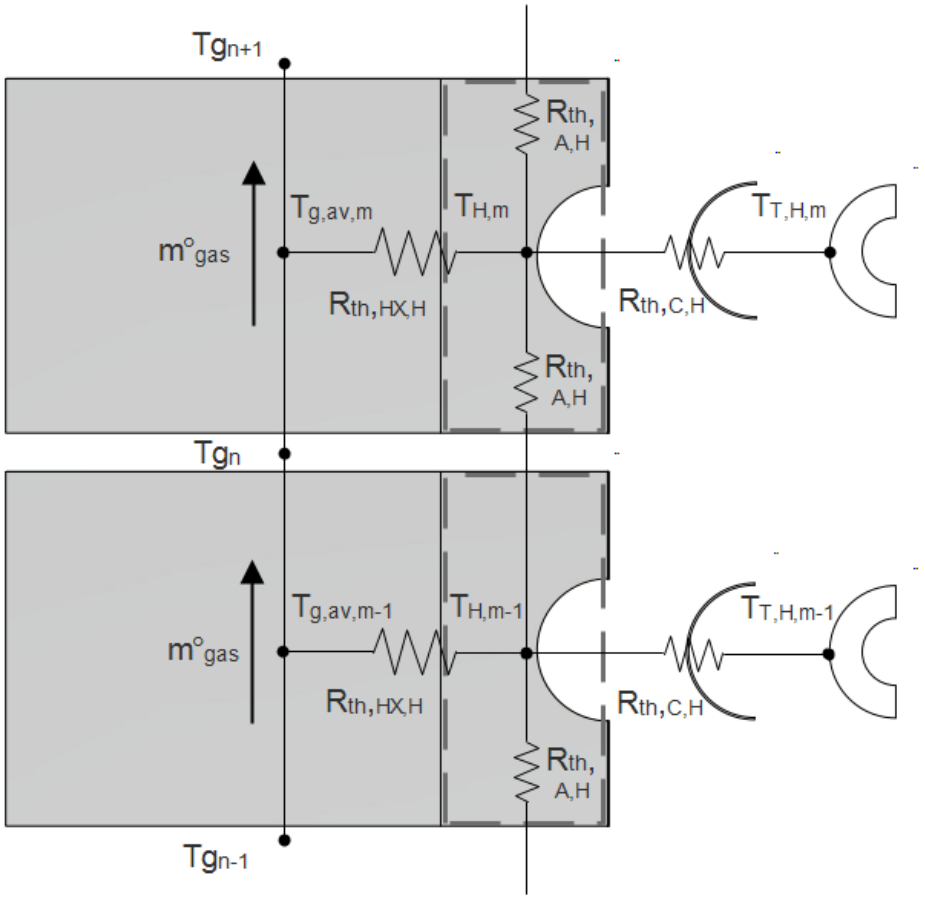

Fig.(4.21) – The next generation TEG POWER heat exchanger with the modelling thermal network.

4.4. Summary

The numerical model was validated using experimental results of the 1st generation TEG POWER systems under different exhaust flow rate conditions, the model results showed a good agreement with the experimental results for power output, efficiency, outlet temperatures of exhaust gas and water, and TEG surfaces temperatures. The next generation TEG POWER heat exchanger design and operating conditions are described, the modelling of different heat exchanger components was described. Temperature dependent thermoelectric properties are used for modelling of annular TEG modules to take into consideration varying average thermoelectric properties between rows. The numerical model will be used as a design tool for the annular TEG modules for optimized performance in the next generation heat exchanger.

Chapter 5

Analysis & Results

5.1. Introduction

In this chapter, the design aspects of thermoelectric generators will be discussed for a multi-row heat exchanger with integrated annular TEGs. Half annular TEG module is presented as a design solution to meet the performance objectives. The effect of different TEG design dimensions performance is analyzed and selection criteria will be discussed. In a multi-row heat exchanger, the interaction between rows at different temperature gradients, due to electrical configuration and conduction through the heat exchanger, is studied. Based on a parametric study, the performance of the next generation TEG POWER heat exchanger is presented under constant operating conditions and dimensions of TEGs is selected.

5.2. Annular TEG design objectives

The performance of TEGs in a heat exchanger is dependent on several different design and operation parameters. These parameters include the TEG design parameters, which in case of annular TEGs are dimensions as TEG diameter ratio and thickness which can be varied to maximize performance. The TEG inner diameter is directly coupled to the heat exchanger pipe diameter. The cold-side thermal resistance ($R_{th,HX,C}$) is relatively constant for the range of small pipe diameters considered and relative to the hot-side thermal resistance ($R_{th,HX,H}$), it only represents 6% of the total thermal resistance, thus ($R_{th,HX,C} \ll R_{th,HX,H}$). So the TEG inner diameter is assumed to have a negligible effect on the analysis. Other TEG arrangement parameters including spacing and module length are kept constant. The heat exchanger design parameters as well as operation parameters (inlet temperatures and flow rates of gas and water) are also kept constant during the analysis.

The TEG design objective is to maximize the power output under electrical current constraint to improve the power characteristics represented in voltage and current output. The current output is limited by a maximum value for the maximum power point tracking (MPPT) system to minimize

losses. The function of the MPPT system is to modulate the voltage and current outputs of the TEGs to match the electrical load while keeping the TEGs operating at maximum power point. The electrical losses and the complexity of MPPT systems increases the higher the difference between the TEG voltage output and the load voltage [33], [55]. Mechanical integrity constraint can also be added as an aspect ratio for the TEG dimensions to avoid failure due to mechanical and thermal stresses that can be evaluated by further modelling and testing of material properties which is not included in this work. It is important to note that, in this study, the power output is considered of more importance than efficiency due to the abundance of waste heat [4]–[7].

5.3. Half annular TEG design performance

The implementation of the annular ring design for TEGs requires some design solutions in order to be integrated in a heat exchanger. Full annular ring design was first developed by Min G. and Rowe D. [12] which offers a modular design that can be fitted on pipes, however using this design in a heat exchanger faces difficulties due to poor contact resistances and cracking due to thermal stresses [12], [14], [16]–[18].

In a full annular ring design, the mismatch in coefficient of thermal expansion (CTE) between the TEG material and the pipe offers poor control on the thermal contact resistance which affects the TEGs performance during operation. Moreover, the temperature difference across an annular TEG can create thermal stresses which induce tensile stresses in the material leading to cracking in the radial direction [17].

A half annular design for TEGs is introduced as a design solution for a heat exchanger since it offers advantages over the full annular design. The advantages include better control on contact resistance by applying pressure on individual halves, an easier assembly for the heat exchanger and reduced thermal stresses.

By comparing performance per unit pipe area of a single row heat exchanger as shown in Fig.(5.1), a half annular TEG (A-TEG) has a higher internal resistance for the same amount of material compared to the full annular design. By splitting the annular TEGs in a heat exchanger, a higher voltage output can be achieved at a lower current for the same power output of the TEGs since the number of TEG couples connected in series is doubled per row.

Using the half annular TEG design, the design objectives can be achieved as it provides lower current output per row which can help achieve the current limit of the MPPT system at a higher power output compared to full annular TEGs.

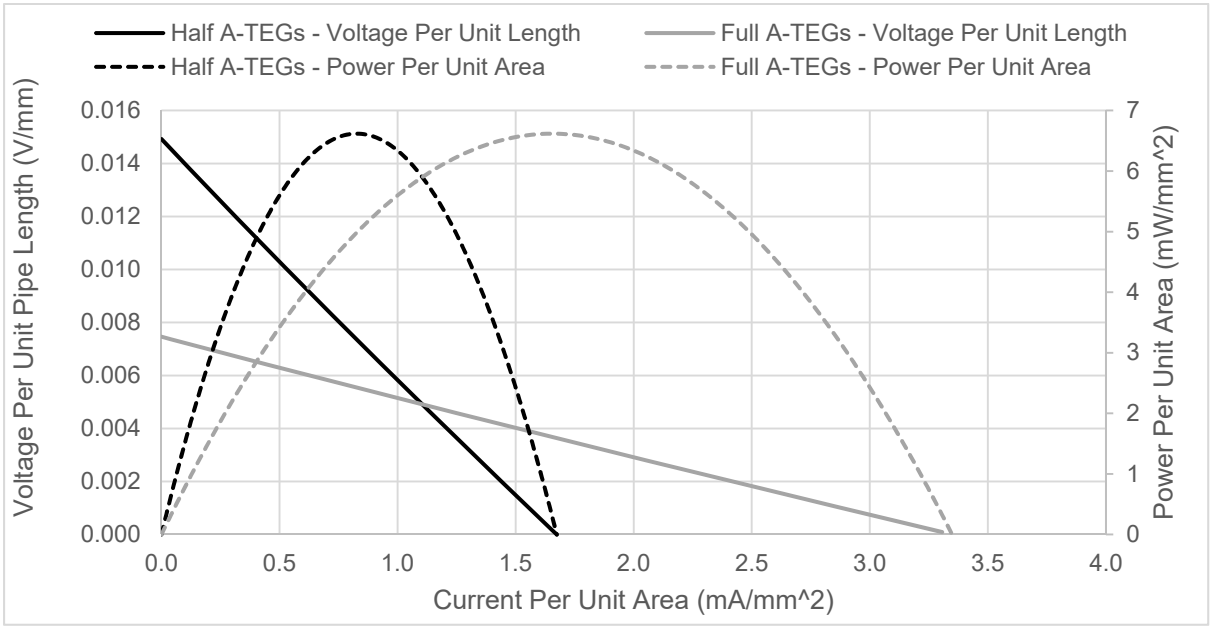

Fig.(5.1) – Comparison between power per unit area and voltage per unit pipe length of half A-TEGs and full A-TEGs by varying the TEG external load.

5.4. Effect of TEG dimensions on performance

The TEG dimensions is one of the important design parameters that affect the annular TEGs performance in a heat exchanger. By changing dimensions, the TEGs thermal conductance and electrical resistance change accordingly which alter the TEGs thermal and electrical performance.

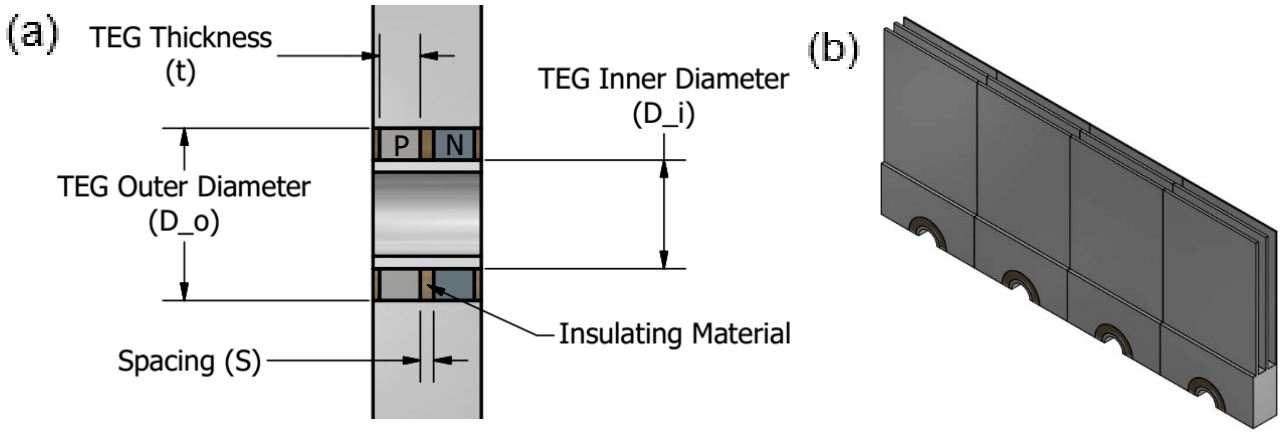

Fig.(5.2) – a) Half A-TEG couple integrated in a multi-row heat exchanger element – b) Isometric view of multi-row heat exchanger element with half A-TEGs

For a fixed heat exchanger design and the TEG design shown in Fig.(5.2), the TEG outer diameter can affect the heat flow and the TEG junctions temperatures due to the low thermal conductivity of the TEG material. By changing the TEG thickness, the TEG electrical resistance which affects the current output and the number of TEG couples that can be fitted per unit length of pipe. The effect of annular TEGs dimensions as the TEG diameter ratio (outer to inner diameter) and thickness is studied on the performance of a single row heat exchanger operating under conditions listed in section (4.3.1). The TEG performance will be presented per unit inner surface (cold-side) area as it remains fixed by keeping the pipe diameter constant.

5.4.1. Effect of changing the annular TEG diameter ratio

The diameter ratio is the ratio of the TEG outer to inner diameter which is an important parameter that affects TEGs performance in a heat exchanger. It directly affect the TEG thermal and electrical resistances. For annular TEGs integrated in a heat exchanger with a fixed inlet temperatures and flow rates for gas and water and fixed thermal resistance of the heat exchanger material, the temperature difference across the TEG junctions is largely affected by the diameter ratio since it controls the TEG thermal resistance. Theoretically the temperature difference ranges from zero, at a diameter ratio equal to one, to an asymptotic value equals to the global temperature difference which is the temperature difference between the gas and water inlets as the diameter ratio goes to infinity.

Since the voltage output is a function of the temperature difference, as the diameter ratio increases, the voltage output increases as shown in Fig.(5.3). The current reaches a maximum value at a low diameter ratio but continue to drop as diameter ratio increases for fixed thickness due to the increase of the electrical resistance. The maximum value of current depends on electrical resistances as conductors and contacts resistances which are fixed during the analysis.

As a result, the TEG power output reaches a maximum value as the diameter ratio increases for a fixed thickness as shown in Fig.(5.4). A similar effect was also reported in literature [3], [6], [7] by varying the flat TEG leg length for a fixed thermal resistance applied on the hot and cold side between fixed temperature heat source and sink. The diameter ratio at maximum power is associated with an increased current output as shown in Fig.(5.3) that can further be controlled by varying the TEG thickness.

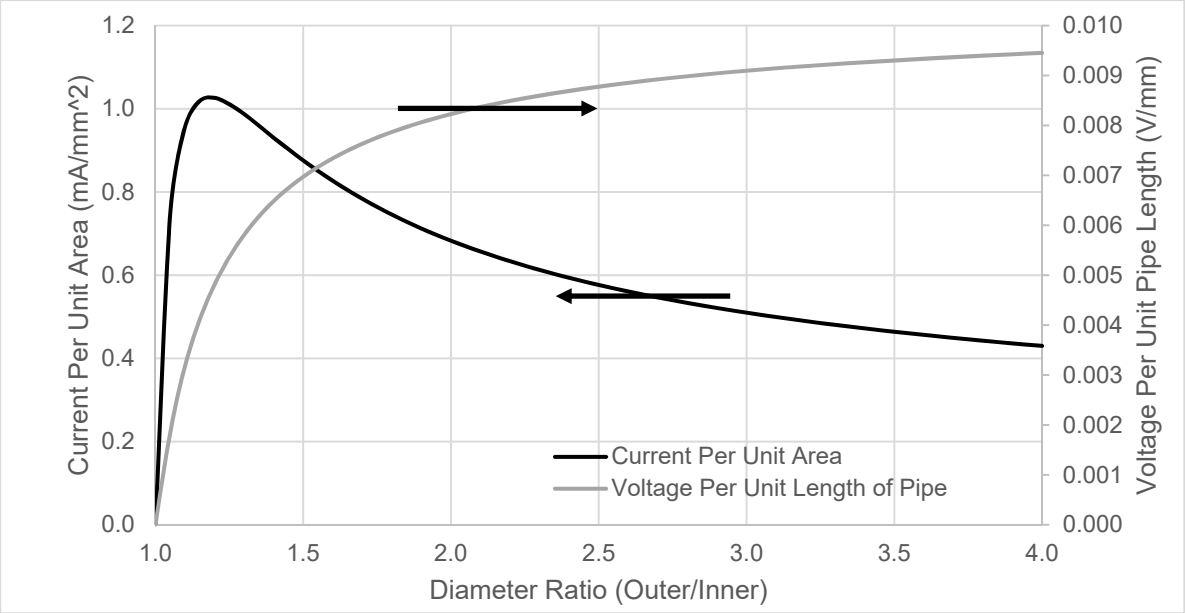

Fig.(5.3) – Current per unit area and voltage per unit pipe length of half A-TEGs at maximum power for different diameter ratios (Outer/Inner).

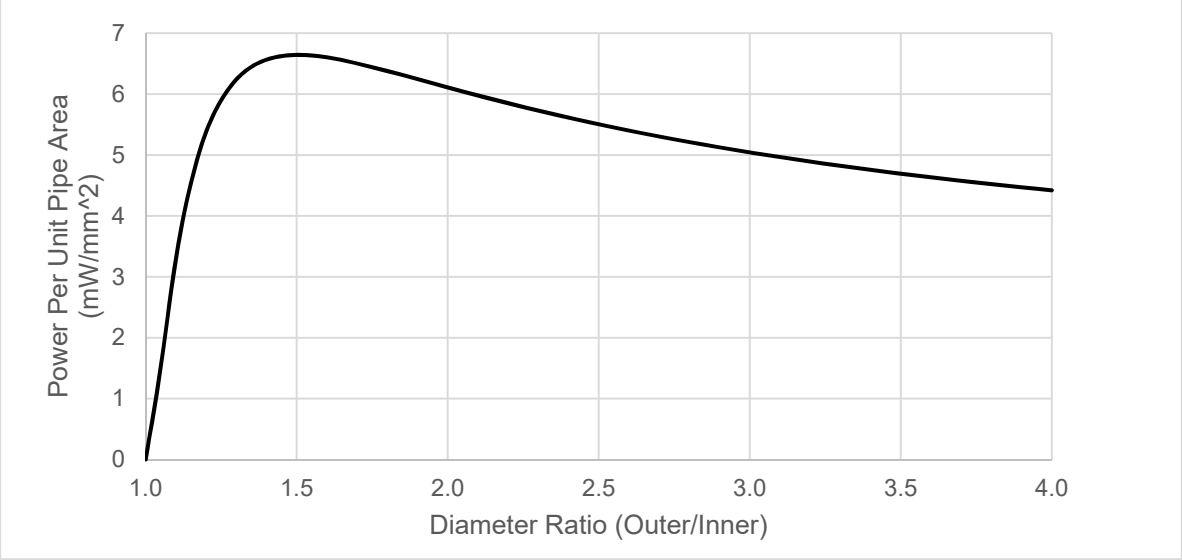

Fig.(5.4) – Maximum power output per unit area of half A-TEGs for different diameter ratios (Outer/Inner).

5.4.2. Effect of changing the annular TEG thickness

For a fixed pipe length in a single row heat exchanger assembly, the TEG thickness controls the current output, as it directly affects the TEGs electrical resistance, as well as the heat flow due to the insulating material that is used to fill the 1 mm spacing between TEGs. The effect of the insulating material shows at small thicknesses of the TEGs as its thermal resistance becomes more effective.

The TEGs power output depends on thickness as shown in Fig.(5.6). By varying N-type TEG thickness, while keeping the P to N thickness ratio constant, it is shown that at small thickness (< 1 mm for the N-type ring), the power output drops as the TEG electrical and thermal resistance increase which causes the heat flow to decrease due to insulation used between the TEGs. In Fig.(5.5), the voltage output increases due to the increased temperature difference as the 1 mm spacing between TEGs affects the heat flow at low thicknesses due to insulation. Theoretically at $t_N = 0$, the voltage would reach a maximum value as the temperature difference maximizes due to the insulating material used between TEGs, there will be no TEG material at this case and the current output reaches zero.

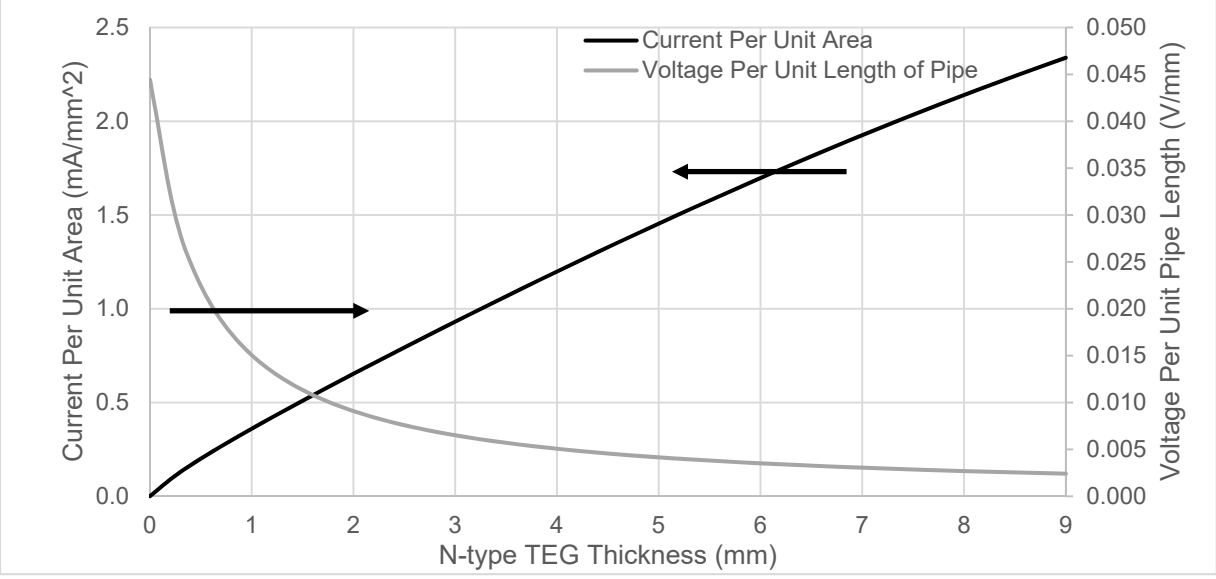

Fig.(5.5) – Current per unit area and voltage per unit pipe length of half A-TEGs at maximum power for different N-type TEG thicknesses.

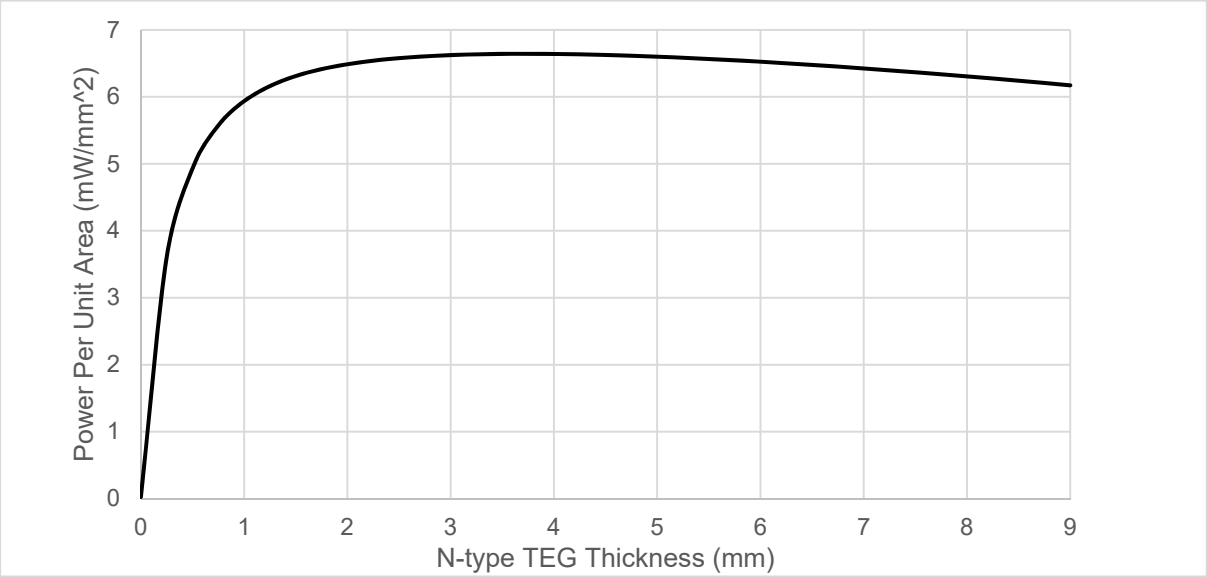

Fig.(5.6) – Maximum power output per unit area of half A-TEGs for different N-type TEG thicknesses.

As the TEGs thickness increases, the power output reaches a maximum at t_N = 4 mm for this case, then it drops as the TEG thermal resistance decreases compared to the spacing material and the Peltier effects become more effective. The temperature difference across the TEG decreases as a result due to increased thermal conductance as well as the gas average temperature as more heat is being absorbed. By increasing the TEGs thickness, the number of TEGs can be fitted per unit length of the pipe decreases which affects the voltage output as well.

5.4.3. Effect of changing the annular TEG P to N thickness ratio

The thickness ratio between the P and N rings can differ according to three different configurations, the thickness ratio depends on the material properties which vary between the TEG P and N materials as discussed in Section (3.2.2.2). The three configurations are Maximum power (MP), Maximum efficiency (ME) and Equal thickness (EQ) which are calculated to be:

$$\left(\frac{t_P}{t_N}\right)_{MP} = 1.29 \ , \ \left(\frac{t_P}{t_N}\right)_{ME} = 1.34 \ , \ \left(\frac{t_P}{t_N}\right)_{EQ} = 1 \quad at \ \bar{T} = \frac{T_{Gas} + T_{Water}}{2}$$

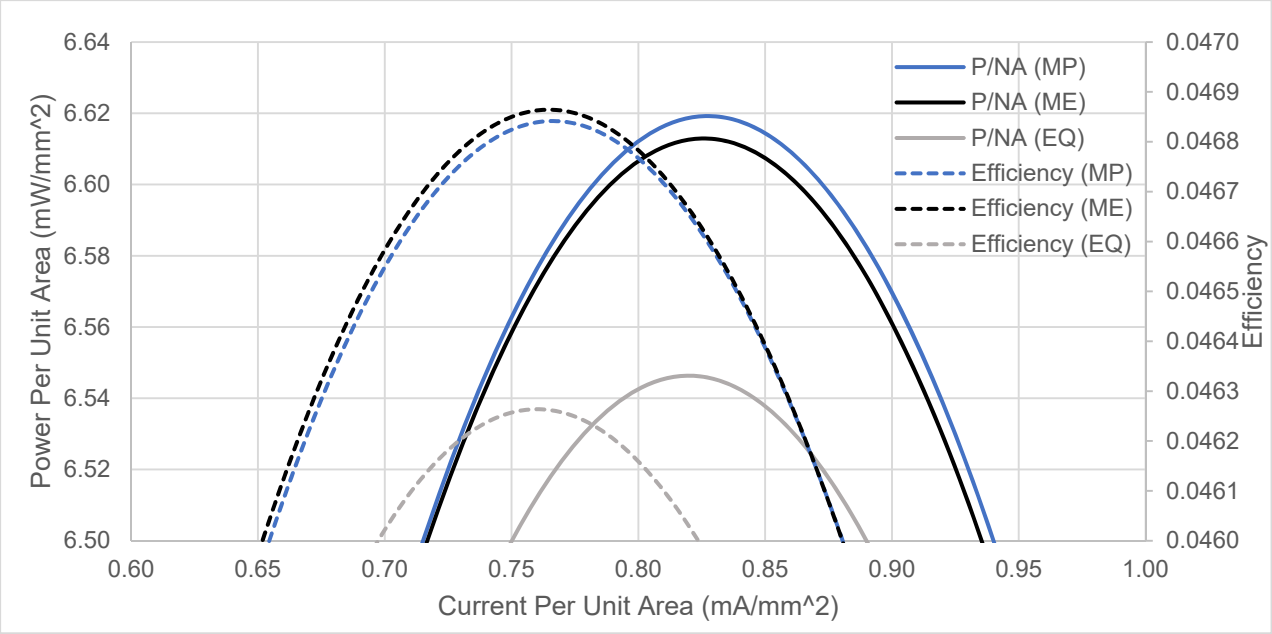

Fig.(5.7) – Power output per unit area and efficiency of half A-TEGs for different P to N thickness ratios by varying the TEG external load.

By keeping the TEG P and N couple length constant and changing the thickness ratio for each configuration, the results in Fig.(5.7) show that the differences in power output and efficiency between MP and ME configurations are small since the thickness ratios in both configurations are very close. The maximum power can be achieved for MP configuration compared to EQ configuration. The MP configuration will be used for the annular TEG design to meet objectives.

5.5. The electrical circuit for TEG rows in a multi-row heat exchanger

In a multi-row heat exchanger assembly with integrated annular TEG rows, the heat is transferred from the gas as it flows through the TEG rows to the water. The temperature of the gas decreases and the water increases as they exit every row which cause the heat source and sink temperatures of the TEGs change per row as well as temperature difference across the TEGs per row.

The performance of every TEG row differs according to the gas and water temperatures which affects the total performance of the TEGs in the heat exchanger due to temperature difference between rows. The electrical connection between the rows will affect the total power output characteristics as voltage and current as well as the losses due to the mismatch. The effect of the electrical connection will be studied for series and parallel connection and compared with the total maximum power output of every individual row.

5.5.1. Temperature mismatch between TEG rows

For a heat exchanger consisting of four TEG rows with equal TEG dimensions for all rows and fixed inlet gas and water temperatures and flow rates, the axial temperature profiles of gas and water are shown in Fig.(5.8). These profiles affect the temperature difference across the TEGs in each row which create a temperature mismatch between TEGs and thus different power output from each row.

In this system of connected TEGs, the outlet temperatures of gas and water from every row depend on the TEGs power output due to Peltier heat which increases the heat conductance through the TEGs.

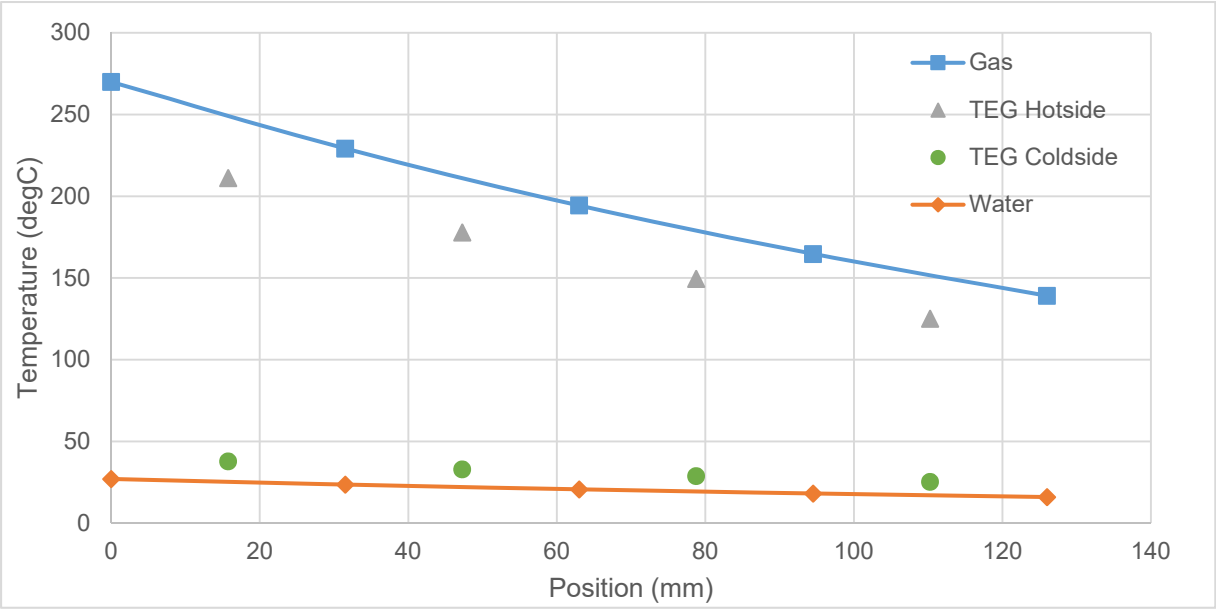

Fig.(5.8) – The temperature variation of gas, water, TEG hot-side and cold-side surfaces along the heat exchanger length using numerical model.

Depending on the electrical connection configuration between rows, the maximum output of the full system of connected TEG rows will differ from the total maximum output of individual rows. In the connected system, the TEG rows will be operating off their maximum individual power output. The maximum power of individual TEG rows is calculated assuming that each row is connected to a separate MPPT system and is operating at its peak power output and the maximum total power will be summation of individual rows power outputs. The effect of the electrical

connection between TEG rows on the power characteristics is studied and compared against the maximum total power of individual rows.

5.5.2. Effect of electrical configuration between rows in a multi-row heat exchanger

For a heat exchanger assembly consisting of four rows, series and parallel electrical configurations are compared for fixed heat exchanger design with equal TEG dimensions for all rows. The variation of power output between the TEG rows, as shown in Fig.(5.9a) and Fig.(5.9b), is a result of the temperature profiles, shown in Fig.(5.8), which affects each TEG row hot-side and cold-side temperatures.

Fig.(5.9a) shows the total power and voltage outputs of the heat exchanger rows for a series connection in which each row voltage output is added for the same value of current, the results show, for series connection, a total maximum power of 391 W at a voltage of 52 V and current of 7.5 A.

Fig.(5.9b) shows the total power and voltage outputs of the heat exchanger rows for a parallel connection in which each row current output is added for the same value of voltage, the results for parallel connection shows a total maximum power of 377 W at voltage of 12.7 V and current of 30 A.

By comparing the results of both cases with the total maximum power output of individual rows which in this case is equal to 396 W, the series connection showed minimal loss of power of 1.1 % due to temperature mismatch compared to the parallel connection which showed approximately 5 % loss of power. In series connection, the operation point of each row is closer to its maximum power point than that in parallel connection. The same effect was found in literature [55] where parallel connection between temperature mismatched TEGs yielded higher percentage of loss in power than series connection.

Series connection is preferred in this case compared to parallel connection as it provides lower current output and higher voltage, however the disadvantage of using series connection is the reliability of the system in case of failure of one TEG module in a heat exchanger which would cause total loss of the heat exchanger power output. On the other hand, a module failure in a parallel connection, the system would continue to produce partial power.

(a)

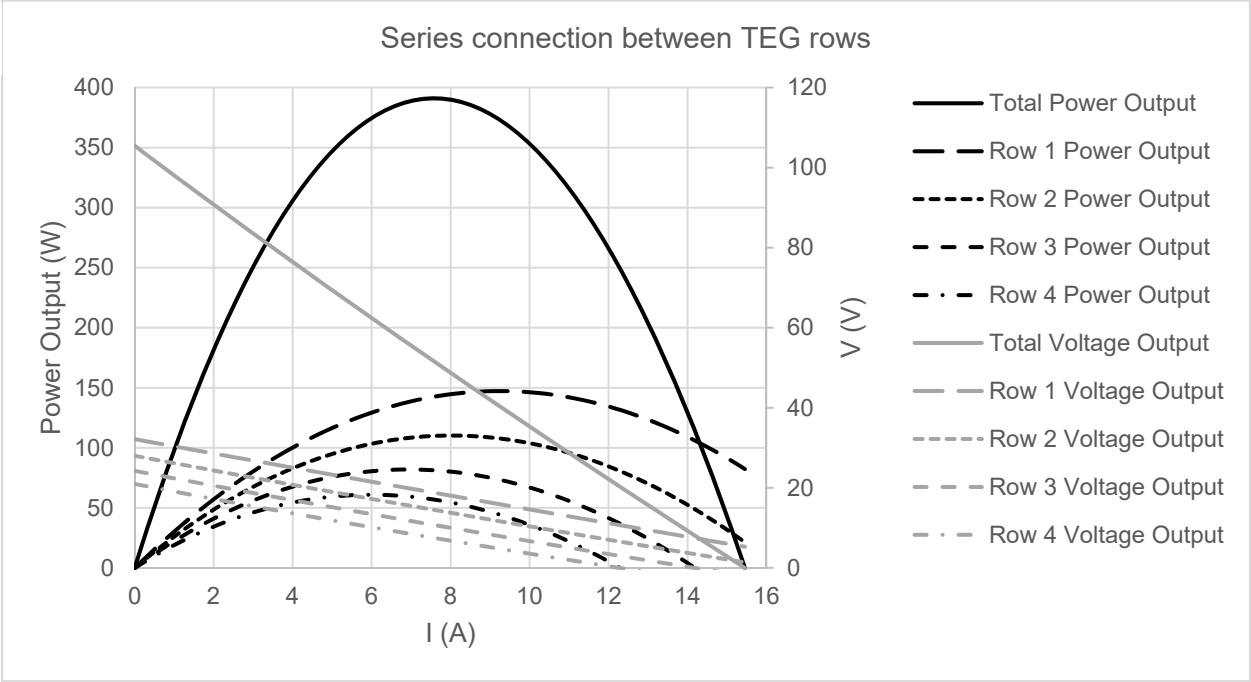

(b)

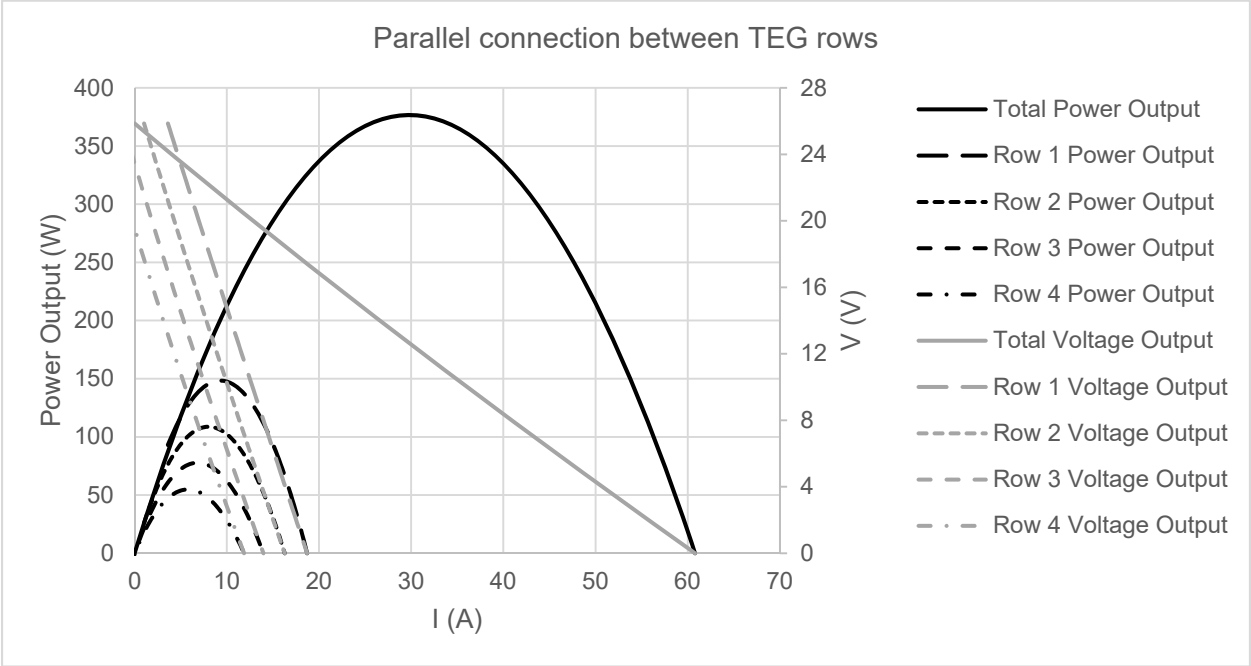

Fig.(5.9) – Total power output, total voltage output and each row power and voltage outputs of a heat exchanger consisting of 4 rows of half A-TEGs connected in for: a) Series – b) Parallel - by varying the external load.

5.6. Effect of axial conduction in metal between TEG rows in a multi-row heat exchanger

The design of a multi-row heat exchanger has numerous parameters that can affect the performance of TEGs in each row. These parameters include the heat transferred between rows in form of conduction in the metal of the heat exchanger structure. Since the heat exchanger is discretized into number of rows equivalent to the TEG rows integrated in the design, these rows can be either separated, which means no axial heat conduction is allowed between rows, or connected to each other through the metal of the hotside fins base. The axial conduction between rows can affect the temperature profiles on gas and water sides and the temperature differences across the TEG rows which is often neglected in literature [39], [40].

5.6.1. Effect of axial conduction on gas temperature profiles

The conduction in metal between rows can significantly affect the gas temperature profile as it flows through the fins. A heat conduction component in the gas direction was added to the numerical model to simulate the effect of conduction between the rows. The results are compared with an ANSYS model for a heat exchanger element to test the model assumptions for conduction as shown in Fig.(5.10). The gas temperature profiles are compared at open circuit, i.e. no thermoelectric effects, to verify the convection and conduction components in the numerical model for a heat exchanger consisting of four rows. Details of the ANSYS model used are presented in Appendix (C).

Same conditions for the water side, convective heat transfer coefficients and average temperatures of water for each, were used in both models. The gas properties is assumed constant and evaluated at average temperature between inlet and outlet for both cases. The material properties of the heat exchanger and TEGs used are the same for both cases and assumed constant with temperature. All thermal contact resistances are neglected in this comparison. For the ANSYS model, The element size was selected to be $5 \times 10^{-4}\ m$ as a compromise between accuracy and computational cost. For the numerical model, the thermal resistance of the fins base metal between rows is assumed to be one dimensional, thus neglecting its thermal resistance in y-direction, and calculated in the z-direction center to center between each two rows with neglecting the space removed for TEGs placement as discussed in section (4.3.2.2).

By simulating the heat exchanger element shown in Fig.(5.10) using an ANSYS model and comparing the results with the numerical model for the same heat exchanger assembly under the same conditions of gas inlet temperature and flow rate, TEG dimensions and material properties, and same water side conditions, the results shows the effect of metal conduction between rows on the TEG hot side temperature profiles in Fig.(5.11).

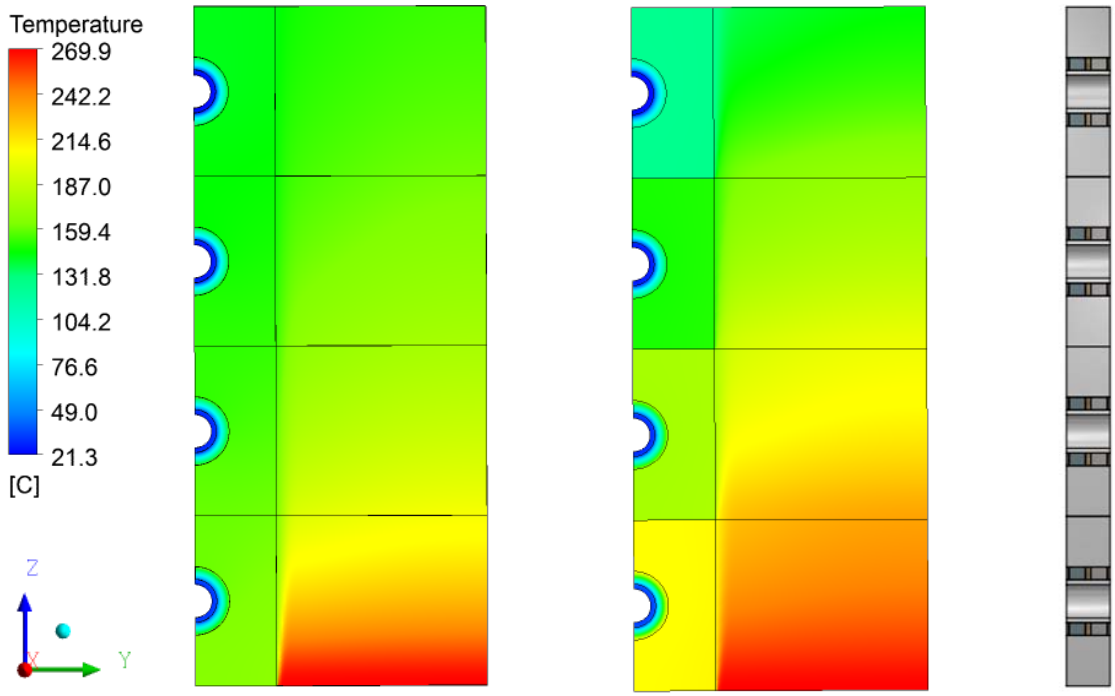

Fig.(5.10) – The variation in temperature of the gas and the fins base metal along the flow direction (Z-direction) in case of: a) With axial conduction – b) No axial conduction / On the left, the heat exchanger element used in ANSYS model.

The gas temperatures in the ANSYS model is averaged at the outlet of each row and the hot side temperature is also obtained by averaging the fins base metal temperature at the center of each row to be compared with the results of the numerical model. The results are compared for two cases, with/without metal conduction, and plotted against the length of the heat exchanger in the direction of gas flow. The radiation between fins in consecutive rows is neglected in both models as the view factor between fin surfaces is found to be less than 0.01 in addition to the low emissivity of the fin material.

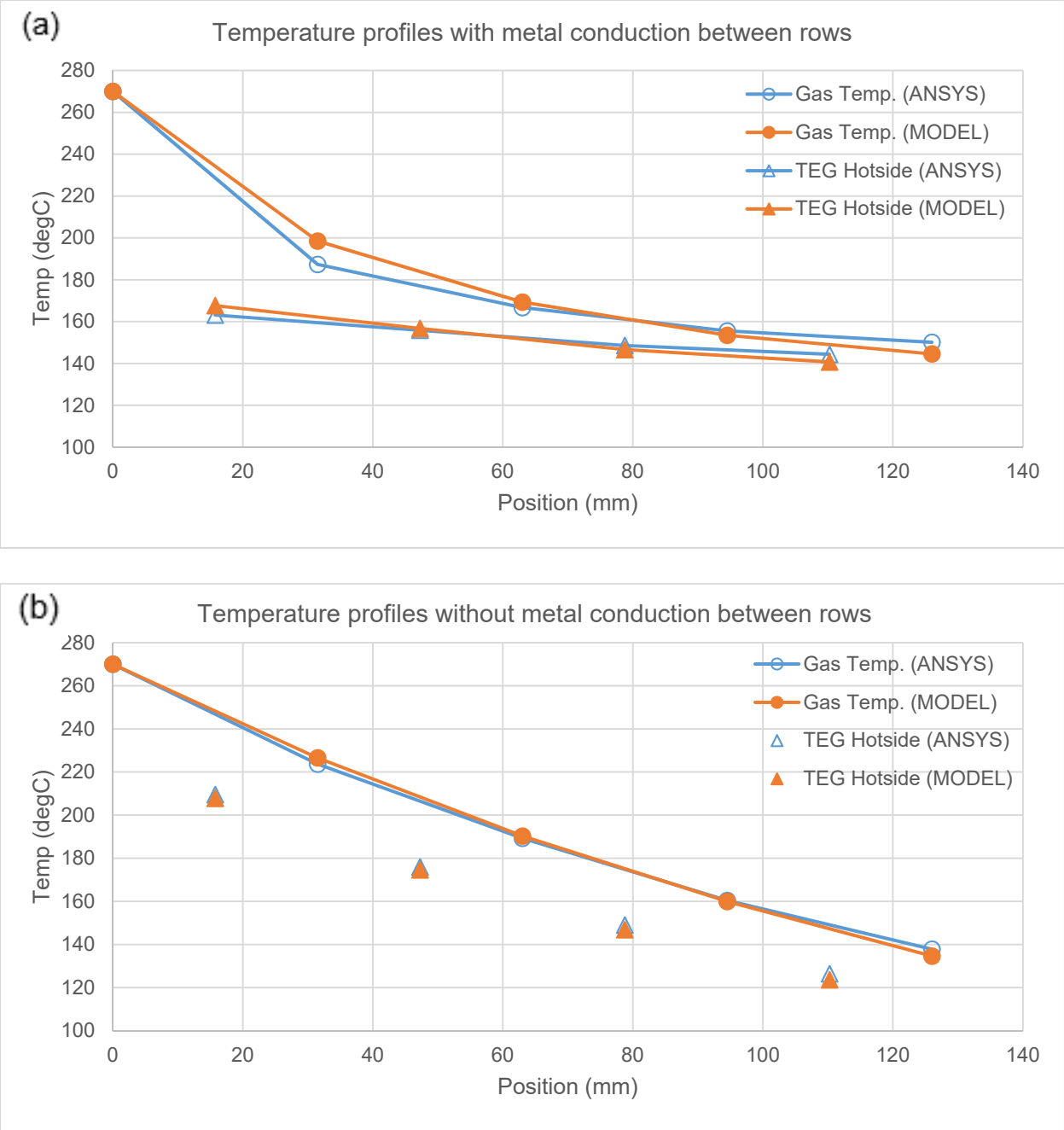

Fig.(5.11) – The variation in average temperature of the gas and the fins base metal profiles along the heat exchanger length in case of: a) With axial conduction – b) No axial conduction

By comparing results for both cases shown in Fig.(5.11a) & Fig.(5.11b), the results of the numerical model show a good agreement with the ANSYS model for the gas temperature and the TEGs hot side profiles at open circuit. The deviation between the models is due to the entrance effects in the gas flow which is captured in the ANSYS model, but neglected in the numerical model as a fully developed correlation was employed. In addition, the low number of discretization

elements in the numerical model led to this inaccuracy as the temperature profile of the gas was assumed linear across each row and the average gas temperature was considered.

The results show the effect of the assumptions used in the numerical model. It also shows the importance of the metal conduction component in the gas direction (z-direction) and its impact on the TEG hot side temperatures which in turn would significantly affect the power output of the TEGs, as discussed in details below.

5.6.2. Effect of axial conduction on TEGs performance

The performance of TEGs is studied under the effect of the metal conduction in the design of the heat exchanger. The results, shown in Fig.(5.12), shows that higher temperature difference is available for the first two rows at open circuit and more energy is recovered in the case without conduction as shown in Fig.(5.13).

The conduction in the fins base causes the temperature difference of the TEG rows to even out compared to the case without conduction, as shown in Fig.(5.12), which shows a larger variation in TEG rows in the gas direction and a significant increase in temperatures of the 1st and 2nd rows compared to the decrease in temperature of the 4th row. The gas outlet temperature in case of no conduction is lower which shows that more energy is recovered in this case compared to the case with conduction.

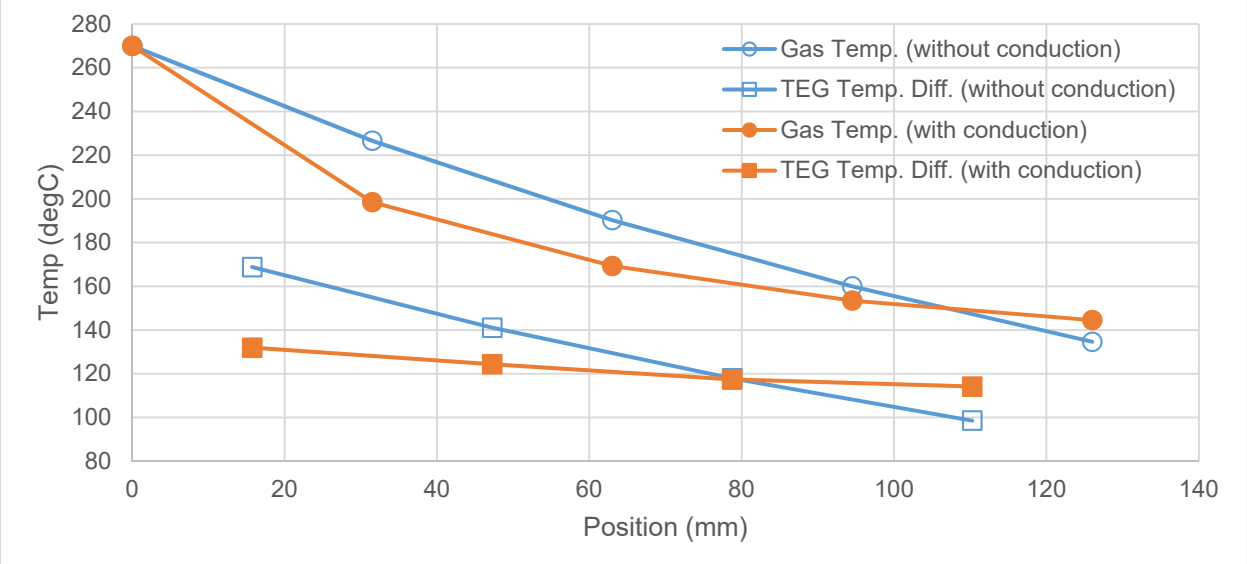

Fig.(5.12) – Comparison between the numerical model results for the average gas temperature profile and the TEG temperature difference in case of with and without axial conduction

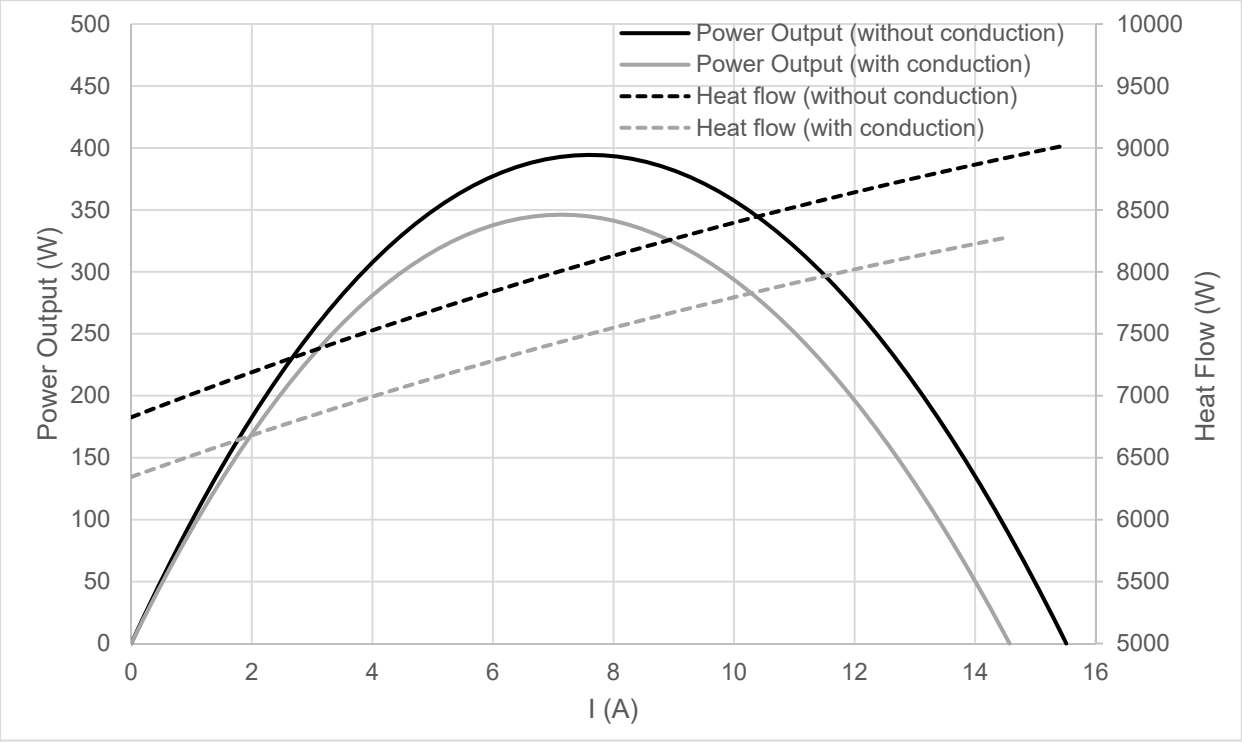

Fig.(5.13) – Comparison between the TEG total power output and heat flow in case of with and without axial conduction by varying the external load

The power output of the case without conduction is higher than that of the case with conduction as shown in Fig.(5.13) which is due to that more heat is recovered in this case since higher gas temperatures are available for rows from 2nd to 4th from comparison of the temperature difference profiles in Fig.(5.12). The results show the importance of the metal conduction in the heat exchanger design with integrated TEGs since the power output can be improved by insulating the TEG rows in the direction of the gas stream as well as increased heat flow which is important for waste heat recovery applications.

5.7. Design criteria for integrated annular TEGs in a multi-row heat exchanger

The performance of annular TEGs integrated in a heat exchanger is influenced by the key design parameters that have been discussed in the previous sections of this chapter as TEG design parameters including TEGs arrangement, dimensions and electrical configuration, and other heat exchanger design parameters such as axial conduction. For a fixed multi-row heat exchanger design, and gas and water inlet temperatures and flow rates, and based on the previous analysis, several design elements are considered. They include the i) half annular TEG design, ii) thickness ratio for maximum power, iii) series connection between TEG rows and iv) insulating between

rows to impede axial conduction in the metal, which can be chosen to satisfy the design objectives that maximizes performance.

However, the annular TEGs dimensions for a multi-row heat exchanger, as diameter ratio and thickness, affect the performance as they can change electrical and thermal resistance of the TEGs as well as the current and voltage output. Through a parametric analysis of the TEGs dimensions, a map was developed to be used as a tool to guide the design of annular TEGs. The parametric analysis map can be used to determine the TEGs dimensions for a heat exchanger with design constraints related to the field of application.

The objective is to provide the criteria to determine the annular TEGs dimensions that maximize the power output and reduce the amount of material used under certain current output constraint. The heat exchanger design and number of rows, material properties as well as other operation parameters, as gas and water inlet temperatures and flow rates, will be kept constant during this analysis.

The analysis is done for a heat exchanger, consisting of four rows of pipes for water fitted with half annular TEGs modules, each consists of eight columns of fixed length. The inlet gas of temperature is 270 °C with a mass flow rate of 0.06 kg/s. An inlet water of temperature 16 °C and flow rate of 10 LPM is connected to a loop as shown in Fig.(5.14). The operating conditions and design are discussed in details in Section (4.3).

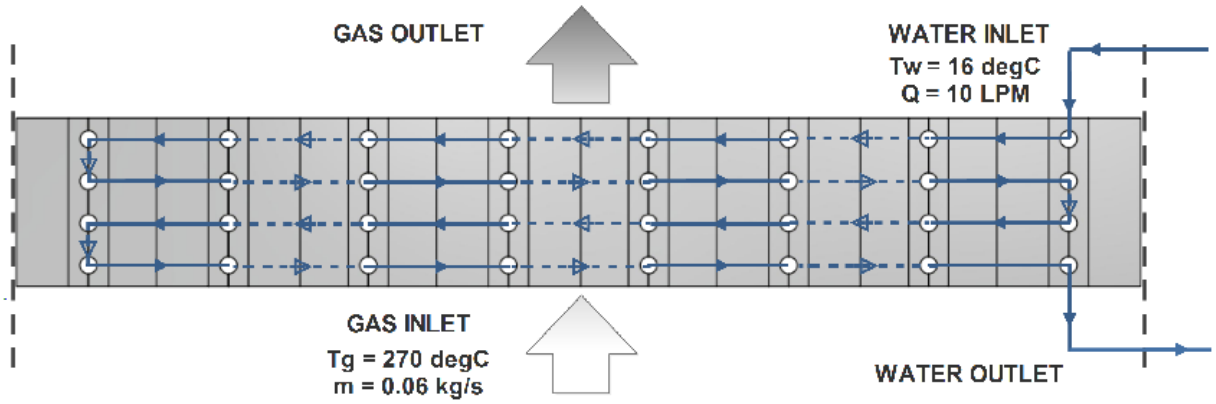

Fig.(5.14) – Schematic for the heat exchanger design listing the operating conditions.

Since the length of pipes in each row is fixed and by changing dimensions as the TEG thickness, the number of TEGs fitted per row will vary accordingly. Series connection between TEG rows will be used for this analysis and the rows are insulated from each other to limit metal conduction in the direction of gas stream, and maximum power configuration for the thickness ratio is used.

5.7.1. Dimensions map for annular TEGs in one row heat exchanger

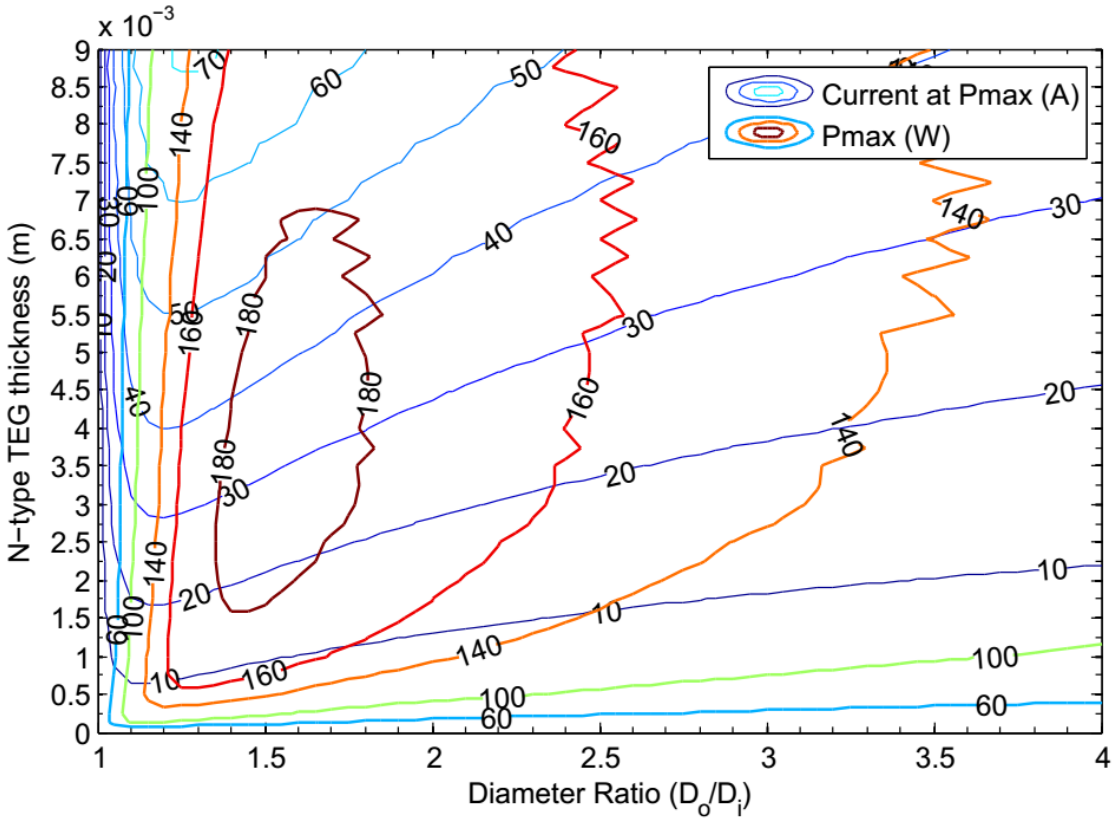

Fig.(5.15) – Dimensions map for one row heat exchanger with half A-TEGs.

By combining the effects of TEG diameter ratio and thickness on performance that was discussed previously in Section (5.4), a map is developed in Fig.(5.15) that shows the contours of maximum power and current output at maximum power calculated using the numerical model using temperature dependent TEG material, gas and water properties. For a set of diameter ratios and N-type TEG thickness, the results show the maximum power available for a single row heat exchanger which guides the choice of TEGs dimensions at these conditions.

It is important to note that the fluctuations in the power output contours at higher values of thickness is due to the abrupt variation in the number for TEGs by varying the thickness since they

are fitted in fixed length modules per row. This causes the number of TEGs to fluctuate by a value of half TEG couple which contributes to the jagged contours of the power output shown in the map.

5.7.2. Dimensionless parameter (β) relating annular TEGs diameter ratio and thickness

For a fixed heat exchanger design with fixed thermal resistance, it is required to determine a value for the annular TEGs thermal resistance that maximizes the power output. Since the dimensions affect the thermal and electrical resistances of annular TEGs, it was important to find a relationship between the TEG diameter ratio and thickness for maximum power output of this heat exchanger design.

$$P = \frac{\alpha^2\left(\bar{T}_g - \bar{T}_w\right)^2}{r} \times \frac{m_L}{(m_L+1)^2} \times \left(\frac{1}{1 + K_T\, R_{th,HX}}\right)^2 \quad (5.1)$$

$$For\ maximum\ power\ \rightarrow K_T = \frac{1}{R_{th,TEG}} = \frac{1}{R_{th,HX}} \quad (5.2)$$

According to the simplified model for TEGs in a heat exchanger in Section (3.2.3.1), the TEG thermal conductance for maximum power output is found to be as shown in eqn.(5.2). This was obtained using eqn.(5.1) by neglecting the Peltier and Joule heating effects, and the contacts and conductors electrical resistance. It shows that a certain value of TEG thermal conductance can achieve a maximum power output. However, eqns.(5.1 and 5.2) would lead to inaccurate results as discussed earlier in Section (2.4.2). Using the numerical model, the optimum TEG thermal resistance can be determined more accurately taking into consideration the factors neglected by the simplified model. The thermal and electrical resistance of half A-TEG module, in one row heat exchanger consisting of (N_{TEGs}), can be written as:

$$K_T = \frac{N_{TEGs}\pi}{\ln(\frac{D_o}{D_i})}\left(\lambda_n t_n + \lambda_p t_p\right)$$

$$= 2\pi L_{pipe}\left(\lambda_n + \lambda_p(t_p/t_n)\right) \times \frac{1}{\ln(\frac{D_o}{D_i}) \times \left(\left(1 + \frac{t_p}{t_n}\right) + \frac{2S}{t_n}\right)} \quad (5.3)$$

$$r_T = \frac{N_{TEGs} \ln\left(\frac{D_o}{D_i}\right)}{\pi}\left(\frac{\rho_n}{t_n}+\frac{\rho_p}{t_p}\right) = N_{TEGs}\,\frac{\left(\rho_n+\frac{\rho_p}{(t_p/t_n)}\right)}{\pi}\times\frac{\ln(\frac{D_o}{D_i})}{t_n} \quad (5.4)$$

$$N_{TEGs} = \frac{2\,L_{pipe}}{L_{couple}} = \frac{2\,L_{pipe}}{t_n\left(1+\frac{t_p}{t_n}\right)+2S} \quad (5.5)$$

By substituting eqn. (5.3, 5.4 & 5.5) in eqn. (5.1) with neglecting the TEG spacing gap thermal resistance, and the electrical and thermal contact resistances, all dimensions parameters can be grouped in one dimensionless parameter (β) which affects the power output as shown.

$$P = \frac{2\pi L_{pipe}\alpha_c^2\left(\bar{T}_g - \bar{T}_w\right)^2}{\left(\rho_n+\frac{\rho_p}{(t_p/t_n)}\right)}\times\frac{m_L}{(m_L+1)^2}\times\frac{\beta}{\left(\beta+2\pi L_{pipe}\left(\lambda_n+\lambda_p(t_p/t_n)\right)R_{th,HX}\right)^2} \quad (5.6)$$

$$where \quad \beta = \ln\left(\frac{D_o}{D_i}\right)\times\left(\left(1+\frac{t_p}{t_n}\right)+\frac{2S}{t_n}\right) \quad (5.7)$$

The result shows the dependence of the power output on the dimensionless parameter (β) which is a function of the diameter ratio and the N-type TEG thickness. The spacing between the TEGs is kept constant and the P-type TEG thickness varies by changing the thickness of the N-type ring according to the constant (MP) thickness ratio.

The results shows that for constant value of parameter (β), the TEG thermal resistance can be kept constant as shown in eqn.(5.3) while varying the TEG diameter ratio and thickness accordingly. The value of β, for a given heat exchanger design, corresponds to the TEG thermal resistance that maximizes the power output. This specific value of β can be used as relationship between the TEG diameter ratio and thickness for the annular TEG design.

For fixed TEG thicknesses and by varying the values of β i.e. varying the diameter ratio, Fig.(5.16a) shows that the maximum power output at any TEG thickness occurs when the parameter (β) is equal to 1.25 under the specified conditions for the heat exchanger described earlier. Fig.(5.16 b) shows that for fixed TEG diameter ratios and by varying the values of β i.e. varying the TEG thickness, the power output reaches a maximum value at (β) approximately equals to 1.25 with an error less than 5 % in the estimation of the maximum power output at a diameter ratio of 1.3 as shown in Fig.(5.16 b). The error is due to simplifying assumptions such as

neglecting the conductor and contact electrical resistances in the derivation of parameter (β) in eqn.(5.7) which is higher in case of varying β using the TEG thickness in Fig.(5.16 b) compared to the case in Fig.(5.16 a).

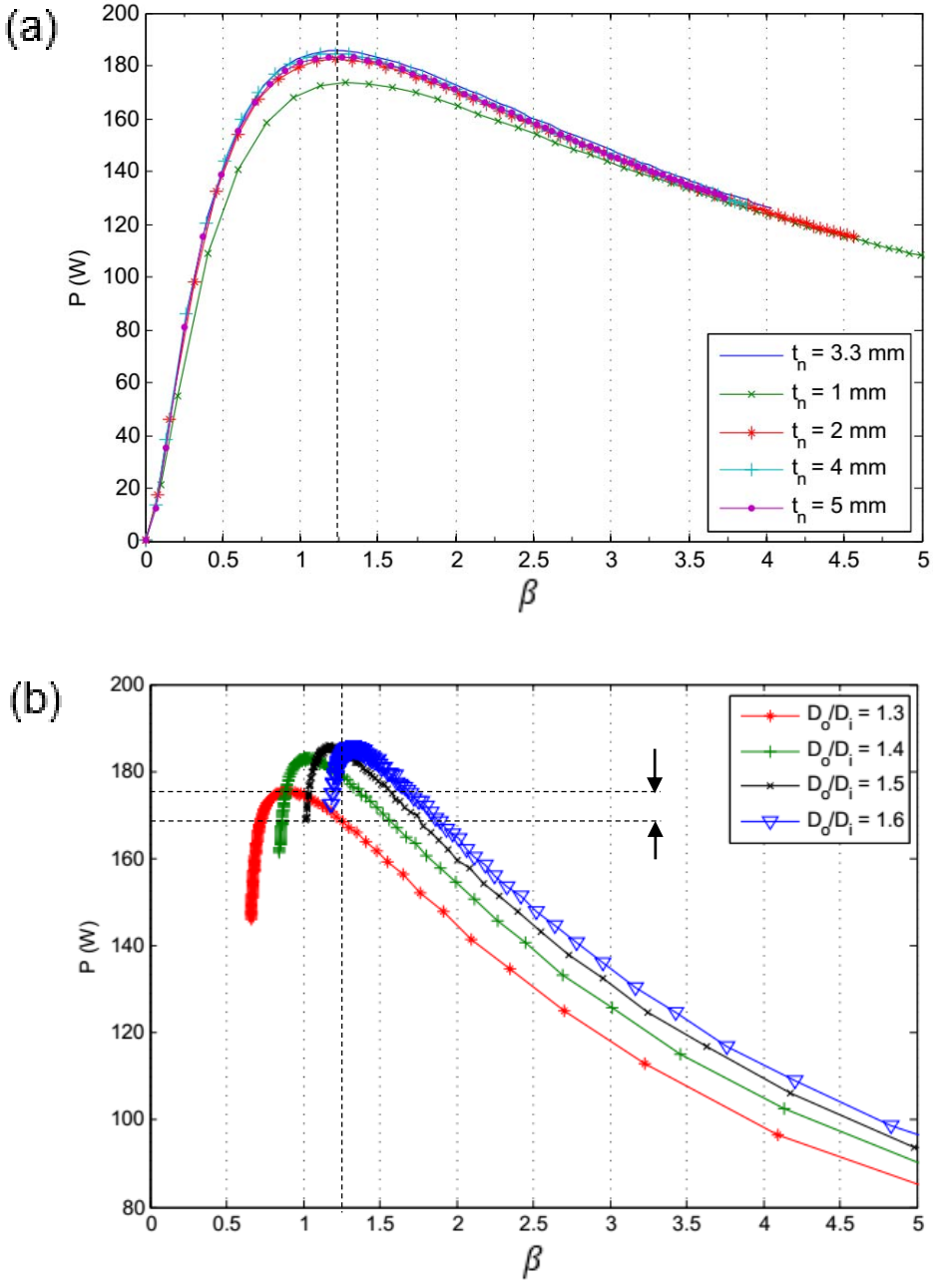

Fig.(5.16) – The variation of the power output with β for: a) Different fixed N-type TEG thicknesses – b) Different fixed diameter ratios

It is important to note that the optimum (β) cannot be predicted using eqn.(5.6). This is because that this equation is based on the simplified analysis which is not equivalent to the numerical model solution. The value of parameter (β) is affected by the thermal and electrical contact resistances and the average gas and water temperatures which indicates that the value of (β) will change between different rows in a multi-row heat exchanger.

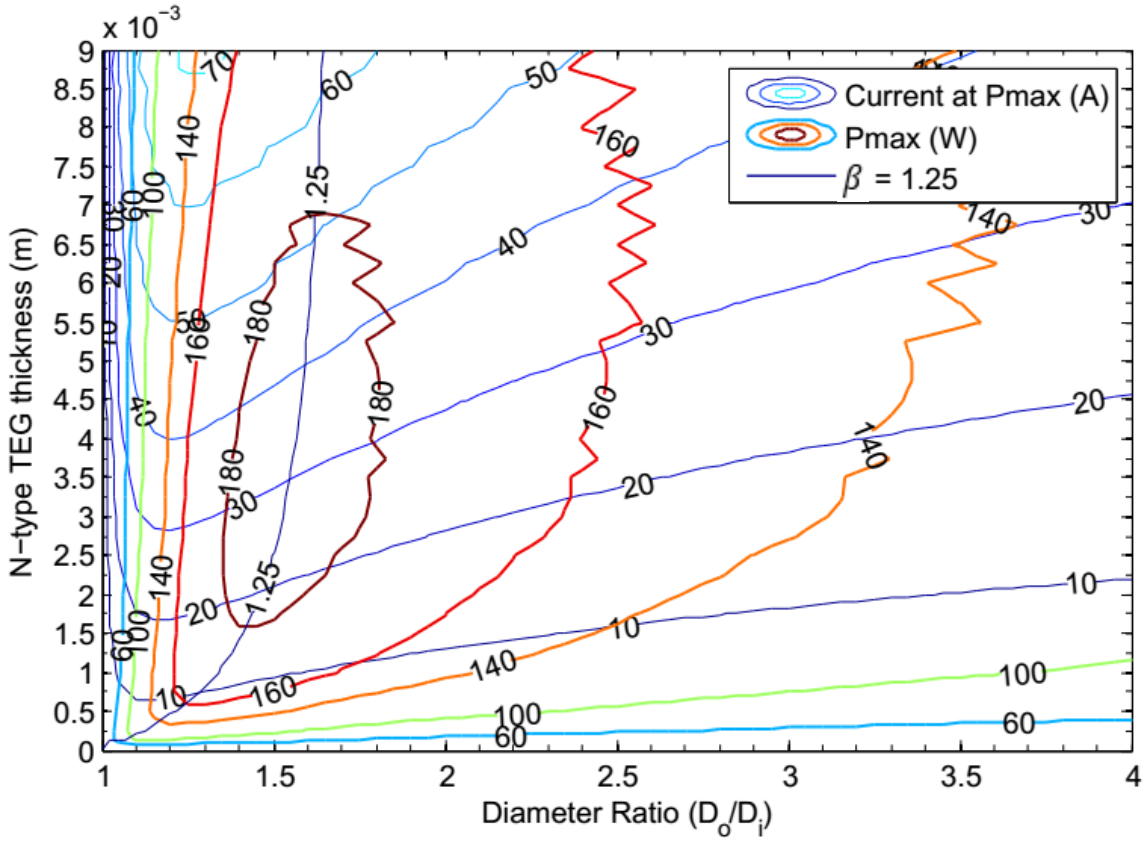

Fig.(5.17) – The dimensions map for one row heat exchanger with half A-TEGs with parameter (β)

As in Fig.(5.17), the results show that the parameter (β) provides a guide to locate the maximum power output region in the dimensions map as it provides a relation between the diameter ratio and the thickness. This map can be used, combined with a set of constraints, as a design criterion for annular TEG dimensions for fixed heat exchanger design and operating conditions. Similar results was found for flat TEG geometry, the optimum aspect ratio, which is TEG leg length (L) to area (A), was found by Freunek et al. [31] based on simplified analysis to be dependent upon heat exchanger thermal resistances, material properties and heat sink temperature.

5.7.3. Dimensions map for annular TEGs in a multi-row heat exchanger

The dimensions map for a heat exchanger consisting of four rows, connected in series, is shown in Fig.(5.18) obtained by using equal diameter ratios and thicknesses in all rows of the heat exchanger. The results show the contours of maximum power output and current for several TEG diameter ratios and thicknesses, a value of $\beta = 2.3$ was calculated for this map using the numerical results. The value of β for this setup is different than the case of a single row since it represents multiple rows connected in series with a temperature mismatch due to the gas and water temperature profiles.

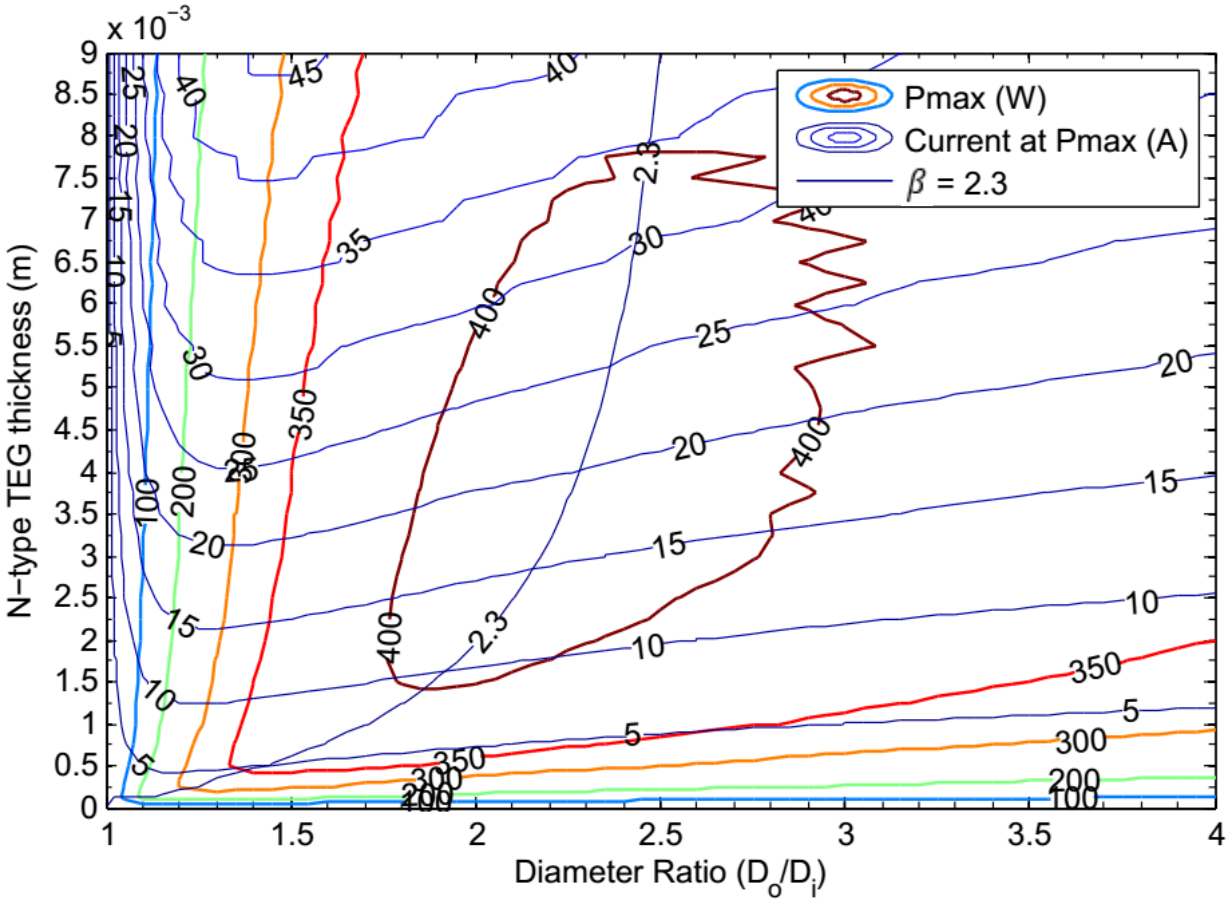

Fig.(5.18) – The dimensions map for four rows heat exchanger with half A-TEGs with parameter (β)

5.7.4. Using the dimensions map as a design criterion for annular TEG dimensions in a four rows heat exchanger

Considering the heat exchanger consisting of four rows under operating conditions as described in the previous section, it is required to select the annular TEG dimensions using the dimension map as a design criterion to maximize the power output of the heat exchanger under a certain current limit as main objectives. The parameter (β) will be used on the map to locate the maximum power output for any TEG thickness or diameter ratio in Fig.(5.19).

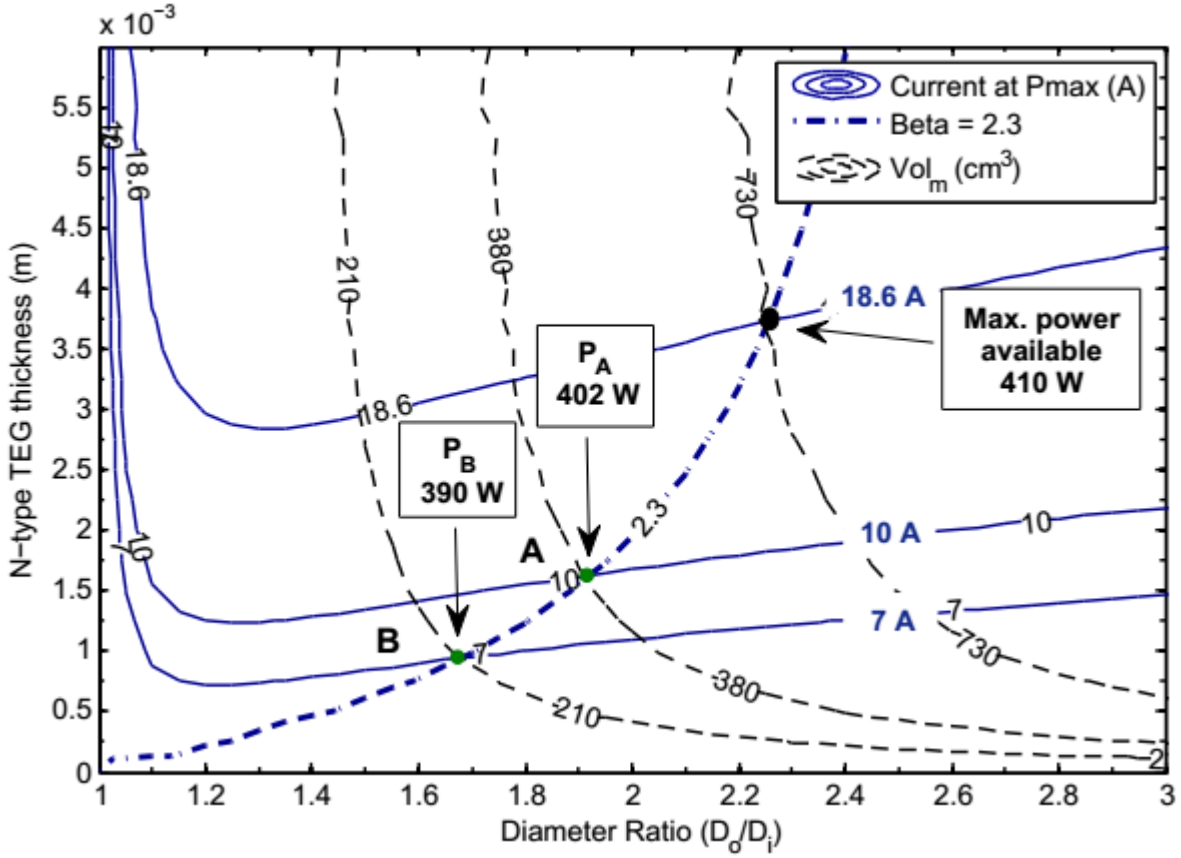

Fig.(5.19) – The dimensions map for four rows heat exchanger with half A-TEGs with parameter (β) and material volume contours.

Along the line ($\beta = 2.3$) in Fig.(5.19), by limiting the current at 10 A, the power output of the heat exchanger becomes 402 W which is equal to 98 % of the maximum power available (410 W). As a result, the current decreased by 46% from 18.6 A to 10 A and the material volume decreased by

48 % from 730 cm^3 (0.56 $\frac{W}{cm^3}$) to 380 cm^3(1.06 $\frac{W}{cm^3}$). The selected dimensions for point (A) is 1.6 mm and 2 mm for N-type and P-type TEG thicknesses and a diameter ratio of 1.9. By further decreasing the maximum current to 7A, the power output decreased to 390 W which is equal to 95 % of the maximum power available and the material volume decreased to 210 cm^3 (1.86 $\frac{W}{cm^3}$). The selected dimensions for point (B) is 1 mm and 1.3 mm for N-type and P-type TEG thicknesses and a diameter ratio of 1.7.

As a conclusion, the results show the benefits of limiting the current output which leads to increased power per unit volume of material used, improve the heat exchanger power output characteristics and increase the efficiency of the MPPT system. However, it should be noted that, although the maximum power output depends on the value of (β) in Fig.(5.16), lower values of (β) can reduce the heat exchanger power output under a current limit. It can significantly decrease the TEG diameter ratio allowing more heat to flow through the heat exchanger which can lead to more compact heat exchanger [36].

5.8. Summary

For an objective of optimizing the next generation TEG POWER heat exchanger with integrated annular TEGs for waste heat recovery, the annular TEGs design aspects were discussed to satisfy a set of design objectives under fixed heat exchanger design and operating conditions. The half annular TEG design was introduced as a design solution to improve the annular TEGs power characteristics. It offers the same power output as the full annular TEGs with higher voltage and lower current outputs in addition to other benefits as easier assembly and better control for thermal contact resistance. The interaction between the heat exchanger rows, by electrical connection between TEG rows and axial conduction, was investigated, the results showed the benefits of thermally isolating the rows from each other and connecting them electrically in series.

The effect of annular TEG dimensions on performance was studied and a map was created to be used as a design tool for optimizing annular TEGs dimensions to meet the design requirements. It was shown that by limiting the electrical current output of TEGs using mapping methodology only slightly reduces the power output, however the material volume can be significantly decreased improving the heat exchanger power per unit volume and the overall cost.

Chapter (6)

Conclusion and Future Work Recommendations

6.1. Conclusion

The design of annular thermoelectric generators (TEGs) for power generation requires certain considerations when implemented in waste heat recovery applications as the next generation TEG POWER systems. Such considerations provide design criteria for integrating TEGs in a heat exchanger to achieve the objective of maximizing the power output while improving the compatibility of the design with the other system components in terms of power characteristics, i.e. voltage and current output, and heat transfer capacity.

Since the performance of TEGs is highly dependent on the temperature difference across them in a heat exchanger, the study of performance requires modelling of the coupling between heat transfer and the thermoelectric effects. Studies have considered modelling of flat TEGs in heat exchangers using constant properties models for the thermoelectric effects and heat transfer models. However, the optimization of the TEGs performance in a multi-row heat exchanger, considering the interaction between consecutive rows due to different electrical connections, flow temperature distribution and heat exchanger design, has not previously been investigated. Other studies, considering annular TEG geometries, were limited to the experimental testing of modules performance, either under set temperature difference or in a heat exchanger, without consideration for the effect of annular TEGs dimensions on performance.

In order to study the annular TEGs performance in TEG POWER heat exchanger and characterize their dimensions, a numerical model was developed to simulate TEGs performance in a multi-row heat exchanger. The model approach takes into consideration effects such as: the flow temperature distribution, the electrical connection (series or parallel between rows), the electrical load matching, the axial conduction of heat through the structure of the heat exchanger, and the variation in thermoelectric properties between rows due to their dependence on temperature. The multi-row TEG heat exchanger model consists of models for TEGs, heat exchanger exhaust-side and water-side components. The model equations are solved numerically for different values of

output current and iteratively between rows to obtain temperature, voltage and power output solutions.

The multi-row TEG heat exchanger model was validated using the 1st generation TEG POWER experimental testing results. The model was able to successfully simulate the heat exchanger performance for different exhaust gas mass flow rates. The results showed a good agreement with the experimental results with maximum error of 6% in the exhaust outlet temperatures. The model was then used to evaluate the performance of the next generation TEG POWER heat exchanger which shares the same exhaust-side heat transfer surface of the 1st generation design. Annular TEGs were integrated in the heat exchanger and the water-side was designed accordingly as a cooling loop using pipes. The next generation heat exchanger is designed to operate at mass flow rate and temperature for; exhaust gas at 0.06 kg/s and 270 °C respectively and water flow rate and temperature at 10 LPM and 16 °C respectively.

The numerical model results for the next generation TEG POWER was verified using an equivalent ANSYS model of an element in a multi-row heat exchanger with integrated annular TEGs consisting of four rows at open circuit conditions. The intent was to test the validity of the simplifying assumptions for heat transfer modelling and evaluate the effect of axial heat conduction between the heat exchanger rows. The numerical results showed a good agreement with ANSYS model and the axial heat conduction was found to have a significant effect on the gas temperature distribution and the TEGs surface temperatures.

By investigating the effect of axial heat conduction on the TEGs power output using the numerical model, it was found that the power output and heat flow through the heat exchanger can be increased by insulating in between rows to impede the axial heat conduction. Series and parallel electrical connections between TEG rows in the heat exchanger were also compared in terms of power characteristics. The series configuration showed better results compared to parallel with lower electrical current output, higher voltage output and lower percentage of power loss due to the temperature mismatch between TEG rows.

The objective of this study is to characterize the dimensions of annular TEGs for a multi-row heat exchanger by maximizing the TEGs power output while maintaining improved power characteristics. The performance of a half annular TEG design was compared to full annular TEG one, the half annular design was able to generate the same power output at double the voltage

output and half the current of the full annular design which improves the heat exchanger power characteristics. The effect of varying TEG outer to inner diameter ratio and thickness on the power output and efficiency was also studied, the results showed that the TEGs power output can be maximized at a certain diameter ratio and thickness which depends on the heat exchanger components thermal resistances.

A dimensions map was developed to be used as a design tool for annular TEG modules in a multi-row heat exchanger. The effects of varying the TEGs diameter ratio and thickness on the power output were shown on a two dimensional map with contours of power output for different configurations. The results showed that a dimensionless design parameter (β), which combines the TEGs diameter ratio and thickness, can be used to locate the maximum power output region on the two dimensional power output map.

Using the dimensions map as a design criterion, the annular TEG dimensions for the next generation TEG POWER heat exchanger was identified. The design parameter (β) was determined using the numerical model results for a heat exchanger, consisting of four rows connected electrically in series, in order to maximize the power output. A current output limit was imposed to increase the heat exchanger voltage output, which in turn improves the power characteristics and decrease losses in the MPPT system, and decrease the volume of TEG material. The results showed that by limiting the current output to 46% of its value at the maximum power available, the material volume was reduced by 48% while keeping the power output at 98% of its maximum value.

6.2. Future work recommendations

The developed numerical model was able to predict the 1st generation TEG POWER heat exchanger performance under different exhaust gas mass flow rates. The next step is to compare the model results with experimental testing results of the next generation TEG POWER heat exchanger to validate the model calculations of the power output.

By integrating the developed heat exchanger numerical model with the chimney exhaust network model developed by Girard J. [8], a full system, consisting a natural gas fired oven, TEG POWER heat exchanger, a chimney and a thermal storage tank, can be modelled simultaneously. It can predict the effect of changes in chimney draft conditions on the electrical power output and the

oven natural gas consumption. Also, combining this model with an MPPT with a DC micro-grid model will be beneficial as the loss in the electrical system and the impact on the electrical load operation can be estimated.

Since the performance of TEGs is significantly influenced by the temperature difference across the modules in a heat exchanger, improvements to the heat exchanger design are suggested. Decreasing the thermal resistance of the heat exchanger components especially on the exhaust-side can increase the TEGs power output and the heat flow through the heat exchanger.

The annular TEGs diameter ratio and thickness were set to be the same for all rows in the heat exchanger, however more reduction in the volume of the material used can be achieved by optimizing the dimensions of each row individually at its temperature range. Other design parameters such as the number of TEG rows in the heat exchanger can yet be optimized for different heat exchanger operating conditions.

The heat exchanger inlet conditions can vary during operation due to changes in either the oven setting, the exhaust temperature, the cooling water temperature due to thermal storage or the chimney draft. It is recommended that the heat exchanger design parameters and the TEG dimensions are optimized over a longer period of operation to maximize the electrical energy generated and the thermal energy harvested.

Appendices

Appendix (A)

Performance Testing of the 1st Generation TEG POWER Heat Exchanger

A.1. Introduction

Waste heat recovery systems are utilized to harvest energy lost from processes in a form of heat from exhaust streams. Such systems can achieve energy savings resulting from the repurposing of waste heat into useful forms as electricity or heating sources for lower temperature applications. Thermal energy is lost from gas-fired appliances in food industry at a steady rate with temperatures up to 400 °C [3] which offers potential for electricity generation using thermoelectric generators (TEGs). These are solid state devices that work under a temperature difference using the Seebeck effect to convert a portion of the heat flow into electric power, they are used in a wide range of applications due to advantages as reliable maintenance-free performance, the ability of generating power at low temperature differences and the capacity to work under unsteady conditions [3].

A heat recovery system was designed to harvest the thermal energy wasted from natural gas-fired ovens with naturally ventilated exhaust stream, referred to as TEG POWER which stands for "Thermal-Electric Generator Pizza Oven Waste Energy Recovery" [8]. The oven is operated continuously to maintain a temperature of 260 °C for baking purposes. As a result, heat is lost at a rate 10 kW through a chimney to the outdoor atmosphere. By transferring part of this heat to a water flow, a temperature difference is created that is suitable for electricity generation using TEGs.

The effect of TEG POWER installation on the chimney performance was investigated by Girard [8] as reducing the exhaust inlet temperature to the chimney will affect the buoyancy forces and thus the exhaust gas mass flow rate. The study showed that by including of TEG POWER heat exchanger and exhaust controls and reducing the dilution air from the draft hood by 45%, the natural gas consumption of the oven decreased by 13% without affecting the oven operation.

For low temperature applications up to 200 °C, Bismuth Telluride alloys are the most suitable for thermoelectric P and N-type materials [1] which form couples that are used to build modules. Commercial TEG modules consist of multiple couples, connected using metallic conductors in a series connection, and fitted between two ceramic substrates. For TEG modules integrated in TEG POWER systems, heat is transferred from the exhaust stream to heat the water at a relatively lower temperature using a heat exchanger, the temperature difference is used for electricity generation with an efficiency that is a function of temperature and thermoelectric material properties.

However, parameters such as the thermal resistances of the heat exchanger components and the thermal contact resistance can affect the TEGs performance [5]. Other operation parameters of the heat exchanger as the inlet conditions of exhaust and water can also have a significant impact on the TEGs power output and efficiency [56]. Since the operating conditions of the chimney can vary the exhaust gas mass flow rate through TEG POWER system [8], the objective is to evaluate the performance of the 1st generation TEG POWER heat exchanger under different draft conditions for the chimney. The heat exchanger performance, TEGs power output, and exhaust gas and water outlet temperatures are tested using an experimental testing facility described Girard J. [8] under different exhaust gas mass flow rates.

A.2. Heat exchanger design

The heat exchanger is designed to transfer heat from the exhaust gas flow to the cooling water through TEG modules arrangement, the design is required to minimize the thermal resistance of the heat exchanger components to increase the heat flow and the temperature difference across the TEGs, and ensure a uniform temperature distribution between TEGs. This is done through heat exchanger design of exhaust side with plate fins attached to a thick metal base and impinging jets for the water side to decrease convection resistance and maintain uniform temperatures for the TEG hot and cold surfaces.

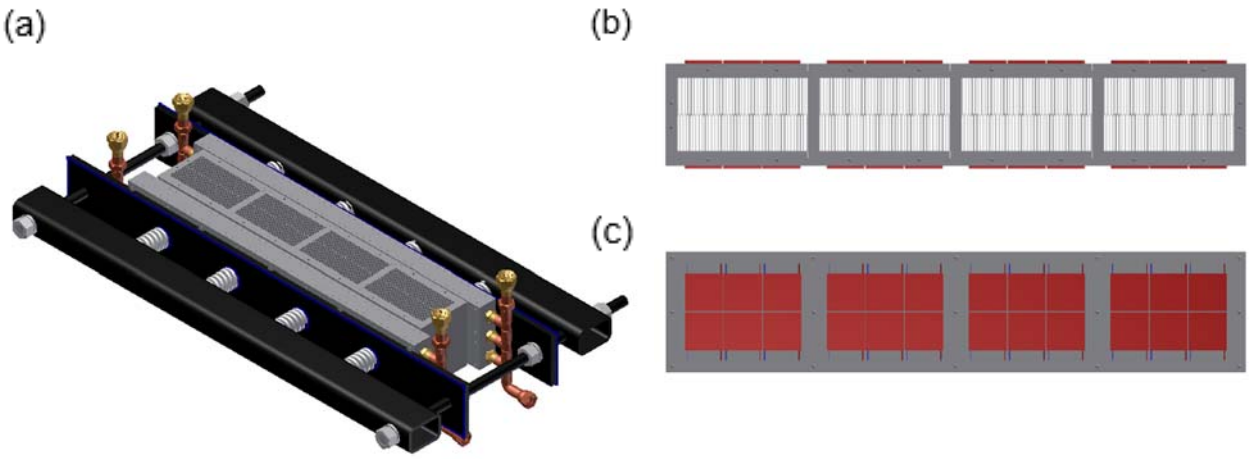

Fig.(A.1) – The 1st generation TEG POWER heat exchanger design: a) Isometric view showing the clamping mechanism and the cold-side heat exchangers arrangement – b) Hot-side heat exchanger design showing the TEGs arrangement on both sides – c) TEGs arrangement on the fin modules base.

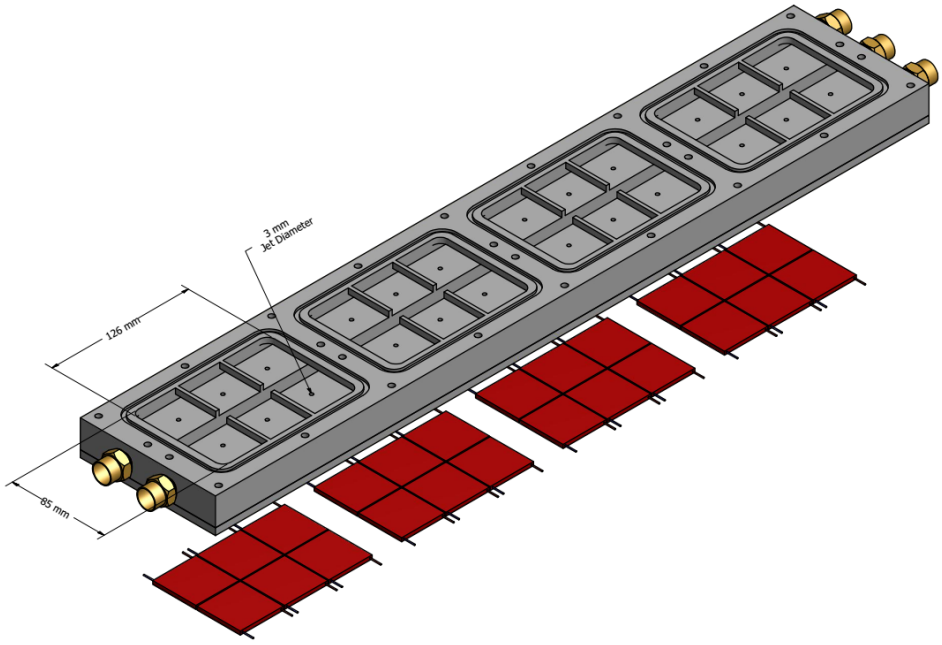

Fig.(A.2) – Cold-side heat exchanger jet impingement design of 1st generation TEG POWER with TEGs arrangement

The heat exchanger consists of four components; exhaust side plate fins, 2 water side jet impingement heat exchanger, 48 TEG modules split into 2 groups and a clamping mechanism as shown in Fig.(A.1 – a). The TEG modules used (TEG1-12610-5.1) are 40 mm x 40 mm in area with maximum power of 5.1 W per module at hot-side temperature of 300 °C and cold-side temperature of 30 °C [9].

The exhaust side consists of 8 plate fin modules made of aluminum, each module has straight fins attached to a base plate, assembled together forming a channel for the exhaust gases. The TEG modules are arranged on two sides of exhaust channel, 24 TEGs per side bundled in 4 groups of 6 TEGs as shown in Fig.(A.1 – b & c). Every 24 TEGs per side are connected electrically in series and both sides are connected together in parallel. The water side is split into two identical heat exchangers, one for each side of 24 TEGs, which are jet impingement heat exchangers that provide cooling for the TEGs. The jet impingement heat exchanger design, shown in Fig.(A.2), was tested and characterized by Hana Y. [49]. The clamping mechanism is used to assemble all components of TEG POWER heat exchanger and maintain pressure on the thermal interfaces between the TEGs, the exhaust side fins and the jet impingement heat exchangers.

A.3. Experimental testing facility

To evaluate the performance of the 1st generation TEG POWER, the heat exchanger was tested using the experimental testing facility described in details by Girard J. [8] under different exhaust flow rates. The facility is comprised of a natural gas fired oven, the TEG POWER heat exchanger mounted on the oven exhaust outlet, a draft hood, an exhaust throttling valve and a chimney to provide draft for the exhaust flow as shown in Fig.(A.3).

For the heat exchanger performance testing shown in Fig.(A.4), the exhaust gas average inlet and outlet temperatures are measured using three inlet and three outlet RTDs (Omega PRTF-11-2-100-1/8-3-E-BX), the exhaust gas flow rate was determined using waste energy balance on the heat transfer between the exhaust gases and the water flow [8]. The TEGs average surface temperatures are measured using 16 T-type thermocouples (TMQSS-032U-6) distributed on the TEGs hot and cold surfaces, the water inlet and outlet temperatures are determined using thermocouples (Omega EMQSS-125U-6) and the water mass flow rate is measured using Coriolis mass flow meter (Endress+Hauser Proline Promass 80E). Finally the TEGs maximum power output was determined by connecting them to an electronic DC load (B&K Precision 8500) and applying a variable electrical load on the TEG system [8], [10] to maximize the TEGs power output at matched load conditions.

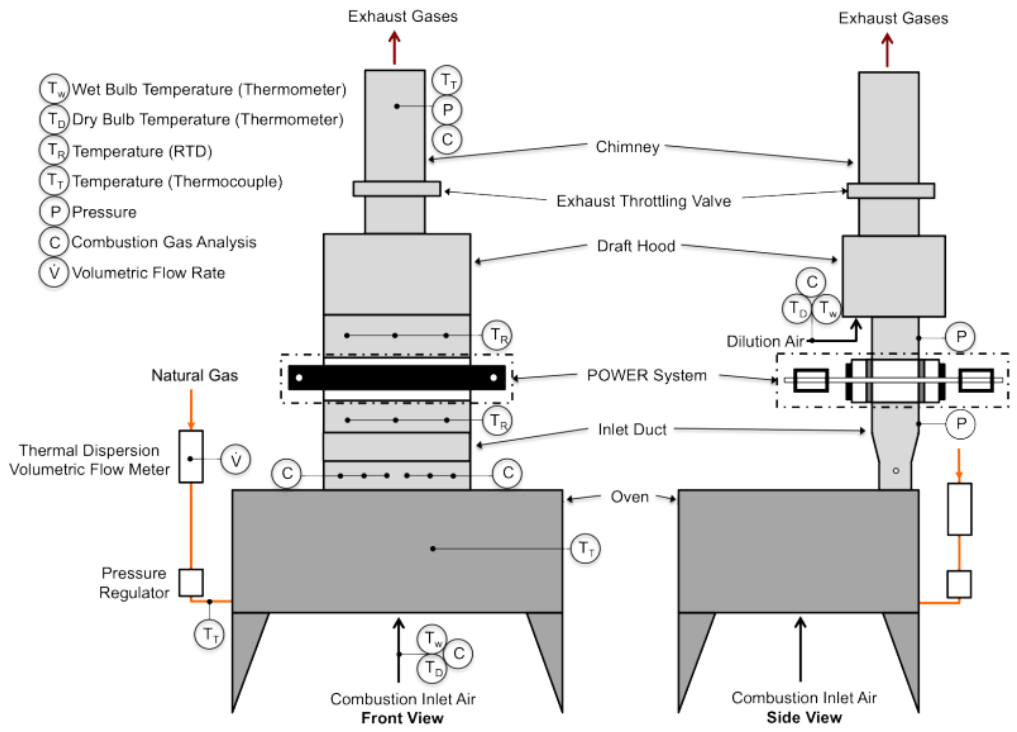

Fig.(A.3) – Experimental testing facility for TEG POWER systems [8]

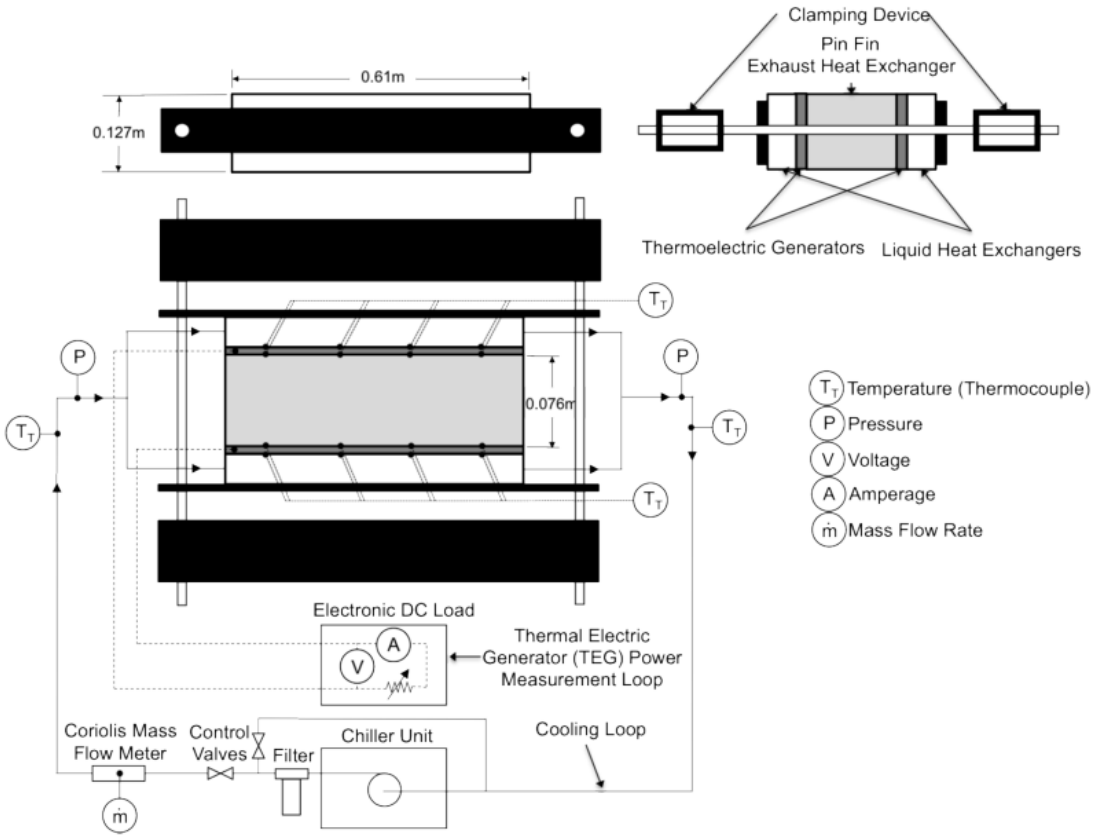

Fig.(A.4) – TEG POWER heat exchanger testing apparatus [8]

The uncertainties in the temperature measurements of the thermocouples and RTDs used in the experimental test facility and the calculated values of gas mass flow rate and TEGs power output are documented by Girard J. [8] and Finnerty D. [10]. The maximum uncertainty in values as; Exhaust temp. ± 1.9 °C, Water temp. ± 0.13 °C, Exhaust gas mass flow rate ± 0.001 kg/s, Water mass flow rate ± 0.0003 kg/s and Power output ± 0.25 W, are listed.

A.4. Results and discussion

By installing the 1st generation TEG POWER heat exchanger on a natural gas-fired oven as shown in Fig.(A.3), the heat exchanger was able to recover the waste heat from the oven exhaust stream at high temperature and transfer this heat to the water cooling loop at low temperature through TEGs which generates an electrical power output due to the temperature difference applied on the TEG hot-side and cold-side surfaces, the TEGs power output is maximized when the electric load is equal to the internal resistance of the TEGs. By varying the setting of the draft hood and the exhaust throttling valve, the heat exchanger performance was tested under different exhaust gas mass flow rates to simulate different draft conditions for the chimney and study the effect on the TEGs power output.

To study the effect of varying the exhaust mass flow rate, the heat recovery system test procedure was followed as described by Girard J. [8] for an oven set temperature of 600 degF (315 °C). The water inlet temperature and mass flow rate was kept constant at approximately 8 °C and 0.07 kg/s respectively, the gas inlet temperature was also maintained by the oven at constant value of 264 °C as shown in Fig.(A.5).

As the exhaust mass flow rate increases, more thermal energy becomes available in the exhaust stream. Since the heat flow through the heat exchanger is affected by the thermal resistance of the components and the temperature difference, the increase in the gas velocity through the channels between fins however does not affect the convection thermal resistance of gas on the fins surface as the flow regime was found to be laminar which is characterized by a constant Nusselt number [48]. Fig.(A.6) shows that the gas-side thermal conductance was found to be nearly constant as well as the water-side and the TEG thermal conductance which means that the total thermal resistance of the heat exchanger remains almost constant by increasing the gas flow rate.

The results in Fig.(A.7) show that the exhaust gas outlet temperature increases by increasing the gas mass flow rate which indicates a rise in the gas average temperature between the inlet and the outlet of the heat exchanger. It can also be seen in Fig.(A.8) that the TEG hot-side surface temperature increases as a result. However, the TEG cold-side surface temperature shows a slight increase compared to the hot-side surface, this is due to the high thermal conductance of the water-side heat exchanger compared to the gas-side as shown in Fig.(A.6) which makes the TEG cold-side surface temperature less affected by the changes in temperature on the gas-side and more influenced by the average water temperature through the heat exchanger. On the other hand, the water outlet temperature in Fig.(A.7) shows very small changes (within 1 °C) compared to the gas temperature which is mainly due to the significant difference in specific heat between exhaust gas and water and the high mass flow rate of water used in the heat exchanger. This causes the water average temperature through the heat exchanger to remain nearly constant as the gas flow rate increases.

The results in Fig.(A.8) show that, by increasing the exhaust gas mass flow rate, the temperature difference across the TEGs increases which is indicative of an increase in the heat flow through the TEGs since their thermal conductance is constant. Consequently, the power output of the TEGs increases by 10% for an increase in the gas mass flow rate from 0.038 kg/s to 0.044 kg/s (16%) as shown in Fig.(A.9) which is the same effect reported by [56], [57], [58], and [59] for increasing the hot fluid flow rate in a heat exchanger with integrated TEGs. On the contrary, the TEGs efficiency shows a smaller increase by 5% compared to the power output within the same range from 0.038 kg/s to 0.044 kg/s, this is due to that the power output is directly proportional to $(\Delta T)^2$ while the efficiency which directly proportional to ΔT, i.e. ΔT is the temperature difference between the TEG hot-side and cold-side temperatures.

Despite the increase in power output and efficiency over the tested range of exhaust mass flow rates, there is a noticeable deviation in the power output and efficiency data points in Fig.(A.9) at approximately 0.037 and 0.046 kg/s which can be improved by testing a wider range of mass flow rates and including more data points which will be considered in further studies, in addition to improvements to the heat exchanger and TEG modules design for higher power output and efficiency.

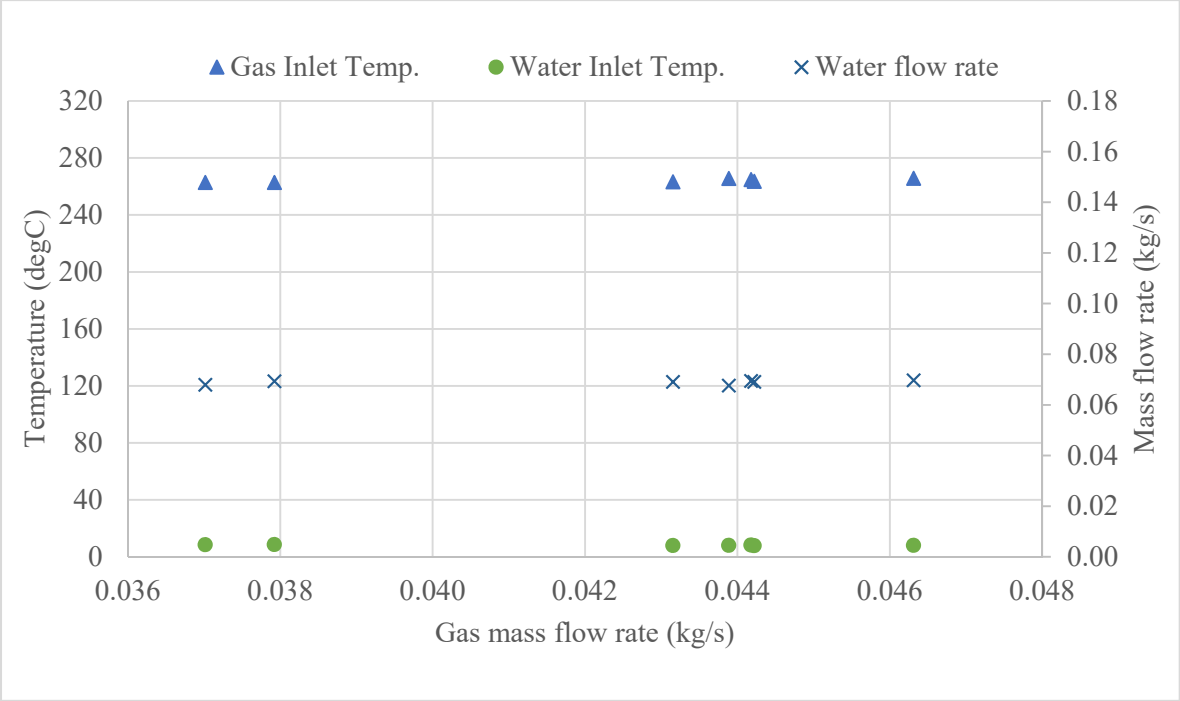

Fig.(A.5) – Heat exchanger gas and water inlet temperatures, and water flow rate at different exhaust gas mass flow rates.

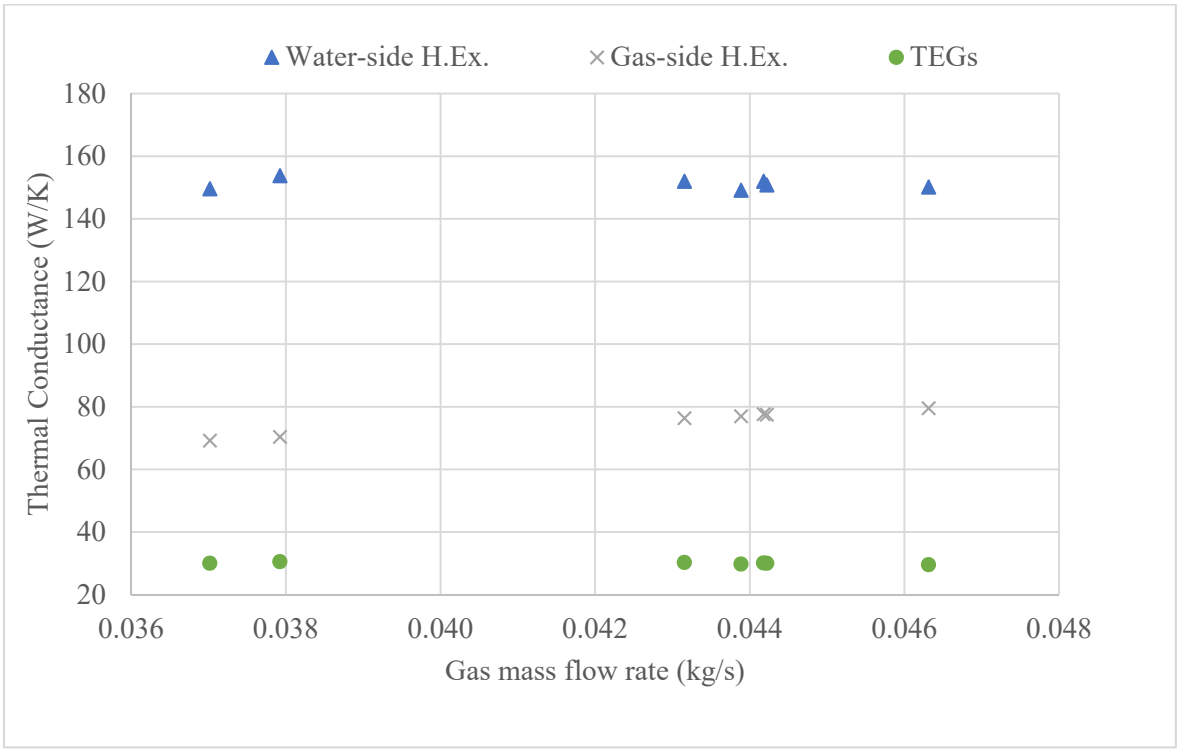

Fig.(A.6) – Thermal conductance of heat exchanger (H.Ex.) components; Water-side, Gas-side and TEGs at different exhaust gas mass flow rates.

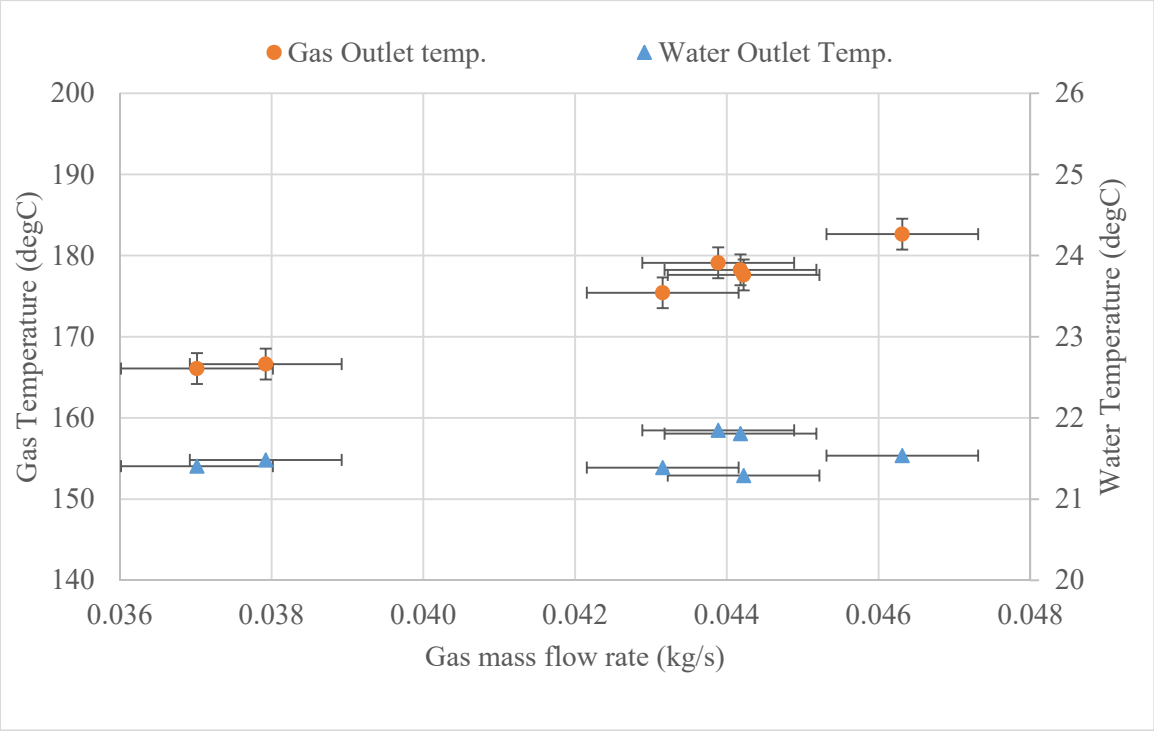

Fig.(A.7) – Heat exchanger exhaust gas and water outlet temperature measurements at different exhaust gas mass flow rates.

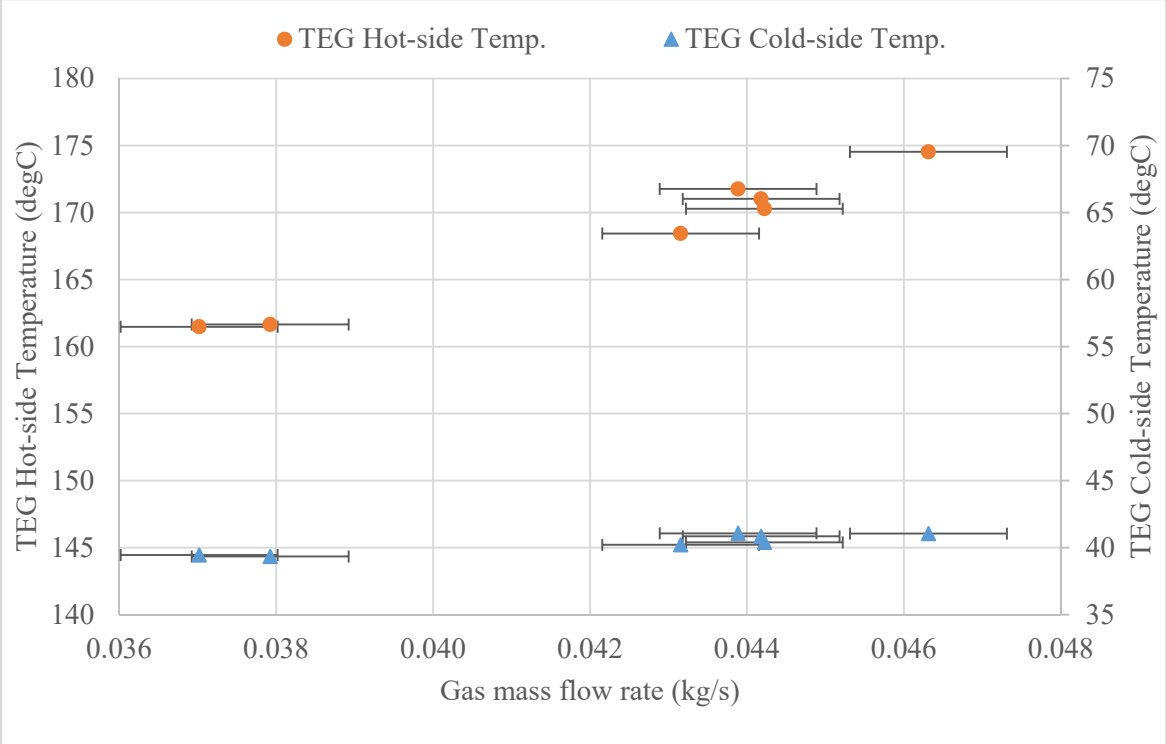

Fig.(A.8) – TEGs hot-side and cold-side surface temperature measurements at different exhaust gas mass flow rates.

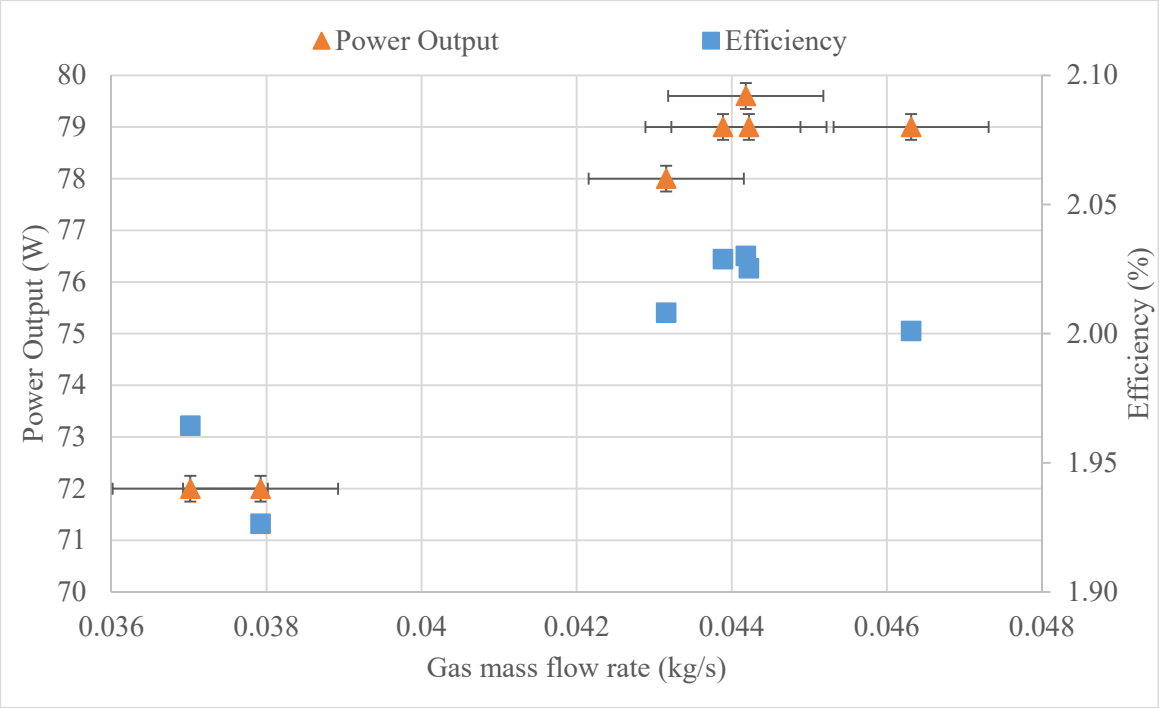

Fig.(A.9) – TEGs power output and efficiency results at different exhaust gas mass flow rates.

A.5. Conclusion

The performance of 1st generation TEG POWER heat exchangers is tested at different exhaust gas mass flow rates to investigate the effect of variation in the chimney draft conditions in a waste heat recovery system for commercial natural gas fired ovens [8], the results are obtained using measurements from an experimental testing facility at different exhaust gas mass flow rates for constant inlet conditions for the heat exchanger. Outlet temperatures, TEGs power output and efficiency results are presented. The results showed a 10% increase in power output and 5% in efficiency as the exhaust gas mass flow rate increases as well as an increase in the heat flow through the heat exchanger. In terms of the system overall performance, TEG POWER heat exchanger is able to recover an average of 3.8 kW of heat out of 10 kW available in the oven exhaust flow which was lost to an ambient of 25 °C while generating 77 kW on average as electrical power output, energy savings can be achieved by thermal storage of the recovered heat in a tank, to offset energy consumption for hot water needs, and the efficient utilization of the electricity generated using a DC microgrid with MPPT system for low power electrical loads.

Appendix (B)

Annular TEGs Material Properties for the Next Generation TEG POWER Heat Exchanger

In order to simulate the thermoelectric material behavior using the multi-row TEG heat exchanger numerical model for the next generation TEG POWER system, the P and N type material properties of the annular TEGs were selected for spark plasma sintered bismuth telluride for 120-180 μm particle sizes. The data provided in [51], [52] was fitted to equations to be used in the model, the curve-fit equations are shown in Fig.(B.1) below:

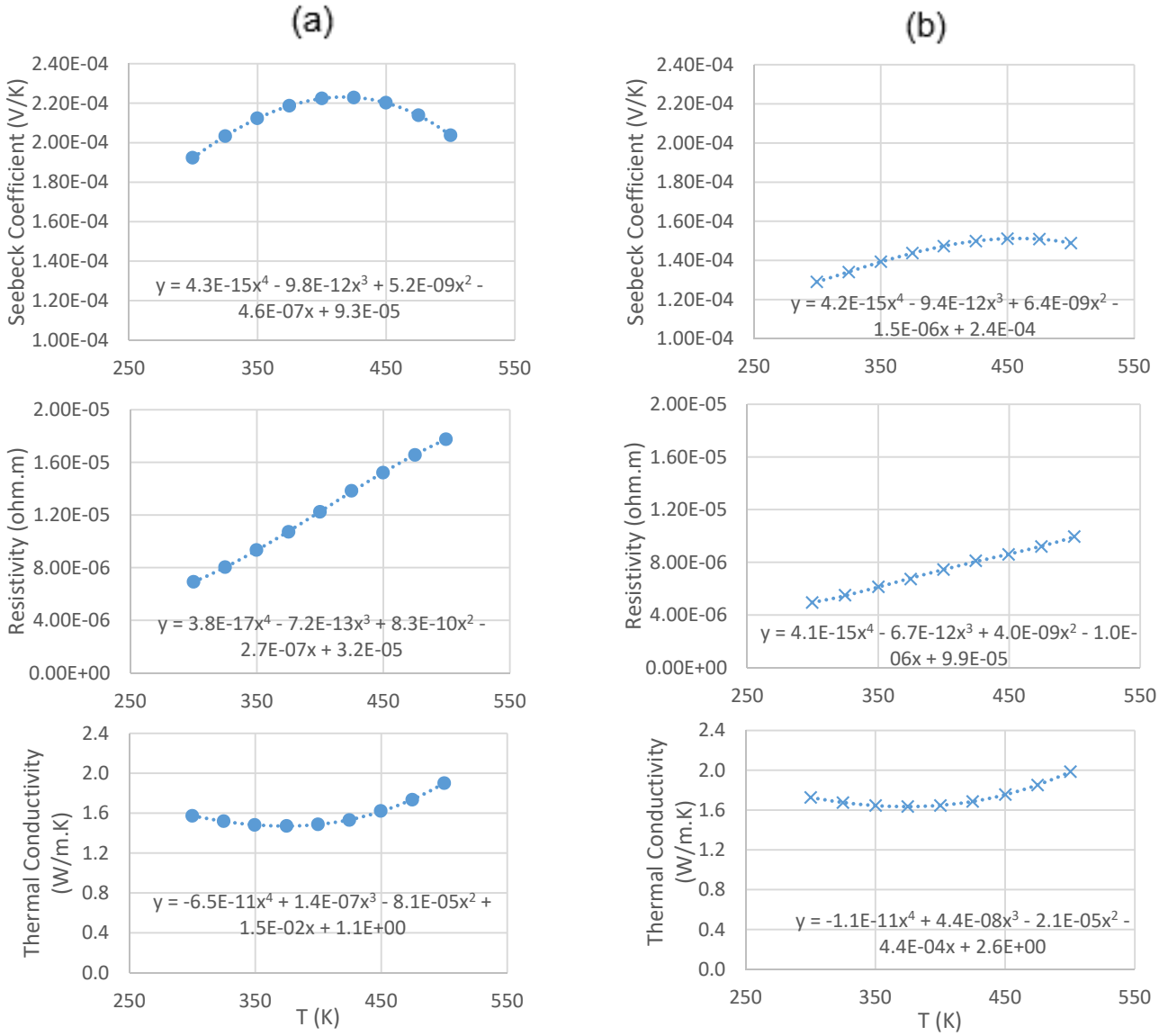

Fig.(B.1) – Thermoelectric properties characterization results [51], [52]: a) P-type SPS Bismuth Telluride – b) N-type SPS Bismuth Telluride

Appendix (C)

Summary of Annular TEG and Heat Exchanger Modelling Using ANSYS

The verification of the numerical model results was discussed in this study using ANSYS models for the performance of an annular TEG couple integrated in a heat exchanger and the effect of axial conduction on the gas temperature profiles of the next generation TEG POWER heat exchanger. Details of the ANSYS models will be presented in this section.

C.1. Modelling of an annular TEG couple integrated in a heat exchanger

An annular TEG couple performance was studied using ANSYS to verify the results of the numerical model. The performance was investigated for constant temperatures of the heat source and the heat sink under different electrical loads. By changing the electrical resistivity of a metallic conductor connected in series to the TEG using copper conductors, the electrical load was varied to simulate the performance under different load ratios. Fig.(C.1) shows a schematic of the ANSYS model of the TEG with the heat exchanger components thermal conductance and a description of the boundary conditions. The thermal resistance of the heat exchanger components was modelled using blocks of known thermal conductivity and dimensions.

The model results at maximum power were obtained using the mesh shown in Fig.(C.2). The mesh independence was tested by reducing the mesh element size from 4 mm to 0.25 mm on five steps. The results were found to be independent of the element size as shown in Table (C.1). The results varied within less than 0.6% by varying the size of the mesh element.

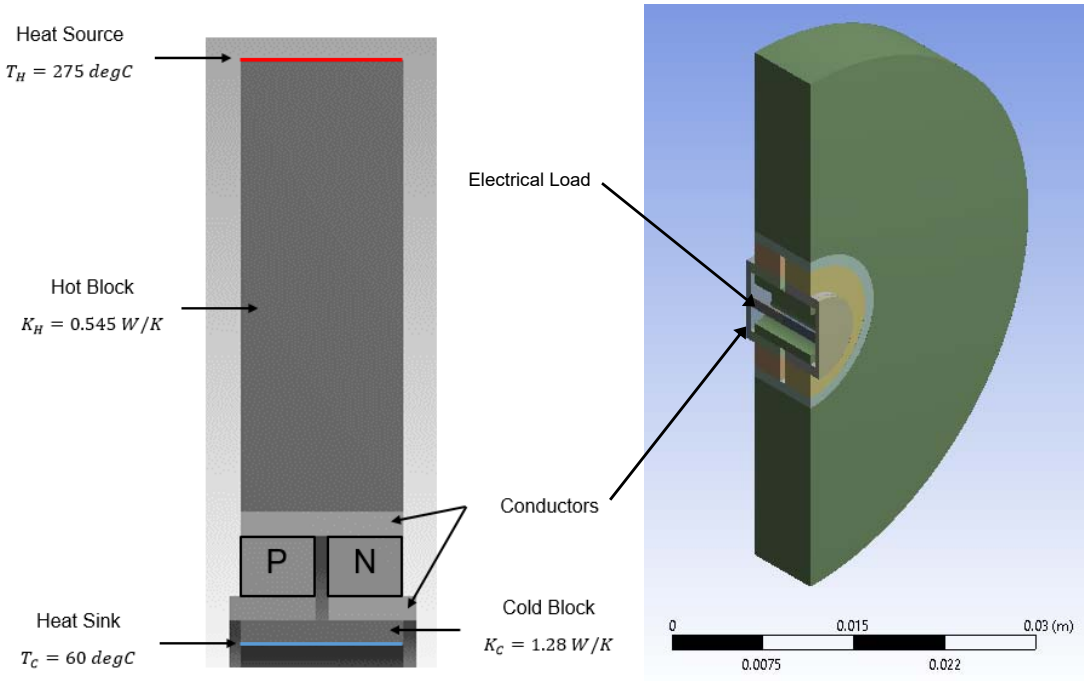

Fig.(C.1) – Description of the ANSYS model for an annular TEG integrated in a heat exchanger

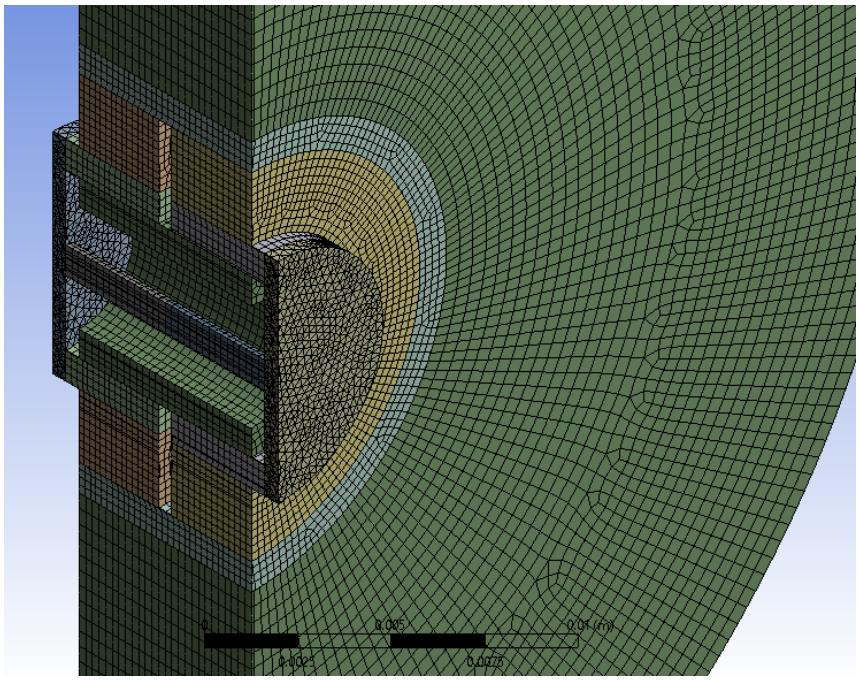

Fig.(C.2) – Section in the model assembly showing the mesh structure with an element size of 0.25 mm.

Element Size (m)	Voltage (V)	Current (I)	Power (W)	Heat Flow (Q_H)
4.00E-03	0.036085	38.82061	1.400842	24.19424
2.00E-03	0.036068	38.83552	1.40072	24.2845
1.00E-03	0.036128	38.7688	1.400639	24.33222
5.00E-04	0.036131	38.73112	1.399394	24.33637
2.50E-04	0.036117	38.69265	1.397462	24.33222
% Change	-0.0886 %	0.330696 %	0.241802 %	-0.56704 %

Table (C.1) – The performance results of the annular TEG model for the mesh independence test.

C.2. Modelling of the gas flow in a heat exchanger element with annular TEGs

The gas temperature profile through the heat exchanger was studied using ANSYS to verify the results of the numerical model for the gas temperatures and the TEGs hot-side surface temperatures at open circuit. The water side was modelled using ANSYS Fluent using a convection boundary condition and an average water temperature of each row that are equal to the results of the numerical model to compare the gas temperatures solution of both models. This was done to check the modelling assumptions used in the numerical model for the TEG hot-side in addition to the modelling of the axial conduction component. Fig.(C.3) shows details of the boundary conditions used in the ANSYS model, noting that all the outer surfaces of the heat exchanger element are insulated.

The model results were obtained at open circuit conditions for the TEGs using the mesh shown in Fig.(C.4). The mesh independence was tested by reducing the mesh element size from 0.75 mm to 0.3 mm on four steps, the average gas temperature results were found to be independent of the mesh element size in the range from 0.3 mm to 0.6 mm as shown in Fig.(C.5).

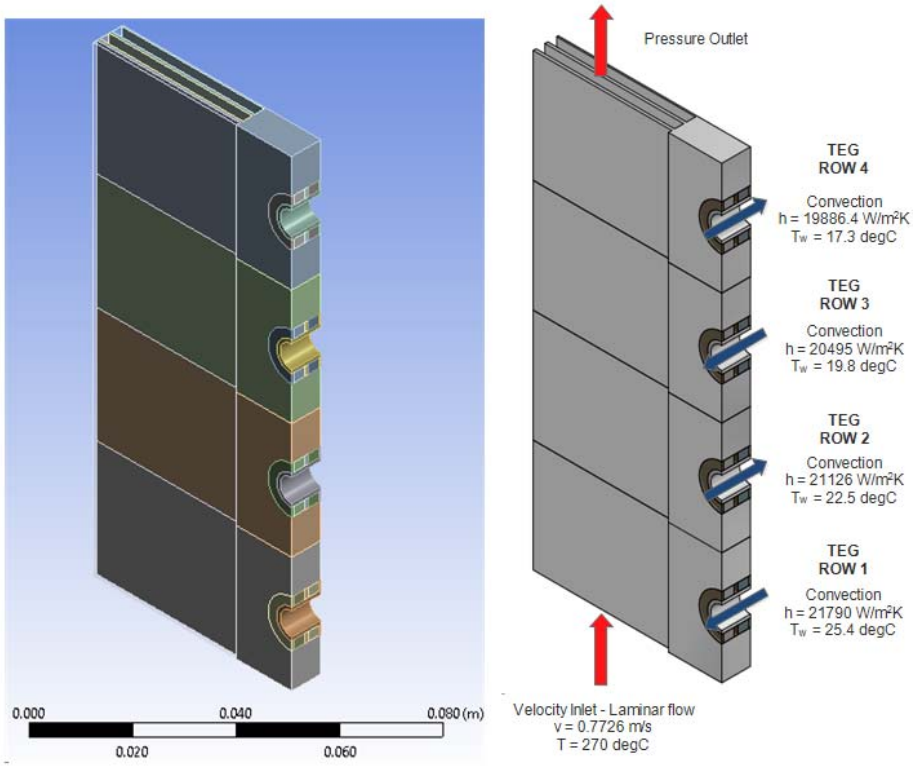

Fig.(C.3) – Description of the ANSYS model for the heat exchanger element with details of the boundary conditions

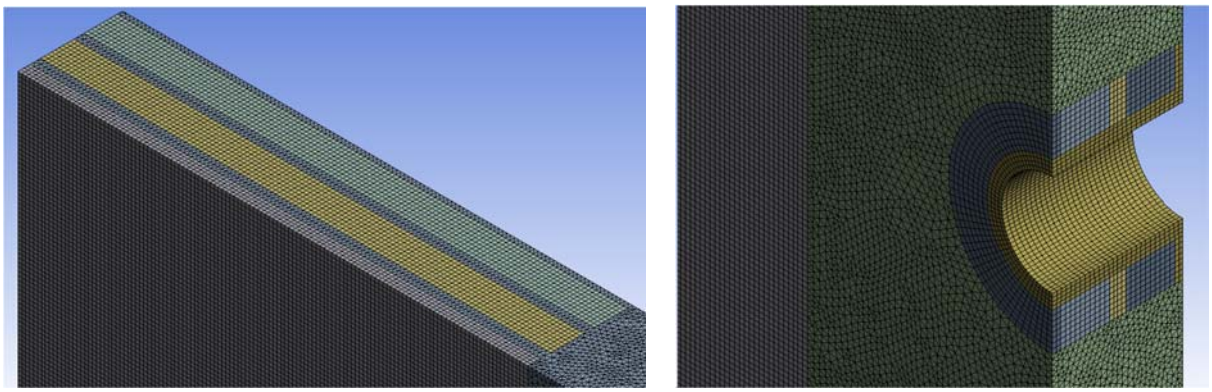

Fig.(C.4) – The ANSYS model mesh structure at an element size of 0.3 mm.

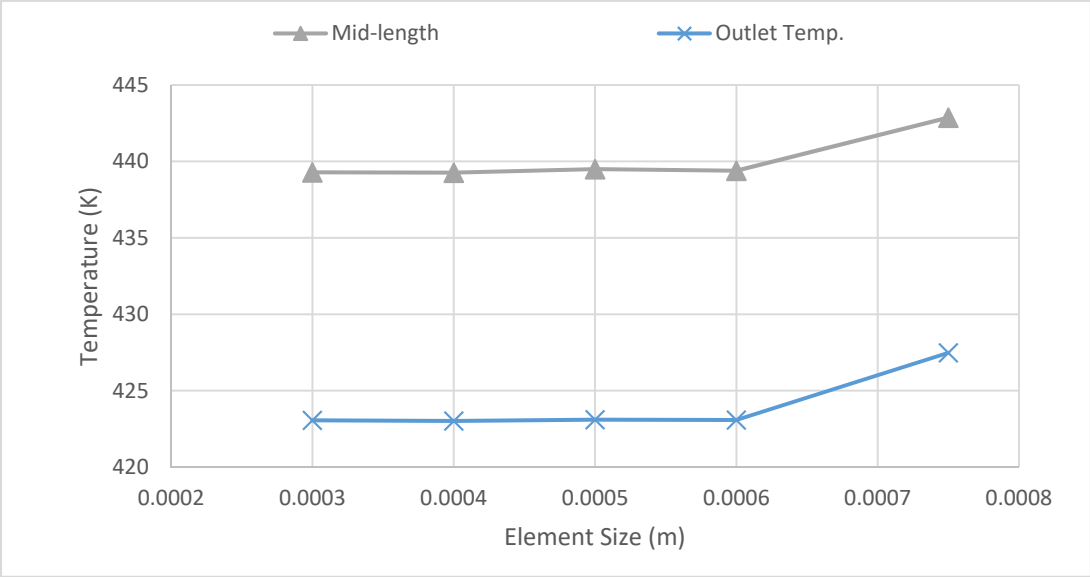

Fig.(C.5) – The variation of average gas temperatures at mid-length and outlet of the fins with the mesh element size

References

[1] D. Rowe, Ed., *Modules, Systems, and Applications in Thermoelectrics*. CRC Press, 2012.

[2] J. L. Pellegrino, N. Margolis, M. Justiniano, M. Miller, and A. Thedki, "Energy Use, Loss and Opportunities Analysis: US Manufacturing and Mining," *DOE/ITP (U.S. Dep. Energy's Iindustrial Technol. Program)*, no. December, p. 169, 2004.

[3] D. Rowe, Ed., *Thermoelectrics Handbook: macro to nano*. CRC Press, 2005.

[4] G. Min and D. M. Rowe, "Optimisation of thermoelectric module geometry for 'waste heat' electric power generation," *J. Power Sources*, vol. 38, no. 3, pp. 253–259, 1992.

[5] D. Rowe and G. Min, "Peltier Devices as Generators," in *CRC Handbook of Thermoelectrics*, CRC Press, 1995.

[6] D. M. Rowe and G. Min, "Evaluation of thermoelectric modules for power generation," *J. Power Sources*, vol. 73, no. Copyright 1998, IEE, pp. 193–198, 1998.

[7] D. M. Rowe and G. Min, "Design theory of thermoelectric modules for electrical power generation," *IEE Proceedings-Science, Meas. Technol.*, vol. 143, no. 6, pp. 351–356, 1996.

[8] J. Girard, "The investigation of exhaust control strategies and waste heat recovery practices of naturally-ventilated exhaust streams," McMaster University, 2016.

[9] TECTEG/Thermal-Electronics, "Specifications TEG Module TEG1-12610-5.1," 2016. [Online]. Available: http://tecteg.com/wp-content/uploads/2014/09/1.pdf.

[10] D. Finnerty, "The Development of Methodologies and a Novel Test Facility for the Characterisation of Thermoelectric Generators," McMaster University, 2013.

[11] J. W. Stevens, "Optimal design of small DT thermoelectric generation systems," *Energy Convers. Manag.*, vol. 42, no. 6, pp. 709–720, 2001.

[12] G. Min and D. M. Rowe, "Ring-structured thermoelectric module," *Semicond. Sci.*

Technol., vol. 22, pp. 880–883, 2007.

[13] A. Bauknecht, T. Steinert, C. Spengler, and G. Suck, "Analysis of annular thermoelectric couples with nonuniform temperature distribution by means of 3-D multiphysics simulation," *J. Electron. Mater.*, vol. 42, no. 7, pp. 1641–1646, 2013.

[14] A. Schmitz, C. Stiewe, and E. Müller, "Preparation of ring-shaped thermoelectric legs from PbTe powders for tubular thermoelectric modules," *J. Electron. Mater.*, vol. 42, no. 7, pp. 1702–1706, 2013.

[15] K. Takahashi, T. Kanno, A. Sakai, H. Tamaki, H. Kusada, and Y. Yamada, "Bifunctional thermoelectric tube made of tilted multilayer material as an alternative to standard heat exchangers.," *Sci. Rep.*, vol. 3, p. 1501, 2013.

[16] A. Sakai, T. Kanno, K. Takahashi, H. Tamaki, and Y. Yamada, "Power Generation and Peltier Refrigeration by a Tubular Pi-Type Thermoelectric Module," *J. Electron. Mater.*, vol. 44, no. 11, pp. 4510–4515, 2015.

[17] N. Mansouri, E. J. Timm, H. J. Schock, D. Sahoo, and A. Kotrba, "Development of a Circular Thermoelectric Skutterudite Couple Using Compression Technology," *J. Energy Resour. Technol.*, vol. 138, no. 5, p. 52003, 2016.

[18] M. Morsy, "Manufacturing and Characterization of Annular Thermoelectric Generators and Verification of a Novel Design," McMaster University, 2015.

[19] C. Goupil, *Continuum Theory and Modeling of Thermoelectric Elements*. Weinheim, Germany: Wiley-VCH Verlag GmbH & Co. KGaA, 2016.

[20] A. F. Ioffe, L. S. Stil'bans, E. K. Iordanishvili, T. S. Stavitskaya, A. Gelbtuch, and G. Vineyard, "Semiconductor Thermoelements and Thermoelectric Cooling," *Phys. Today*, vol. 12, no. 5, pp. 42–42, May 1959.

[21] J. E. Sunderland and N. T. Burak, "The influence of the Thomson effect on the performance of a thermoelectric power generator," *Solid. State. Electron.*, vol. 7, no. 6, pp. 465–471, Jun. 1964.

[22] P. Lau and R. Buist, "Calculation of thermoelectric power generation performance using

finite element analysis," *XVI ICT "97. Proceedings ICT"97. 16th International Conference on Thermoelectrics (Cat. No.97TH8291)*. pp. 563–566, 1997.

[23] G. Fraisse, J. Ramousse, D. Sgorlon, and C. Goupil, "Comparison of different modeling approaches for thermoelectric elements," *Energy Convers. Manag.*, vol. 65, pp. 351–356, 2013.

[24] C. Jincan and Y. Zijun, "The influence of Thomson effect on the maximum power output and maximum efficiency of a thermoelectric generator," *J. Appl. Phys.*, vol. 79, no. 1, pp. 111–119, 1996.

[25] H. J. Goldsmid, "Conversion Efficiency and Figure-of-Merit," *CRC Handb. Thermoelectr.*, pp. 32–39, 1995.

[26] M. H. Cobble, "Calculations of Generator Performance," *CRC Handb. Thermoelectr.*, vol. 2, no. 3, pp. 489–492, 1995.

[27] J. Henderson, "Analysis of a Heat Exchanger- Thermoelectric Generator System," *14th Intersoc. Energy Convers. Eng. Conf.*, vol. 2, pp. 1835–1840, 1979.

[28] W. Glatz, S. Muntwyler, and C. Hierold, "Optimization and fabrication of thick flexible polymer based micro thermoelectric generator," *Sensors Actuators, A Phys.*, vol. 132, no. 1 SPEC. ISS., pp. 337–345, 2006.

[29] M. Strasser, R. Aigner, M. Franosch, and G. Wachutka, "Miniaturized thermoelectric generators based on poly-Si and poly-SiGe surface micromachining," *Sensors Actuators, A Phys.*, vol. 97–98, pp. 535–542, 2002.

[30] M. Freunek, L. M. Reindl, and W. D. Walker, "Modified Model for Thermoelectric Generators," *Ect2008*, vol. 49, no. 0, pp. 1–4, 2008.

[31] M. Freunek, M. Müller, T. Ungan, W. Walker, and L. M. Reindl, "New physical model for thermoelectric generators," *J. Electron. Mater.*, vol. 38, no. 7, pp. 1214–1220, 2009.

[32] M. Strasser, R. Aigner, C. Lauterbch, T. F. Sturm, M. Franosch, and G. Wachutka, "Micromachined CMOS thermoelectric generator as on-chip power supply," *TRANSDUCERS '03. 12th Int. Conf. Solid-State Sensors, Actuators Microsystems (IEEE,*

2003). p. 45–48., 2003.

[33] I. Laird and D. D. C. Lu, "High step-up DC/DC topology and MPPT algorithm for use with a thermoelectric generator," *IEEE Trans. Power Electron.*, vol. 28, no. 7, pp. 3147–3157, 2013.

[34] E. Brownell and M. Hodes, "Optimal design of thermoelectric generators embedded in a thermal resistance network," *IEEE Trans. Components, Packag. Manuf. Technol.*, vol. 4, no. 4, pp. 612–621, 2014.

[35] D. T. Crane, G. S. Jackson, and D. Holloway, "Towards Optimization of Automotive Waste Heat Recovery Using Thermoelectrics," in *Thermal systems management and geat exchangers*, SAE International, 2001, pp. 53–66.

[36] D. T. Crane and G. S. Jackson, "Optimization of cross flow heat exchangers for thermoelectric waste heat recovery," *Energy Convers. Manag.*, vol. 45, no. 9–10, pp. 1565–1582, 2004.

[37] D. T. Crane, J. W. L. Grandeur, F. Harris, and L. E. Bell, "Performance Results of a High-Power-Density Thermoelectric Generator : Beyond the Couple," vol. 38, no. 7, pp. 1375–1381, 2009.

[38] D. T. Crane and L. E. Bell, "Progress Towards Maximizing the Performance of a Thermoelectric Power Generator," 2006.

[39] S. Kumar, S. D. Heister, X. Xu, R. James, and G. P. Meisner, "Thermoelectric Generators for Automotive Waste Heat Recovery Systems Part I : Numerical Modeling and Baseline Model Analysis," vol. 42, no. 4, pp. 665–674, 2013.

[40] S. Kumar, S. D. Heister, X. Xu, J. R. Salvador, and G. P. Meisner, "Thermoelectric generators for automotive waste heat recovery systems part II: Parametric evaluation and topological studies," *J. Electron. Mater.*, vol. 42, no. 6, pp. 944–955, 2013.

[41] J.-H. Meng, X.-D. Wang, and W.-H. Chen, "Performance investigation and design optimization of a thermoelectric generator applied in automobile exhaust waste heat recovery," *Energy Convers. Manag.*, vol. 120, pp. 71–80, 2016.

[42] J.-H. Meng, X.-X. Zhang, and X.-D. Wang, "Characteristics analysis and parametric study of a thermoelectric generator by considering variable material properties and heat losses," *Int. J. Heat Mass Transf.*, vol. 80, pp. 227–235, 2015.

[43] T. Kyono, R. O. Suzuki, and K. Ono, "Conversion of unused heat energy to electricity by means of thermoelectric generation in condenser," *IEEE Trans. Energy Convers.*, vol. 18, no. 2, pp. 330–334, 2003.

[44] Z. G. Shen, S. Y. Wu, and L. Xiao, "Theoretical analysis on the performance of annular thermoelectric couple," *Energy Convers. Manag.*, vol. 89, pp. 244–250, 2015.

[45] E. Brownell and M. Hodes, "Optimal Design of Thermoelectric Generators Embedded in a Thermal Resistance Network," vol. 4, no. 4, pp. 612–621, 2014.

[46] S. W. Angrist, *Direct energy conversion*, 3rd ed. Allyn and Bacon Inc., 1976.

[47] M. K. Khorasgani, "Synthesis and Characterization of Bismuth Telluride- Based Nanostructured Thermoelectric Composite Materials," 2014.

[48] S. Kakaç, R. K. Shah, and W. Aung, Eds., *Handbook of single-phase convective heat transfer*. New York : Wiley, c1987, 1987.

[49] Y. Hana, "Characterization of Flat-Plate Heat Exchangers for Thermal Load Management of Thermoelectric Generators," McMaster University, 2014.

[50] Fujipoly, *Sarcon - Thermal Managment Materials*. 2012.

[51] J. Jiang, L. Chen, S. Bai, and Q. Yao, "Thermoelectric performance of p-type Bi-Sb-Te materials prepared by spark plasma sintering," *J. Alloys Compd.*, vol. 390, no. 1–2, pp. 208–211, 2005.

[52] J. Jiang, L. Chen, S. Bai, Q. Yao, and Q. Wang, "Fabrication and thermoelectric performance of textured n-type Bi2(Te,Se)3 by spark plasma sintering," *Scr. Mater.*, vol. 52, no. 5, pp. 347–351, 2005.

[53] L. W. da Silva and M. Kaviany, "Micro-thermoelectric cooler: Interfacial effects on thermal and electrical transport," *Int. J. Heat Mass Transf.*, vol. 47, no. 10–11, pp. 2417–2435, 2004.

[54] F. P. Incropera and D. P. DeWitt, *Fundamentals of Heat and Mass Transfer*, 7th ed. John

Wiley & Sons, 2011.

[55] A. Montecucco, J. Siviter, and A. R. Knox, "The effect of temperature mismatch on thermoelectric generators electrically connected in series and parallel," *Appl. Energy*, vol. 123, pp. 47–54, 2014.

[56] X. Niu, J. Yu, and S. Wang, "Experimental study on low-temperature waste heat thermoelectric generator," *J. Power Sources*, vol. 188, no. 2, pp. 621–626, 2009.

[57] D. T. Crane and L. E. Bell, "Design to Maximize Performance of a Thermoelectric Power Generator With a Dynamic Thermal Power Source," *J. Energy Resour. Technol.*, vol. 131, no. 1, p. 12401, 2009.

[58] J. Yu and H. Zhao, "A numerical model for thermoelectric generator with the parallel-plate heat exchanger," *J. Power Sources*, vol. 172, no. 1, pp. 428–434, 2007.

[59] S. Kumar, S. D. Heister, X. Xu, and J. R. Salvador, "Optimization of Thermoelectric Components for Automobile Waste Heat Recovery Systems," *J. Electron. Mater.*, vol. 44, no. 10, pp. 3627–3636, 2015.